UNITED NATIONS EDUCATIONAL, SCIENTIFIC AND CULTURAL ORGANIZATION
INTERNATIONAL ATOMIC ENERGY AGENCY
INTERNATIONAL CENTRE FOR THEORETICAL PHYSICS
I.C.T.P., P.O. BOX 586, 34100 TRIESTE, ITALY, CABLE: CENTRATOM TRIESTE

H4.SMR/942-2

Third Workshop on 3D Modelling of Seismic Waves Generation Propagation and their Inversion

4 - 15 November 1996

Modelling of Seismic Input

G.F. Panza

Dept. of Earth Sciences/ICTP
Trieste, Italy

Realistic modelling of observed seismic motion in complex sedimentary basins

Donat Fäh(1)(*) **and Giuliano F. Panza**(1)(2)
(1) *Istituto di Geodesia e Geofisica, Universita di Trieste, Italy*
(2) *International Center for Theoretical Physics, Trieste, Italy*

Abstract
Three applications of a numerical technique are illustrated to model realistically the seismic ground motion for complex two-dimensional structures. First we consider a sedimentary basin in the Friuli region, and we model strong motion records from an aftershock of the 1976 earthquake. Then we simulate the ground motion caused in Rome by the 1915, Fucino (Italy) earthquake, and we compare our modelling with the damage distribution observed in the town. Finally we deal with the interpretation of ground motion recorded in Mexico City, as a consequence of earthquakes in the Mexican subduction zone. The synthetic signals explain the major characteristics (relative amplitudes, spectral amplification, frequency content) of the considered seismograms, and the space distribution of the available macroseismic data. For the sedimentary basin in the Friuli area, parametric studies demonstrate the relevant sensitivity of the computed ground motion to small changes in the subsurface topography of the sedimentary basin, and in the velocity and quality factor of the sediments. The relative Arias Intensity, determined from our numerical simulation in Rome, is in very good agreement with the distribution of damage observed during the Fucino earthquake. For epicentral distances in the range 50 km-100 km, the source location and not only the local soil conditions control the local effects. For Mexico City, the observed ground motion can be explained as resonance effects and as excitation of local surface waves, and the theoretical and the observed maximum spectral amplifications are very similar. In general, our numerical simulations estimate the maximum and average spectral amplification for specific sites, *i.e.* they are a very powerful tool for accurate micro-zonation.

Key words *wave-propagation modelling – seismic strong ground motion – sedimentary basins – seismic micro-zonation*

1. Introduction

The presence of unconsolidated sediments with irregular geotechnical characteristics makes sedimentary basins the zones which are most vulnerable to earthquakes. In fact, when the shear-wave velocity at the surface is low, quite large amplifications of the ground motion are observed, and localized amplification of the signals are often related to lateral irregularities in the subsurface topography (*e.g.* Jackson, 1971). Even smooth variations of the near-surface structure can cause large differential motion, and in relatively close points it is possible to observe signals with significantly different amplitude and duration.

It is well-known that incident plane waves are amplified when the seismic wave travels through an interface from a medium with high rigidity, into a medium with low rigidity. For vertically incident waves, the frequencies of the mechanical resonance which can occur in sedimentary basins, are given by $f_n = (2n + 1)\beta/4h$, where β is the shear wave

(*) *Now at:* Institut für Geophysik, ETH-Hönggerberg, CH-8093 Zürich, Switzerland.

15

velocity in the basin and h is its thickness (Haskell, 1960, 1962). An irregular interface between bedrock and sediments can cause the focusing of waves (*e.g.* Aki and Larner, 1970; Boore *et. al.*, 1971; Sánchez-Sesma *et al.*, 1988), and can excite local surface waves (*e.g.* Trifunac, 1971; Bard and Bouchon, 1980a,b). These local surface waves can be excited not only by body waves but also by the incidence of surface waves (Drake, 1980). Bard and Bouchon (1985) demonstrated that the occurrence of local surface waves is determined primarily by the depth of the basin and by the contrast between the shear-wave velocity of the basin and that of the bedrock. When the wavelength of the incident wave is comparable with the depth of the basin, the local surface waves can have larger amplitudes than the direct signal, and, if the contrast in the elastic parameters between the sediments and the underlying bedrock is high, they can be reflected at the edges of the basin, causing a long duration of the ground motion in the basin. This behavior does not change if a vertical stratification of the sediments, with a large vertical velocity gradient, is considered (Bard and Gariel, 1986).

For preparedness purposes, it is crucial to estimate the seismic ground motion, before an earthquake occurs, and to include these results in the assessment of seismic hazard or in (micro)-zonation studies. A powerful tool to estimate the amplification effects in complex structures are numerical simulations. One major problem which is encountered when doing such simulations is the large number of parameters which have to be specified as input. The choice of these parameters should be based on all available seismological, geological and geotechnical information for the area under consideration. At a specific site, the numerical simulation can predict the seismic response only if the properties of the seismic source and the mechanical (density, velocity, damping, etc.) and geometrical (such as layer thickness) parameters of the path from the source are reasonably well-known. In general this is not the case, and parametric studies are necessary to quantify the variability of the expected ground motion. Whenever possible, such simulations, must be compared with observed ground motion.

The method we use for the modelling of the wave propagation in two-dimensional complex media, is the hybrid technique, which combines modal summation (Panza, 1985; Florsch *et al.*, 1991) and the finite difference technique (Korn and Stöckl, 1982; Virieux, 1986), described by Fäh (1992), Fäh *et al.* (1993a; 1993b), and Fäh *et al.* (1994). The propagation of waves from the source to the sedimentary basin is treated with the mode summation method, applied to plane layered, anelastic structures which represent the average crustal properties along the source-basin path. In our modelling, this structure is used as the reference, bedrock model. The wavefield computed for this bedrock model is used as incident wavefield for the explicit finite difference schemes, which are used to simulate the propagation of seismic waves in the two-dimensional, anelastic model of the sedimentary basin. This hybrid method allows us to take into account the source and propagation effects, including local soil conditions, even when dealing with path lengths of a few hundred kilometers.

In the following, we illustrate a comparison between numerical simulations, and observed strong ground motion or the space distribution of the available macroseismic data. We will focus on the different effects of the source, the path and the local soil conditions. Special emphasis is given to understanding the different features of ground motion in sedimentary basins, and the application of numerical simulations for seismic zonation. The three applications include sites close to the source (a sedimentary basin near to the epicenter of the September 11, 1976, Friuli aftershock at 16 h 35 min 4 s), at an intermediate distance (Rome, about 80 km from the epicenter of the January 13, 1915, Fucino earthquake), and sites that are far from the source (Mexico City, about 400 km from the epicenter of the September 19, 1985, Michoacan earthquake).

2. The sedimentary basins in the Friuli area

The September 11, 1976 Friuli aftershock (16 h 35 min 4 s) was recorded by a few accelerographic stations (CNEN-ENEL, 1977). Records from one of the nearest stations – the three-component records at Buia station (fig. 1) – are considered and compared with the theoretical computations. We focus on the variability of ground motion within the sedimentary basin, and on the sensitivity of the computed ground motion to small changes in the subsurface topography of the sedimentary basin, and in the velocity and quality factor of the sediments. The interpretation of the observed data will here be given in terms of the near-surface geological model by keeping the source and long-distant propagation path unchanged for all numerical simulations.

The bedrock model, describing the average mechanical properties of the path from the epicenter to the sedimentary basin, has been proposed by Fäh *et al.* (1993a), and its uppermost layers are shown in fig. 2. The source-depth used in the numerical modelling is 7.1 km, the angle between the strike of the fault and the epicenter-station line 19°, the dip 28°, the rake 115°, and the source duration is 0.6 s (Florsch *et al.*, 1991).

The area where the station of Buia is located is characterized by terrigenous sediments (Flysch), widely outcropping at Monte Buia (fig. 1), which are covered locally by a thin quaternary layer, forming a sedimentary basin, and which overlap a carbonatic mesozoic sequence. The thickness of the quaternary sediments is well-known (Giorgetti and Stefanini, 1989) and locally can reach 100 m. The aver-

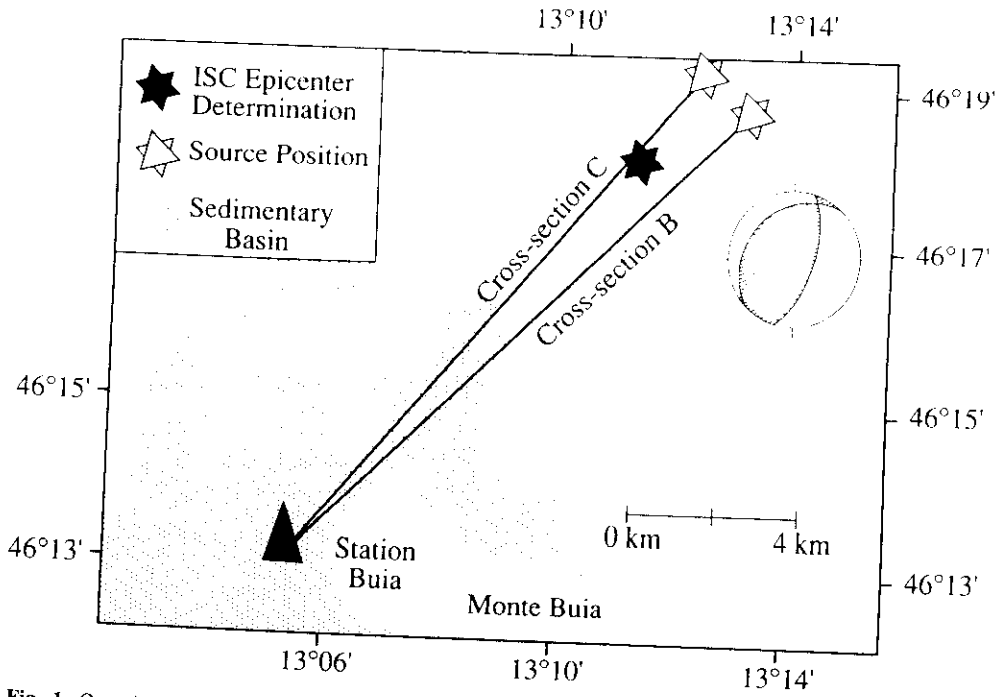

Fig. 1. Overview of the Friuli seismic region, showing the presence of the quaternary basin, the ISC epicenter determination of the September 11, Friuli 1976 aftershock (16 h 35 min 4 s), and the position of Buia station. The solid lines indicate the position of the two cross-sections for which 2D modelling has been performed.

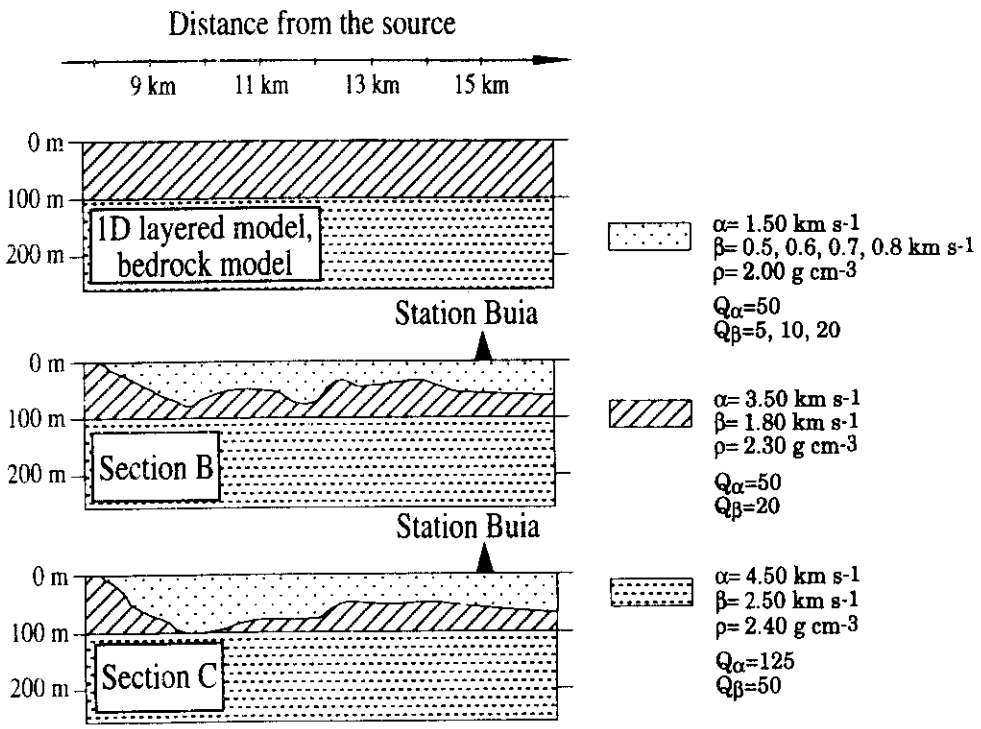

Fig. 2. Surficial layers of the one-dimensional model, describing the propagation of waves from the source position to the sedimentary basin (Fäh *et al.*, 1993a), and of the 2D models corresponding to cross-sections B and C in fig. 1. Only the part near to the surface is shown, where the 2D models are different from the bedrock model.

age model for the sedimentary basin is represented by the cross-section B, while the part of the basin with a thick sedimentary cover is well represented by the cross-section C, both shown in fig. 2.

The accelerograms obtained in correspondence with the cross-section B, with the shear-wave velocity of the unconsolidated sediments equal to 0.6 km/s and the quality factor Q_β equal to 20, are shown in fig. 3. At sites with a thick layer of low-velocity material near the surface, the peak acceleration of the radial component is up to two times larger than the vertical component, while, due to the source radiation pattern, the transverse component is the same size as the radial component.

The heterogeneity, with size comparable to the wavelength of the incident wavefield, causes significant spatial variations in the ground motion (fig. 3). There are three major effects which are caused by the presence of the sedimentary cover: 1) the excitation of surface waves at the edge of the sedimentary basin; 2) the resonance in parts of the basin due to the subsurface topography of the bedrock, and 3) the excitation of very dispersed local surface

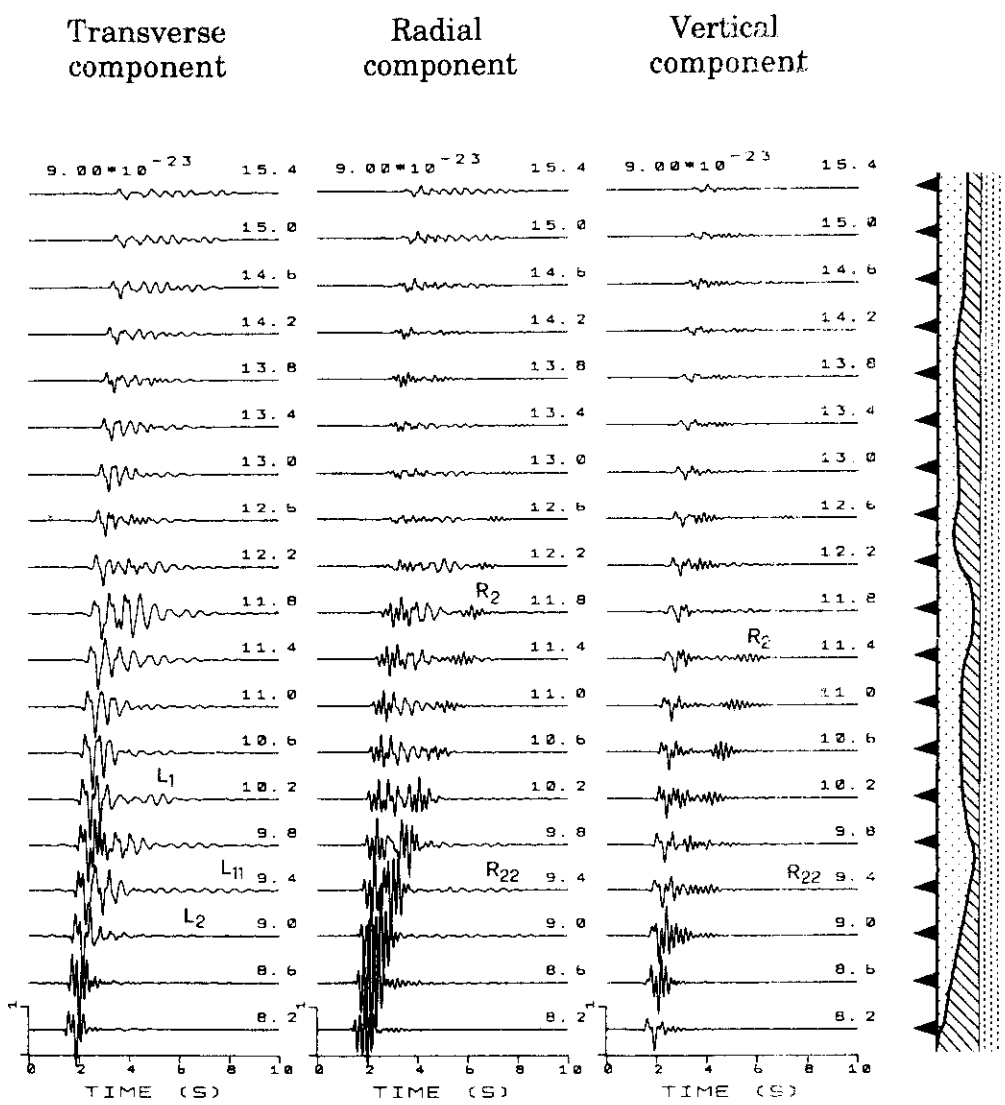

Fig. 3. Acceleration time series for *SH* and *P-SV* waves at an array of receivers, for cross-section B shown in fig. 2 ($\beta = 0.6$ km/s and $Q_\beta = 20$ for the unconsolidated sediments). All amplitudes are related to a source with a seismic moment of 10^{-7} N m. The signals are normalized to the peak acceleration given in units of cm s^{-2}. The distance to the source for each seismogram is given in units of km. The time scale is shifted by 2 s from the origin time (0 s in the figure is really 2 s from the origin time).

20

waves, with peak energy at about 2 Hz, within the sedimentary basin for epicentral distances larger than 14 km.

Multiple reflections of *SH*-waves can generate local surface waves (phase L_1) – forming the coda of the signals (fig. 3) – which are excited as soon as the fundamental Haskell's frequency of resonance (Haskell, 1960, 1962) for the sedimentary basin is reached. These local surface waves can be reflected inside the basin at places where the sediments become thin. One example is given by the phase L_{11} in fig. 3, which corresponds to the reflected local surface wave L_1. Also for *P-SV*-waves, a dipping layer at the edge of a sedimentary basin gives rise to multiple reflections of body waves and the excitation of local surface waves (phase R_2 in fig. 3), which are characterized by larger amplitudes on the radial than on the vertical component of motion, and can be the dominant part of the wavefield at the edge of the sedimentary basin. The reflections of the local Rayleigh waves inside the sedimentary basin (R_{22} in fig. 3) do not appear as clear as in the case of Love waves, since their amplitudes are small in comparison with the amplitudes of the primary waves.

Resonance occurs in those parts of the basins with smooth variations of the interface between the bedrock and the sediments, and originates from the superposition of forward propagating local surface waves with their reflections, within sub-basins of the sedimentary cover. Examples are seen for the two sub-basins in cross-section B, especially at 9.8 km and at 11.8 km from the source (fig. 3). The resonance is stronger for *SH*- than for *P-SV*-waves, and in general can give rise to very large duration and amplitude, as can be seen from the signal computed at 11.8 km from the source. The excitation of strongly dispersed local surface waves by subsurface lateral heterogeneities can be observed in correspondence with the cross-section B at epicentral distances larger than 14 km, both for *SH*- and *P-SV*-waves.

The synthetic accelerograms, obtained from the numerical modelling, can be used to compute some ground motion related quantities. These quantities are: 1) the peak ground acceleration PGA and 2) the quantity W defined as:

$$W = \lim_{t \to \infty} \int_0^t [x(t)(\tau)]^2 d\tau$$

where $x(t)$ is the time series describing the ground displacement. The Arias Intensity is proportional to the quantity W by a factor $\pi/(2g)$, where g is the acceleration of gravity. To discuss the site effects with respect to the bedrock model it is convenient to consider the quantities PGA(2D), and W(2D), *i.e.* PGA and W obtained from the accelerograms computed for the two-dimensional model, and PGA(bedrock) and W(bedrock), *i.e.* PGA and W obtained from the accelerograms computed for the model representing the average properties of the source-basin path. The ground motion computed for the different sites in the two-dimensional model is normalized with respect to the ground motion obtained for the same source-receiver distance considering the bedrock model.

The spatial distribution of the values of the relative PGA (PGA(2D)/PGA(bedrock)) and relative Arias Intensity (W(2D)/W(bedrock)) for the transverse component of motion, and for different shear-wave velocities and quality factors of the unconsolidated sediments are shown in fig. 4. The relative PGA increases only slightly when the shear-wave velocity of the sediments is reduced, whereas the relative Arias Intensity is very sensitive to small changes in the shear-wave velocity of the sediments. A low shear-wave velocity induces the largest amplitudes and dispersion of the local surface waves. These effects give the dominant contribution to the relative Arias Intensity at sites where resonance effects and excitation of local surface waves are important (for example at 11.8 km from the source). The relative PGA and relative Arias Intensity have been computed for three different quality factors Q_β of the sediments, by keeping the shear-wave velocity fixed at 0.6 km/s (right part of fig. 4). The attenuation of waves increases with decreasing quality factor. This causes the reduction of the duration of the signals at sites

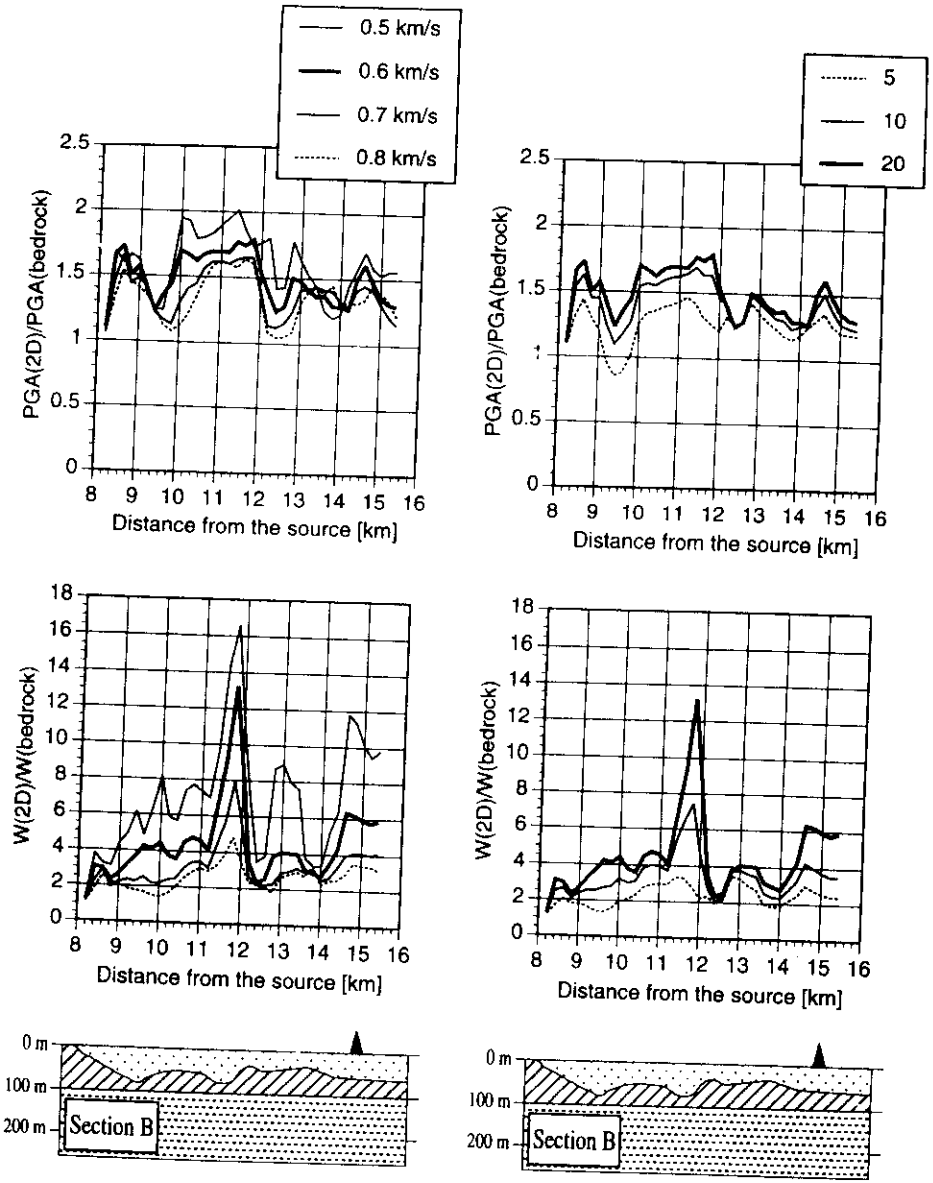

Fig. 4. Relative peak ground acceleration PGA(2D)/PGA (bedrock) and relative Arias Intensity W(2D)/W (bedrock) obtained for cross-section B. The values are shown for four different shear-wave velocities (0.5 km/s, 0.6 km/s, 0.7 km/s and 0.8 km/s), and for three different quality factors ($Q_\beta = 5$, $Q_\beta = 10$, and $Q_\beta = 20$) of the unconsolidated sediments.

where resonance effects and excitation of local surface waves are important phenomena. The smaller the quality factor of the unconsolidated sediments, the shorter is the duration of the resonance, and the smaller the propagation distance of the local surface waves. Consequently, low quality factors strongly reduce the relative Arias Intensity.

In fig. 5a-c, we compare the synthetic signals computed for the two cross-sections B and C, shown in fig. 1, with the accelerograms recorded at Buia station. In correspondence with the recording station, which is at 15 km from the source, the thickness of the sedimentary cover is the same in the two cross-sections.

For the transverse component of motion, the local surface waves have amplitudes that are too large in comparison with the observation. In the choice of the geometry of the bedrock-sediment interface, we have restricted ourselves to that given by Giorgetti and Stefanini (1989). However, to reproduce the observed transverse component, the heterogeneity inside the sedimentary basins, responsible for the excitation of these local surface waves, would have to be different. The considered heterogeneity is either too close to Buia station or the bedrock-sediment interfaces are too close to the free surface. In the radial component the excitation of local surface waves is not very clear. When dealing with *P-SV*-waves, there are two sources of local surface waves: the edge of the sedimentary basin and the places where the bedrock-sediment interface approaches the free surface. From the signals computed for the two cross-sections, it can be concluded that the closer the sediment-bedrock interface is to the free surface, the greater are the amplitudes of the local Rayleigh waves. On the other hand, this lateral heterogeneity can cause the reflection of most of the local Rayleigh waves, generated at the sedimentary basins edge which is closer to the seismic source.

The comparison of the synthetic signals with the observed radial component shows good agreement between the observation and

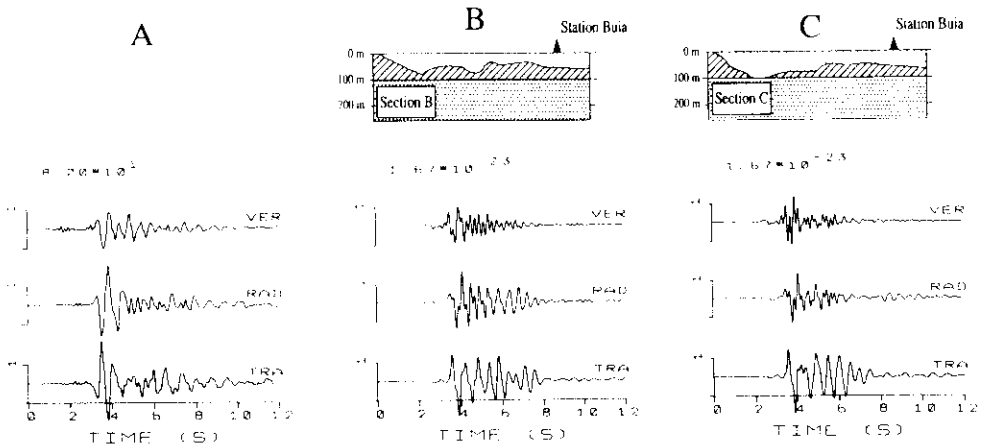

Fig. 5a-c. Comparison between (A) the recorded transverse, radial and vertical components of acceleration, and synthetic signals, computed for (B) the cross-section B and (C) the cross-section C. The time-scale is shifted by 2 s from the origin time. The recorded seismograms are aligned to agree with the synthetic signals. All amplitudes of the synthetic signals correspond to a source with a seismic moment of 10^{-7} N m. The synthetic signals are normalized to the same peak acceleration which is given in units of cm s^{-2}.

the signal obtained for cross-section C. Due to the small amplitudes of the coda in the observation, it can be concluded that the local surface waves have travelled through the deeper parts of the sedimentary basin, and that the lateral heterogeneity within the basin has reflected a relevant part of the local surface waves, which is excited at the edge of the basin. To reproduce the observed signal, the lateral heterogeneity within the basin cannot be strong; a strong heterogeneity, in fact, would excite large-amplitude local surface waves inside the basin, and these are not observed experimentally.

The vertical component of the observed ground motion, especially at low-frequency (below 4 Hz), is quite similar to the synthetic signals, which do not change significantly from one cross-section to the other. The relatively small sensitivity of the vertical component of motion to the lateral variation of sedimentary basins has been observed also at different sites in Mexico City, and the results illustrated in this paper suggest considering this fact a quite general property of sedimentary basins. The high-frequency component, not observed experimentally, but present in the synthetic signals for models B and C, is due to the resonance effects in the shallow part of the sedimentary cover. This difference between the computed and the observed signals indicates once again that, in the modelling, either the shallow parts of the sedimentary cover are too close to the observation point, or the bedrock-sediment interfaces are too close to the free surface.

3. The Rome area and the 1915 Fucino earthquake

The area of Rome, considered here, is characterized by several sedimentary basins of considerable thickness, which, in some parts, are covered by volcanic rocks. The area is very vulnerable to earthquakes, as indicated, for example, by the well documented damage distribution caused by the January 13, 1915, Fucino (Italy) earthquake ($M_L = 6.8$) (fig. 6). Since no strong motion records are available for this event, we have applied the hybrid technique to explain the observed damage distribution (Fäh *et al.*, 1993b). The source parameters, the bedrock model, describing the path from the source to Rome, and the two-dimensional model for the area of Rome are described in Fäh *et al.* (1993b).

To demonstrate that not only the local soil conditions are important to explain a local distribution of damage, but that there are also important regional effects due to the source location, we compare the results of two sets of computations, made by changing only the distance of the seismic source from the city of Rome (fig. 7). The epicenter of the Fucino event is about 85 km east of Rome, and the other hypothetical source, source 2 in fig. 7, is located at a distance of about 65 km, in the same direction.

The synthetic accelerograms are used to compute the quantity $W(2D)$, and the relative Arias Intensity, $W(2D)/W$ (bedrock), of ground motion. The results for the transverse component of motion, corresponding to the two source positions are shown in fig. 8a,b. They are compared with the histogram of the damage distribution, which has been constructed by projecting each observation of damage, shown in fig. 6, on the cross-section used in the numerical modelling (Fäh *et al.*, 1993b). Only those points of the distribution have been used which are located in an area where the geometry of the structure does not differ too much from the geometry of the two-dimensional cross section. This area is delimited in fig. 6 by the two dotted lines. Since neither the type of buildings nor the density of the urbanization can be known in great detail, the histogram shown in fig. 8a,b should be interpreted only in a qualitative manner.

The quantity W, and the relative Arias Intensity, computed for the numerical simulation of the Fucino event are quite well correlated with the damage distribution, as is shown in fig. 8a,b (Fäh *et al.*, 1993b). There are four relative peaks: two at the edges of the Tiber basin, one within the alluvial valley of the Aniene river, and a broad peak where the Sicilian low-velocity zone gets close to the surface. The largest values are observed at the margins

22

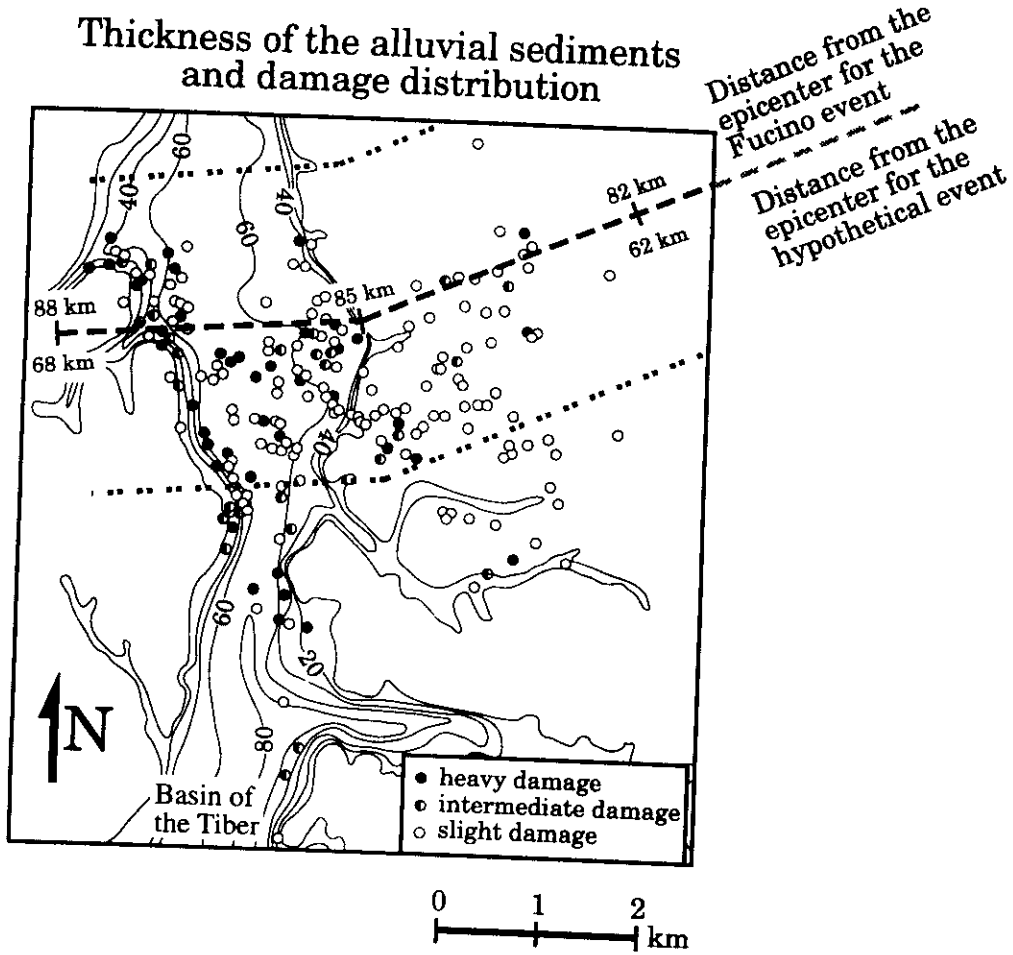

Fig. 6. Damage distribution in Rome caused by the January 13, 1915 Fucino earthquake (after Ambrosini *et al.*, 1986), and thickness of the alluvial sediments (given in meters) (Ventriglia, 1971; Funiciello *et al.*, 1987; Feroci *et al.*, 1990). Three types of damage are distinguished: slight damage (cracking of plaster, the downfall of small pieces of mouldings), intermediate damage (between slight and heavy damage), and heavy damage (deep and diffuse damage of indoor and outdoor walls, downfall of large parts of mouldings and of chimneys). The dashed line indicates the position of the cross section, for which numerical modelling has been performed. The distribution of damage within the area limited by the two dotted lines has been projected on the cross section to construct the histograms, shown in fig. 8a,b.

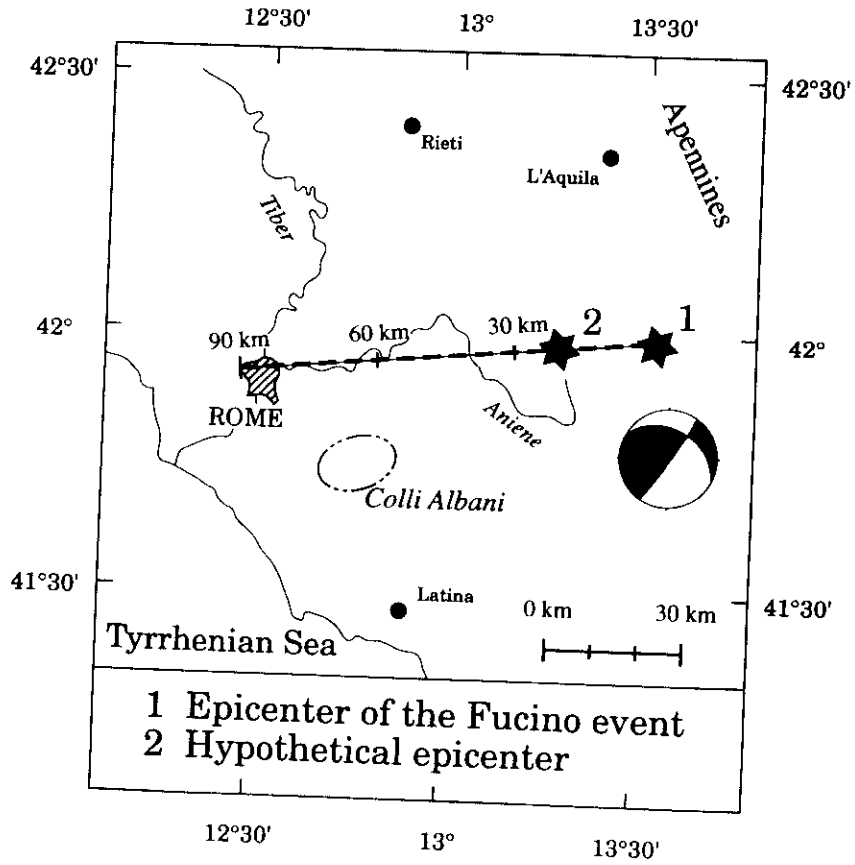

Fig. 7. Approximate epicenter location of the January 13, 1915 earthquake in the Fucino valley (1), and of a hypothetical event (2) located at about 65 km from Rome. The dashed line indicates the cross section along which the numerical modelling has been performed. The source depth is 8 km, the angle between the strike of the fault and the epicenter-station line is 38°, the fault dip 39°, and the rake with respect to the strike 172°. The seismic moment is 10^{19} N m (Fäh *et al.* 1993b).

of the Tiber bed. There the signals have the largest amplitudes and duration, due to the low impedance of the alluvial sediments, the excitation of local surface waves, and resonance effects. Minimum values can be observed for sites placed above the volcanic layer overlying the Paleotiber basin, which acts as a shield, and reflects part of the incoming energy: the thicker the volcanic layer, the smaller are the W values observed at the surface. As is shown in Fäh *et al.*, (1993b), similar conclusions can be drawn for the radial and the transverse components of acceleration, with the difference that the amplitudes of the transverse component are about half the size of those of the radial component. This is due to the *SH* and *P-SV* radiation patterns of the source.

The results of our modelling, obtained considering source 2, are quite different if compared with the modelling of the Fucino event.

23

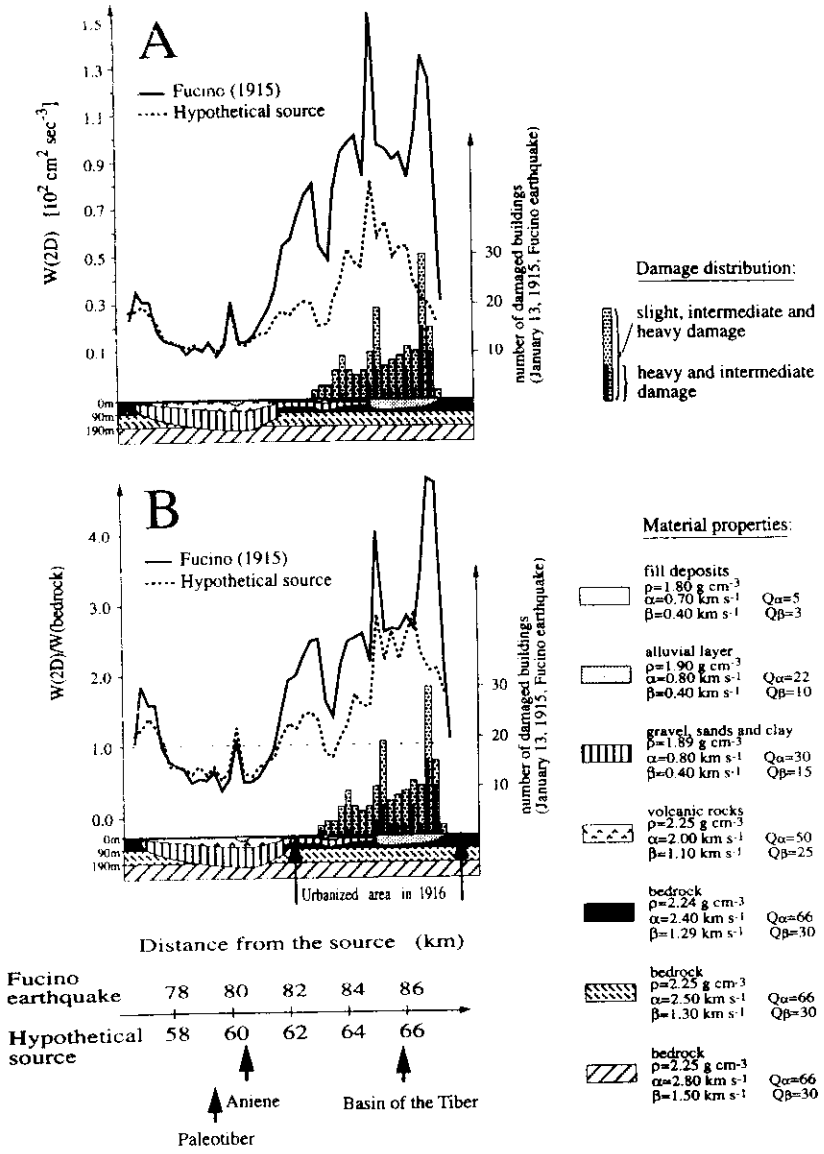

Fig. 8a,b. (A) Quantity $W(2D)$ obtained for the two-dimensional model and the two source positions given in fig. 7, and (B) corresponding relative Arias Intensity $W(2D)/W(\text{bedrock})$. The results are compared with the histogram of the damage distribution caused by the January 13, 1915 Fucino earthquake. The part of the structure near to the surface, where the 2D model deviates from the bedrock model, is given at the bottom of both parts of the figure.

The quantity W and the relative Arias Intensity are similar in the area of the Paleotiber basin, whereas in the other areas the values obtained considering source 2 are considerably smaller, and the two peaks at the margin of the Tiber basin are significantly reduced. A comparison of W, determined from the two numerical experiments, shows that the total energy associated with the Fucino event is significantly larger than the one carried by source 2, even if the former event is 20 km farther from Rome than the latter.

These differences can be explained by the attenuation of PGA and W with distance. The example concerning the transverse component of motion, computed for the bedrock model, is shown in fig. 9a,b. The PGA and W are not monotonically decreasing with distance. This behavior is due to the fact that for epicentral distances less than 50 km, the PGA and W are essentially controlled by the crustal Sg phase, while at greater distances they are increasing owing to the contribution of several S-wave phases reflected mostly at the Moho (Suhadolc and Chiaruttini, 1985), which gradually become a part of the Lg waves and further increase PGA and W.

At distances of the order of 80 km (average distance of the Paleotiber from the Fucino event) and 60 km (average distance of the Paleotiber from the hypothetical source), the W values in our modelling are about the same. This explains the similar values of W in the area of the Paleotiber (fig. 8a,b) computed considering the two events. Similarly, it is possible to explain the values of W observed at distances in the range 61 km-67 km from source 2 (fig. 8a,b), which are smaller than the ones corresponding to the Fucino event in the epicentral distance range 81 km-87 km. Finally from fig. 9a,b, it is evident that, when dealing with earthquakes occurring in the Apennines, for epicentral distances between 50 and 100 km, the largest damage, for a given seismic moment tensor, can be expected from an event as far as 90 km from Rome.

The Fourier-spectrum of the signal computed at 85 km from the source, corresponding to the epicentral distance of the margin of the Tiber basin from the Fucino event, is quite

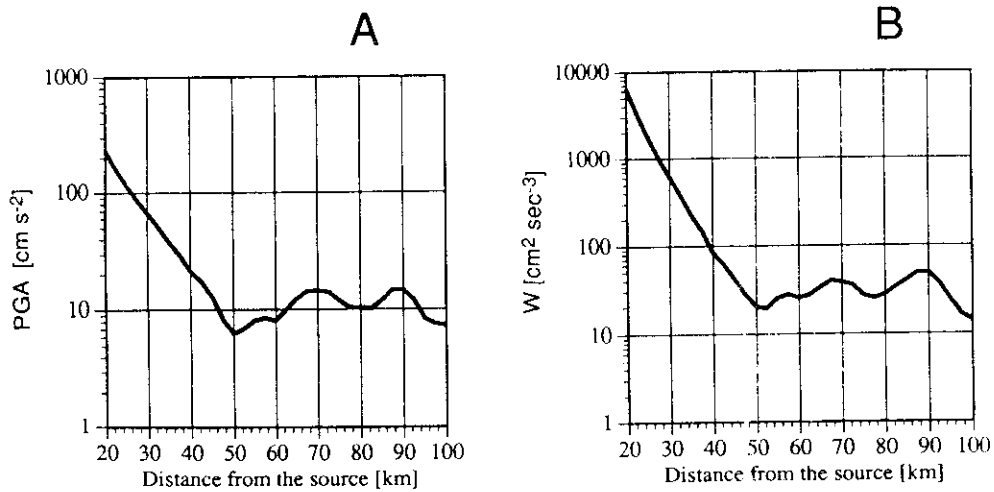

Fig. 9a,b. (A) Attenuation of PGA(bedrock), and (B) attenuation of W(bedrock) with distance from the seismic source for the one-dimensional layered model (bedrock model).

24

large for frequencies below 2.5 Hz if compared with the spectrum of the signal obtained at 65 km from the source, which corresponds to the epicentral distance of the margin of the Tiber from source 2 (fig. 10). As we will see later, for frequencies below 2.5 Hz strong amplifications occur at the margins of the Tiber basin. Since the incident wavefield computed for source 2 contains relatively small energy at frequencies below 2.5 Hz, resonance effects and excitation of local surface waves are not the dominant phenomena, and this justifies the absence of the peak in W at the margin of the Tiber basin computed for source 2. Thus, for epicentral distances in the range 50 km-100 km, the source location and not only the local soil conditions control the local site effects.

All the quantities used to measure strong ground motion like the maximum amplitude, the duration and the Fourier spectrum provide only a very limited description of the ground motion and certainly do not quantify its damage producing potential. A better quantity is the spectral acceleration Sa of the earthquake ground motion. A representation of the local soil effects is given by the spectral amplification $Sa(2D)/Sa(\text{bedrock})$ computed from the spectral accelerations obtained for the two-dimensional and the bedrock models. This procedure allows us to identify the frequency bands and sites at which amplification and attenuation effects occur. For SH-waves, the spectral amplification for zero damping are shown in fig. 11a,b for the two simulated events, as a function of frequency and of the spatial location along the section. The darker an area is, the stronger the amplifications due to the two-dimensional effects. The greatest amplification is observed for the numerical simulation of the Fucino event at the western edge of the sedimentary basin of the Tiber river (about 87 km from the source), for frequencies around 2 Hz. The maximum amplification is of the order of 5-6, and it is due to the combination of resonance effects and the excitation of local surface waves. This amplification effect is responsible for the relative peak in the quantity W at the margin of the Tiber basin (fig. 8a,b).

The global distribution of the shaded areas can be related to the geometry of the structural model. The results are similar for the Fucino event and for source 2, except at the margins of the Tiber basin. An amplification over almost the entire frequency band is observed outside the Paleotiber basin (82-87 km from the source for the Fucino event, 62-67 km from source 2). Some amplification occurs in the Aniene basin, for frequencies above 2 Hz. For frequencies above 0.8 Hz, in the Paleotiber basin, the volcanic layer acts as a shield reflecting part of the incoming energy, and the values of the spectral amplification are smaller than 1. The underlying sedimentary complex (Sicilian) causes spectral amplification of the order of 2-3, due to resonances, which are most pronounced at frequencies around 0.4 Hz, where the fundamental resonance of this low-velocity zone is excited. In this part of the Paleotiber, in the frequency band 1.5-2.0 Hz,

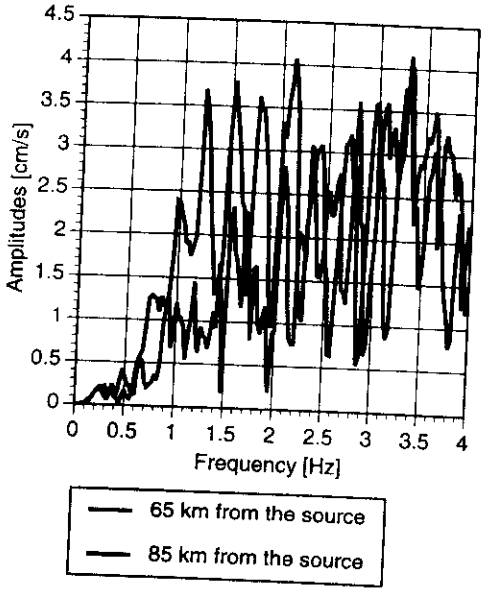

Fig. 10. Fourier-spectra of the signals obtained at 65 km and 85 km from the source for the one-dimensional layered model. The distances correspond to the distance of the eastern margin of the Tiber basin from source 2 and from the Fucino earthquake.

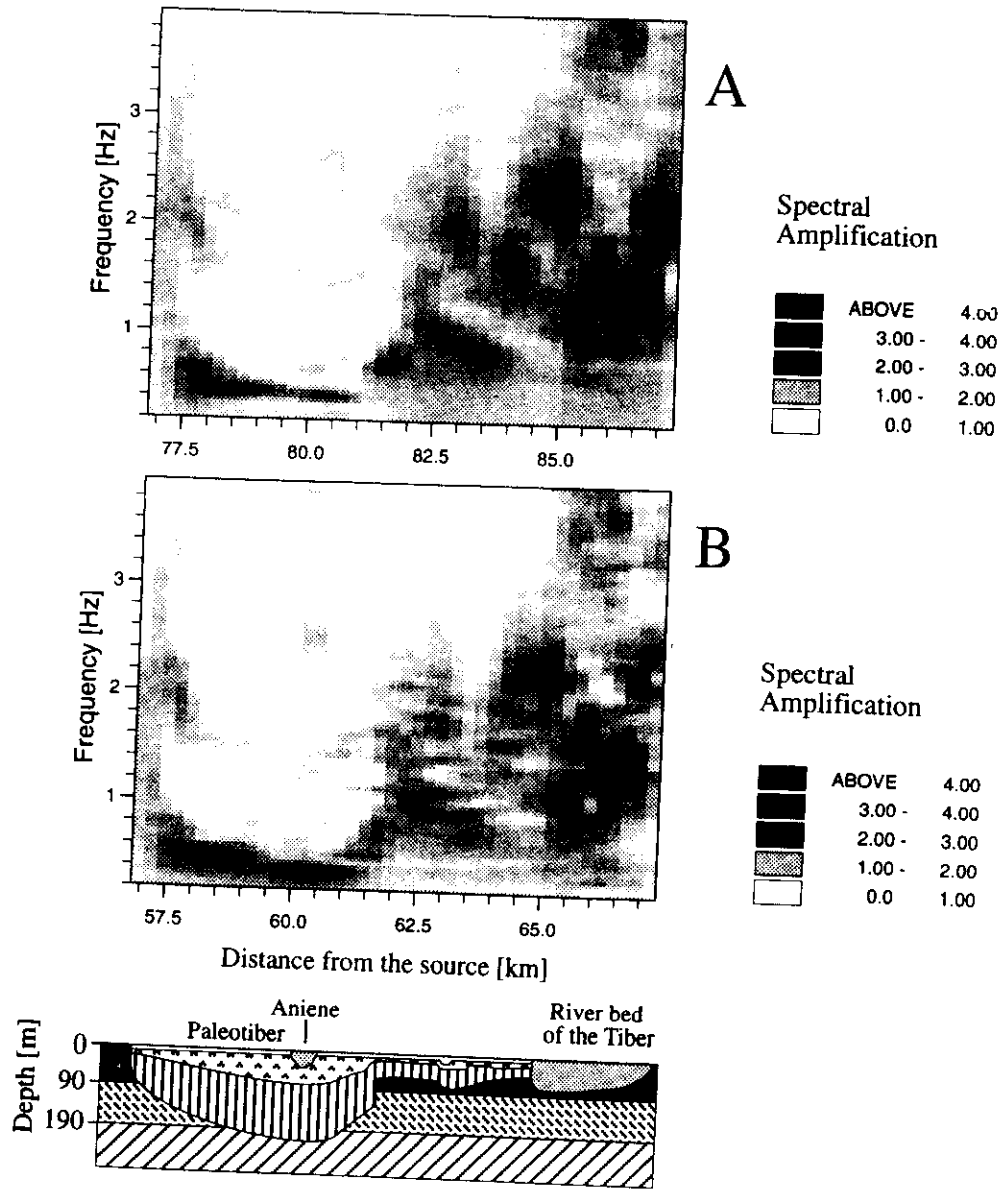

Fig. 11a,b. Spectral amplification for the transverse component of motion over the entire cross section, (A) for the Fucino event and (B) for the hypothetical earthquake. The reference signals are the one obtained for the one-dimensional layered model. At the bottom of the figure, the geometry of the two-dimensional cross-section is given, while its mechanical parameters are given in fig. 8a,b.

there is also evidence for the excitation of some higher modes of resonance. At distances of the order of 82-83 km from the Fucino event, and 62-63 km from source 2, between the Paleotiber and the Tiber basins, where the wave guide and overlying volcanic cover are thinning, focusing of seismic energy occurs and most of the trapped energy reaches the surface. This leads to amplifications, of the order of 2, over almost the entire frequency band considered. Therefore, the presence of a near-surface layer of rigid material is not sufficient to classify a site as a «hard-rock site». Reliable determinations of local soil effects, in addition to the knowledge of the frequency content and direction of the incoming signal, require the knowledge of both the thickness of the surficial layer and of the deeper parts of the structure, down to the real bedrock. This is especially important in volcanic areas, where pyroclastic material often covers alluvial basins.

4. Mexico City

Mexico City is an area of particular interest since extensive damage occurred in the lake-bed zone during the Michoacan earthquake of September 19, 1985. This can be attributed to the geotechnical and geometrical characteristics of the unconsolidated sediments in this zone. From the geotechnical point of view, the valley of Mexico City can be divided into the hill zone, the transition zone, and the lake-bed zone (fig. 12). The hill zone is formed by alluvial and glacial deposits, and by lava flows. The transition zone is mainly composed of sandy and silty layers of alluvial origin. The surficial layers in the lake-bed zone consist mainly of clays. These deposits are poorly consolidated, with a high water content and very low rigidity. The thickness of this surficial layer varies between 10 m and 70 m, and increases regularly towards the east (Suarez *et al.*, 1987). The clay layer is overlying the so-called «deep sediments» found below 10-70 m. These deeper deposits reach depths of the order of 700 m, with an uncertainty which may be as large as a few hundred meters (*e.g.* Bard *et al.*, 1988). There are three outcrops of the basement: at Chapultepec, Peñon, and Cerro de la Estrella (fig. 12). In the last years, a strong motion network has been operating in the valley of Mexico City (*e.g.* Mena *et al.*, 1986; Espinosa *et al.*, 1990), and the positions of the stations used in this study are shown in fig. 12.

Today's research, to understand the extensive damage caused by the 1985 earthquake and the recorded ground motion in Mexico City, has shown the importance of considering source and propagation effects, including local soil conditions. This is dealt with explicitly in the recent work by Fäh *et al.* (1994) in which the hybrid technique has been applied to study the ground motion in Mexico City. The model used by Fäh *et al.* (1994) explains the observed difference in amplitudes for receivers located inside and outside the lake bed zone. The ratio between the computed, horizontal peak ground displacements inside and outside the lake-bed zone reaches values ranging from 5 to 7, and about the same ratio is obtained for the observed ground motion. The validity of the modelling is further confirmed by the fact that the spectral ratios obtained for the horizontal components of the synthetic seismograms are very similar to comparable spectral ratios obtained from observations. For the 1985 Michoacan event, the energy contributions of the three subevents are important to explain the observed durations in the lake-bed zone (Fäh *et al.*, 1994).

The structural model used in the numerical simulations for the 1985 Michoacan event, and a detailed parametric study of the effects of different soil properties in Mexico City is given in Fäh *et al.* (1994). The flat-layered structure in table I describes the path from the seismic source to the valley of Mexico City (Campillo *et al.*, 1989), and was deduced directly from refraction measurements in the Oaxaca, Southern Mexico region (Valdes *et. al.*, 1986). The depth of the Moho is about 45 km, and the upper five kilometers are composed of low-velocity material. The two-dimensional structure for the Mexico City valley, modelling the Chapultepec-Peñon cross-section (solid line in fig. 12), is shown in fig. 13. The structure is rather simple, in agreement with the resolving power of the available data.

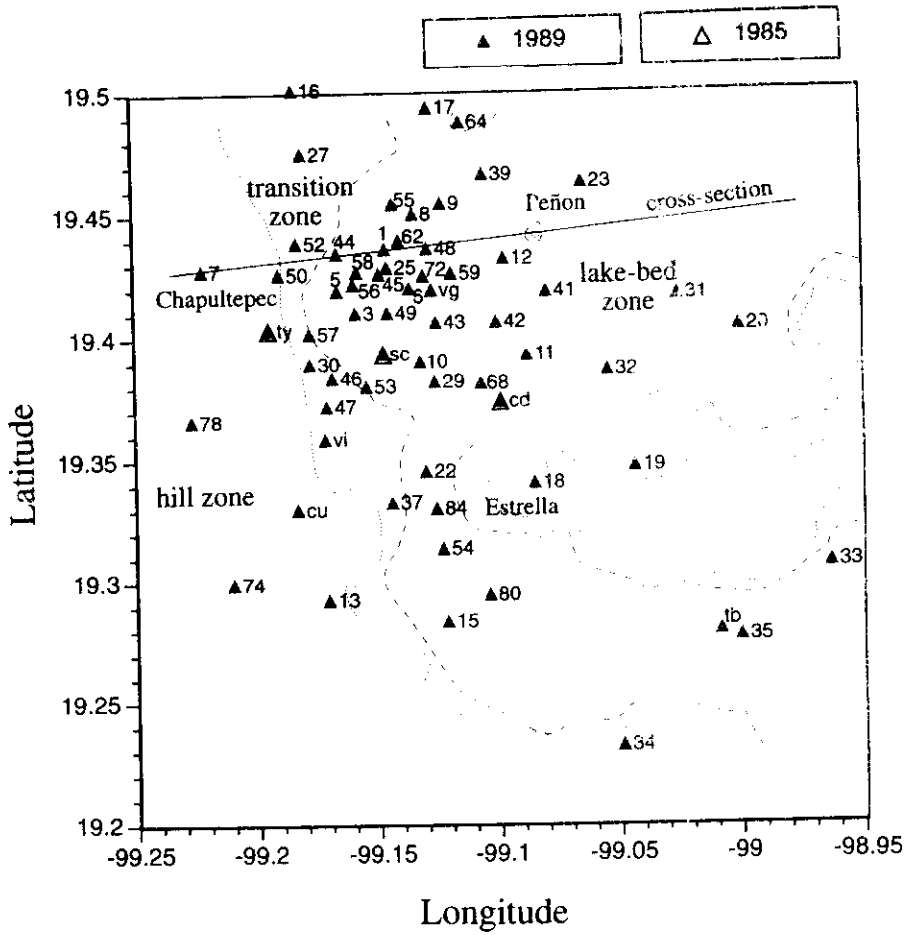

Fig. 12. Map of the area of Mexico City showing the locations of strong motion accelerometric stations. The stations represented by large triangles were operating during the 1985 Michoacan event, while the small gray triangles represent the stations which recorded the April 25, 1989 event. The solid line indicates the position of the cross-section, for which the 2D modelling was performed.

As in Fäh *et al.* (1994), to keep the source model as simple as possible and to avoid any, *a priori*, enhancement of resonance effects at the longer periods (above 2 s), we consider first a constant, frequency independent, seismic moment rate spectrum. The focal mechanism is the one proposed by Campillo *et al.* (1989), based on the results of Houston and Kanamori (1986) and Riedesel *et al.* (1986). The distance from the source to the valley of Mexico City is 400 km, the angle between the strike of the fault and the epicenter station line is 220°, the source depth is 10 km, the dip 15°, and the rake is 76°.

26

Table I. Numerical parameters for the schematic crustal model describing the path from the source in the Michoacan subduction zone, to Mexico City (Campillo *et al.*, 1989).

Layer	Thickness (km)	ρ (g/cm³)	α (km/s)	β (km/s)	Q_α	Q_β
1	5.0	2.67	4.30	2.53	800	500
2	10.0	2.77	5.70	3.30	800	500
3	15.0	3.09	6.80	4.03	800	500
4	15.0	3.09	7.00	4.10	800	500
5	∞	3.30	8.20	4.82	800	500

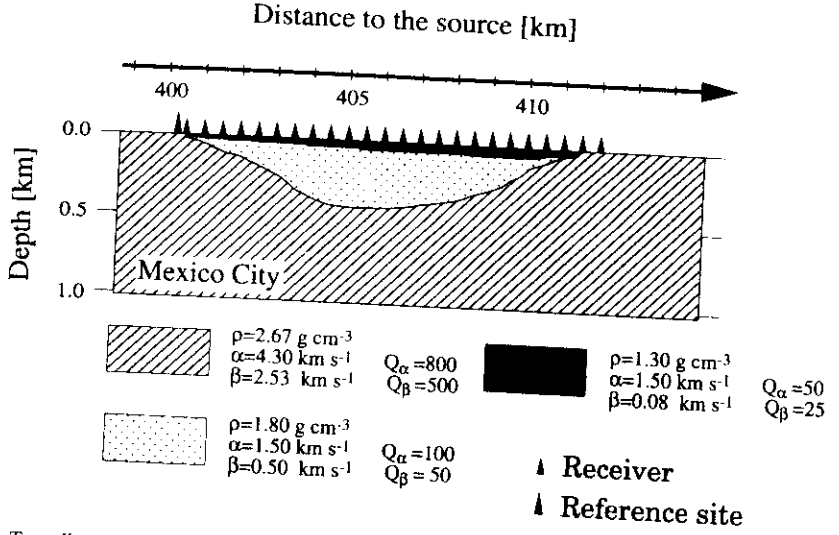

Fig. 13. Two-dimensional model of the Chapultepec-Peñon cross-section. Only the part of the structure near to the surface is shown, where the 2D model deviates from the bedrock model (table I).

The use of an instantaneous time-function gives rise to synthetic signals that contain too much energy at high frequency (above 0.6 Hz), and we can remove this drawback applying the ω^2 scaling law for the seismic moment rate spectrum, proposed by Kanamori *et al.* (1993) for the events occuring in the Mexican subduction zone:

$$\hat{M} = M_0\, \omega_c^2\, (\omega^2 + \omega_c^2)^{-1} \qquad (4.1)$$

where $\hat{M}$ is the seismic moment rate spectrum, M_0 is the seismic moment, and ω_c is the corner angular frequency. Following Kanamori *et al.* (1993), $\omega_c = 0.196\ s^{-1}$ and $M_0 = 0.5\ 10^{21}$ Nm. With these values we obtain a good reproduction of the shape of the observed signals at station CD (fig. 14a-c), especially for the radial and vertical component of motion (fig. 14b). The absolute observed accelerations are underestimated (fig. 14b). This discrepancy can be

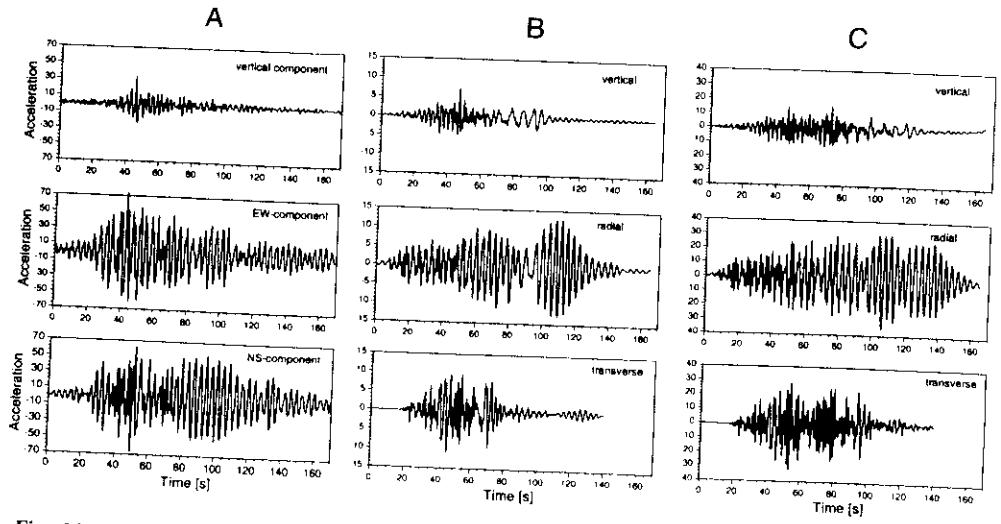

Fig. 14a-c. Comparison between (A) the recorded ground motion at station CD for the 1985 Michoacan earthquake with (B, C) synthetic signals, computed at the eastern edge of the basin, 409.5 km from the source (see fig. 13). All signals are low-pass filtered with a 5-pole butterworth filter having its corner frequency at 1 Hz. The accelerations are given in units of cm s^{-2}. A) Observed horizontal and vertical components of acceleration at station CD. Both horizontal components of motion are characterized by *SH*-waves as well as *P-SV* waves (see text); B) synthetic accelerations due to one point source. The synthetic signals are scaled assuming the seismic moment rate spectrum proposed by Kanamori *et al.* (1993); C) synthetic accelerations due to three point sources, all located at a depth of 10 km and the same distance. The three point sources have different weights and time shifts (1.0, 1.0, 0.2 and 0 s, 26 s, 47 s). The synthetic signals are scaled assuming the seismic moment rate spectrum proposed by Singh *et al.* (1990) for the 1985 Michoacan event.

reconciled considering the errors affecting the estimates of ω_c and M_0, and taking into account the subsequent rupture episodes of the Michoacan event, mainly the one occurring about 26 s after the origin time. If we assume a seismic source that is composed of three subevents, as proposed by Houston and Kanamori (1986), with the seismic moment rate spectrum proposed by Singh *et al.* (1990), the durations increase by about 45 s (fig. 14c) compared to those relative to a single event (fig. 14b). The computed radial component of motion (in fig. 14c) is very similar to the observed horizontal ground motion (fig. 14a). The underestimate in amplitude of the synthetic signals, and the remaining difference between synthetics and observations, is due to the simple source model in our modelling, the absence of dynamic irregularities in the rupture process, and the fact that only one cross-section of the sedimentary basin is considered.

Spectral amplification at the site of interest computed with respect to a reference site gives a good representation for micro-zoning purposes, especially from the engineering point of view (Fäh and Suhadolc, 1994). We compute the spectral amplification, *i.e.* the relative spectral velocities $Sv(2D)/Sv(Ref)$, for zero damping and 5% damping. $Sv(2D)$ is the spectral velocity obtained for the receivers in the two-dimensional structural model shown in fig. 13. $Sv(Ref)$ is the value obtained for the reference station shown in fig. 13. For all the receivers, we have computed the relative spectral velocities for one hundred frequencies of the oscillator in the range 0.1-1.0 Hz. From these values

27

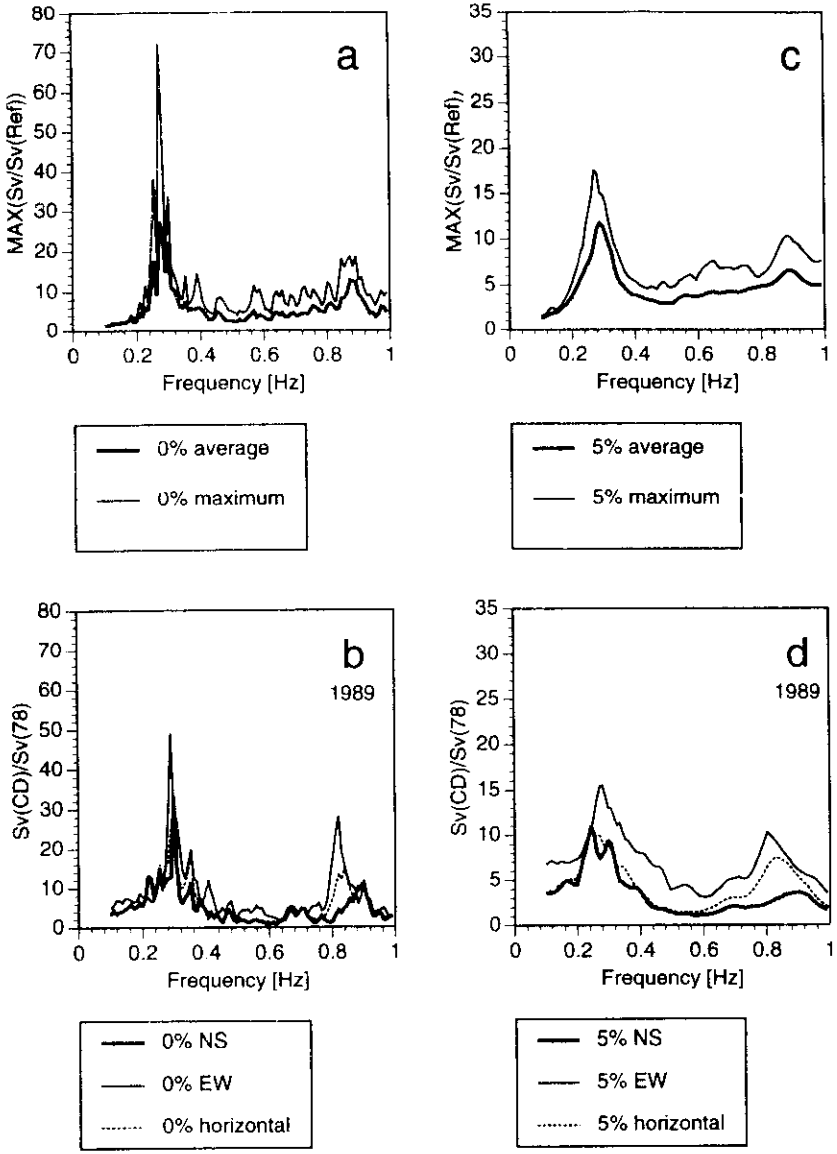

Fig. 18a-d. Average and maximum relative spectral velocities for zero damping (a), and 5% damping (c), computed with the synthetic signals obtained for the receivers at distances between 408.5 and 410 km from the source. They are compared with the observed relative spectral velocities $Sv(CD)/Sv(78)$ for the 1989 earthquake, for zero damping (b), and 5% damping (d), determined from the station CD using station 78 as reference.

ferent sites within the lake-bed zone, and therefore each peak in the MSA (fig. 17b) is obtained from a different receiver. The maximum values obtained theoretically and from the observations are about the same, and the greater complexity in the observed MSA for zero damping, with respect to the theoretical one, which has only two peaks around 0.27 Hz and 0.47 Hz (fig. 15a,b), is not surprising since our numerical model is restricted to one cross-section. In our model the maximum clay thickness is 65 m and, therefore, the MSA shown in fig. 15a-d is valid only for sites in the lake-bed zone that are characterized by a clay layer with a thickness not exceeding this value.

For 5% damping, the theoretical (fig. 15c,d) and the observed MSA (fig. 17d) are very similar, both in shape and in maximum values, and the two-dimensional model under study can be considered representative for the general geological situation in Mexico City. This is a valuable contribution for micro-zoning purposes, and it permits for each site, where the stratigraphy is reasonably well-known, a realistic estimate of the maximum and average spectral amplification with respect to a bedrock site. An example of the theoretical prediction, based on our results, appropriate for a site similar to the one of station CD (see fig. 12), is shown in fig. 18a,c: the theoretical MSA values are quite satisfactorily compared with the observations made at the station CD in connection with the 1989 event (fig. 18b,d).

5. Conclusions

The hybrid technique presented in this study makes it possible: 1) to study local effects even at large distances (hundreds of kilometers) from the source; 2) to include the seismic source, and 3) the propagation path. This technique can assist in the interpretation and prediction of ground motion at a given site. It can be applied in (micro-)zonation studies, and provides realistic estimates of spectral amplifications for detailed two-dimensional, anelastic models.

The synthetic signals explain the major characteristics (relative amplitudes, spectral amplification, frequency content) of the considered seismograms, and the space distribution of the available macroseismic data, even when quite simple source models are assumed. The theoretical computations show that waveforms and frequency content of seismograms are sensitive to small changes in the subsurface topography of the sedimentary basin, the velocity and quality factor of the sediments. The absence of dynamic irregularities in the rupture process in our simulations, in general, causes only an underestimate of the absolute accelerations.

To achieve a realistic simulation of seismic ground motion, it is necessary to include source, path and local soil effects, to study both *SH* and *P-SV* wave propagation, and to consider anelastic absorption. The reasons for the damage caused by the Michoacan earthquake and the Fucino event can be found not simply in the local site conditions, but also in the effects of the seismic source and of the long-distance propagation path in the crust. The dynamic irregularities of the rupture process and the properties of wave propagation in the crust control the frequency content of the incident wavefield; if a relevant amount of energy is present in the frequency band close to the resonance frequency of the unconsolidated sediments, local surface waves and resonance effects may dominate the horizontal components of motion within the sedimentary basin.

One aspect which is not included in our discussion is the influence of surface topography on ground motion. This approximation can be justified for sites inside sedimentary basins, where topographic features are in general small. However, topography can become important at the edges of sedimentary basins and near outcrops, especially in mountainous regions (Fäh and Suhadolc, 1994).

Acknowledgements

We would like to thank Prof. Peter Suhadolc and Dr. Claudio Iodice for their contribution to this research, ENEA for allowing us the use of the IBM3090E computer at the ENEA INFO BO Computer Center, and the Instituto de Ingeniería of the University UNAM.

30

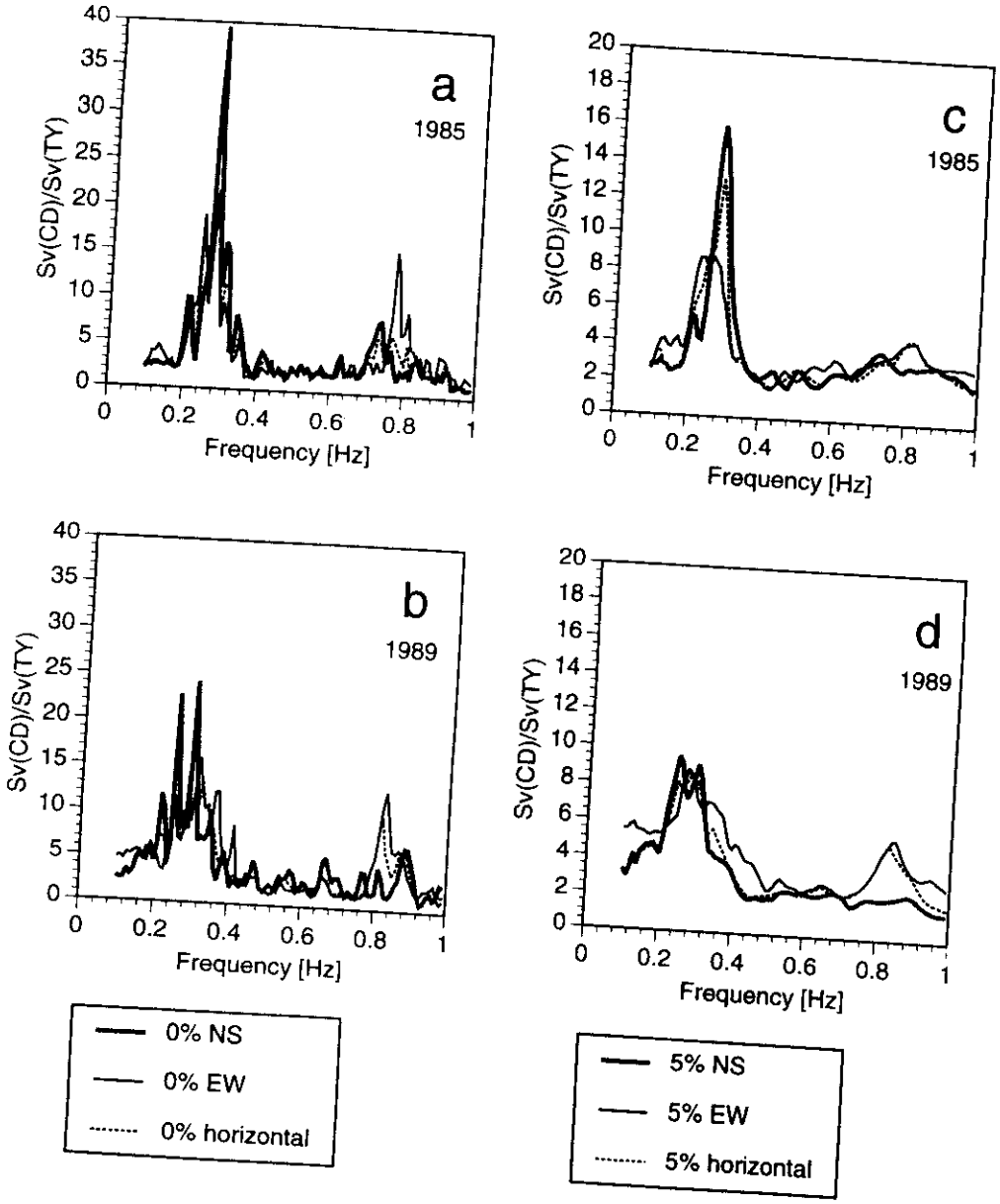

Fig. 16a-d. Relative spectral velocities Sv(CD)/Sv(TY), for zero damping (a,b) and 5% damping (c,d). They are determined from the stations CD using TY as reference. Results are shown for the 1985 Michoacan earthquake (a,c) and the April 25, 1989 event (b,d).

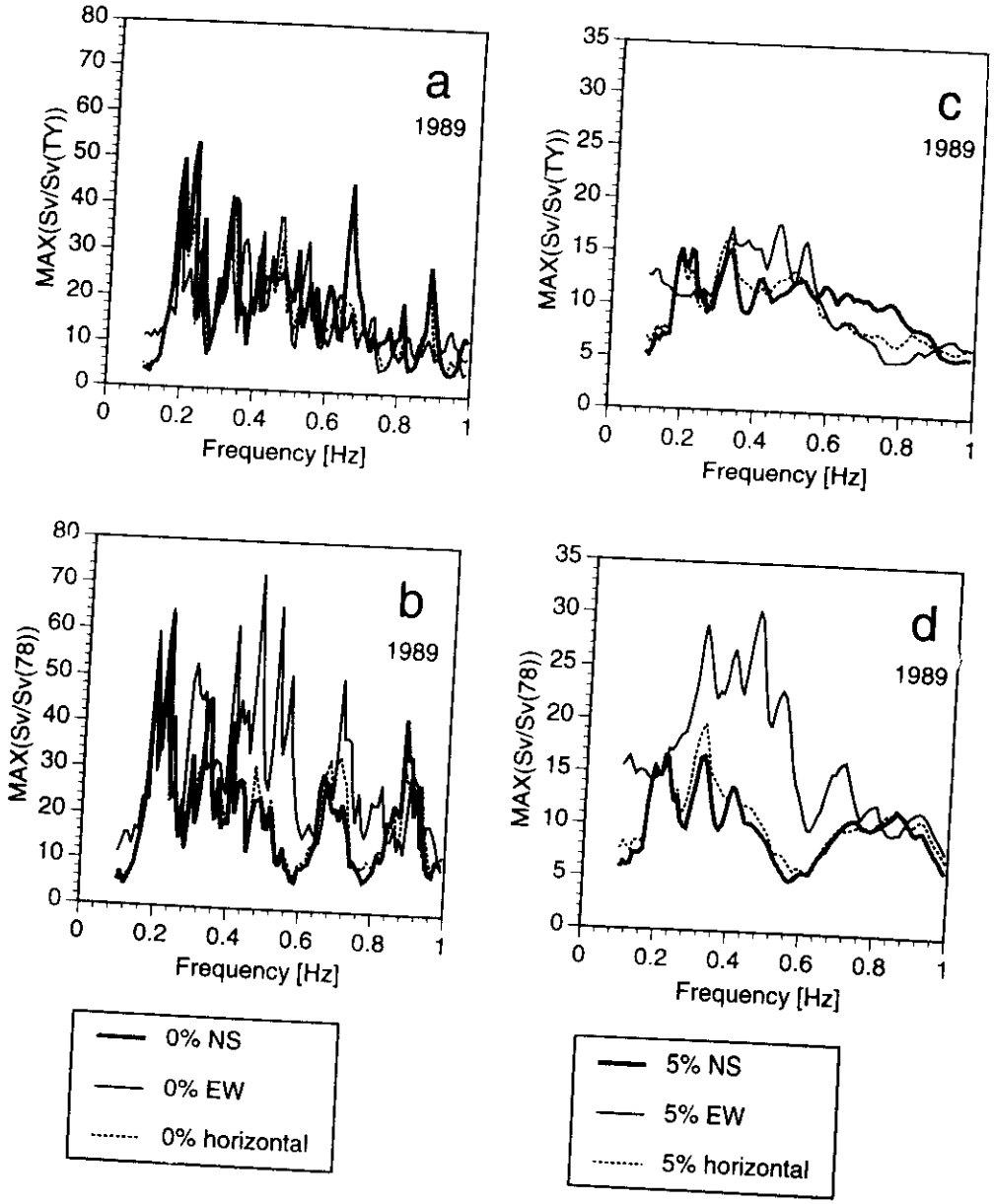

Fig. 17a-d. Maximum relative spectral velocities Sv/Sv(TY) and Sv/Sv(78) observed during the 1989 event, for zero damping (a,b) and 5% damping (c,d), obtained for all stations shown in fig. 12, using as reference station TY (a,c) and station 78 (b,d), respectively.

29

Application of numerical simulations for a tentative seismic microzonation of the city of Rome

Donat Fäh(1)(*), **Claudio Iodice**(1), **Peter Suhadolc**(1) **and Giuliano F. Panza**(1)(2)
(1) *Istituto di Geodesia e Geofisica, Università degli Studi di Trieste, Italy*
(2) *International Center for Theoretical Physics, Trieste, Italy*

Abstract
A hybrid technique, based on mode summation and finite differences, was used to simulate the ground motion induced in the city of Rome by possible earthquakes occurring in the main seismogenetic areas surrounding the city: the Central Apennines and the Alban Hills. The results of the numerical simulations are used for a seismic microzonation in the city of Rome, which can be used for the retrofitting of buildings of special social and cultural value. On the basis of our analysis Rome can be divided into six main zones: (1) the edges and (2) the central part of the alluvial basin of the River Tiber; (3) the edges and (4) the central part of the Paleotiber basin; the areas outside the large basins of the Tiber and Paleotiber, where we distinguish between (5) areas without, and (6) areas with a layer of volcanic rocks close to the surface. The strongest amplification effects have to be expected at the edges of the Tiber basin, with maximum spectral amplification of the order of 5 to 6, and strong amplifications occur inside the entire alluvial basin of the Tiber. The presence of a near-surface layer of rigid material is not sufficient to classify a location as a «hard-rock site», when the rigid material covers a sedimentary complex. The reason is that the underlying sedimentary complex causes amplifications at the surface due to resonance effects. This phenomenon can be observed in the Paleotiber basin, where spectral amplifications in the frequency range 0.4-1.0 Hz reach values of the order of 3 to 4.

Key words *Rome - wave-propagation modelling - seismic strong ground motion - seismic microzonation*

1. Introduction

Numerical simulations play an important role in the estimation of strong ground motion. They can provide synthetic signals for areas where recordings are absent and are, therefore, very useful for engineering design of earthquake-resistant structures and for the retrofitting of particularly important buildings. Lateral heterogeneities and sloping layers, commonly present in nature, can cause effects that dominate the ground motion: the excitation of local surface-waves, focusing and defocusing of waves, and resonance effects. In such circumstances, at least two-dimensional techniques are necessary for a realistic estimate of the ground motion.

To include both a realistic source model and a complex structural model of the site of interest, a hybrid method has been developed that combines modal summation and the finite difference technique (Fäh, 1992; Fäh *et al.*, 1993, 1994). The propagation of the waves from the source up to the local structure at the site is computed with the mode-summation method for plane layered anelastic structures (Panza

(*) *Now at*: Institut für Geophysik, ETH-Hönggerberg, CH-8093 Zürich, Switzerland.

32

the Centro de Instrumentación y Registro Sismico of the Fundación Javier Barros Sierra, and the Fundación del Grupo Ingenieros Civiles Asosiados for the use of the strong motion data recorded in Mexico City. D.F. was supported by the Swiss National Science Foundation under Grant N. 8220-037189. This study was made possible by CNR contracts 191.02692.CT15, 91.02550.PF54 and 92.02867.PF54, and EEC contract EPOC-CT91-0042. This research has been carried out in the framework of the ILP Task Group II.4 contributions to the IDNDR project «Physical Instability of Megacities».

REFERENCES

Aki, K. and K.L. Larner (1970): Surface motion of a layered medium having an irregular interface due to incident plane *SH* waves, *J. Geophys. Res.*, **75**, 933-954.

Ambrosini, S., S. Castenetto, F. Cevolani, E. Di Loreto, R. Funiciello, L. Liperi and D. Molin (1986): Risposta sismica dell'area urbana di Roma in occasione del terremoto del Fucino del 13 gennaio 1915. Risultati preliminari. *Mem. Soc. Geol. It.*, **35**, 445-452.

Bard, P.-Y. and M. Bouchon (1980a): The seismic response of sediment-filled valleys. Part 1: The case of incident *SH* waves, *Bull. Seismol. Soc. Am.*, **70**, 1263-1286.

Bard, P.-Y. and M. Bouchon (1980b): The seismic response of sediment-filled valleys. Part 2: The case of incident P and SV waves, *Bull. Seismol. Soc. Am.*, **70**, 1921-1941.

Bard, P.-Y. and M. Bouchon (1985): The two-dimensional resonance of sediment-filled valleys, *Bull. Seismol. Soc. Am.*, **75**, 519-541.

Bard, P.-Y. and J.-C. Gariel (1986): The seismic response of two-dimensional sedimentary deposits with large vertical velocity gradients, *Bull. Seismol. Soc. Am.*, **76**, 343-366.

Bard, P.-Y., M. Campillo, F.J. Chavez Garcia and F.J. Sánchez-Sesma (1988): The Mexico earthquake of September 19, 1985 - A theoretical investigation of large - and small-scale amplification effects in the Mexico City valley, *Earthquake Spectra*, **4**, 609-633.

Boore, D.M., K.L. Larner and K. Aki (1971): Comparison of two independent methods for the solution of wave-scattering problems: response of a sedimentary basin to vertically incident *SH* waves, *J. Geophys. Res.*, **76**, 558-569.

Campillo, M., J.-C. Gariel, K. Aki and F.J. Sánchez-Sesma (1989): Destructive strong ground motion in Mexico City: source, path, and site effects during great 1985 Michaocan earthquake, *Bull. Seismol. Soc. Am.*, **79**, 1718-1735.

CNEN-ENEL (1977): *Accelerograms from the Friuli, Italy, earthquake of May 6, 1976 and aftershocks, Part 3: Uncorrected accelerograms*, Rome, Italy, November 1977.

Drake, L.A. (1980): Love and Rayleigh waves in an irregular soil layer, *Bull. Seismol. Soc. Am.*, **70**, 571-582.

Espinosa, J.M., G. Ibarrola, O.R. Contreras, V.R. Silva, L. Camarillo and C. Pineda (1990): Sumario de acelerogramas colectados durante 1990, *Centro de instrumentación y registro sísmico, a.c., fundación javier barros sierra, a.c.*

Fäh, D. (1992): *A hybrid technique for the estimation of strong ground motion in sedimentary basins*, Ph.D. thesis No. 9767, Swiss Federal Institute of Technology, Zurich.

Fäh, D., P. Suhadolc and G.F. Panza (1993a): Variability of seismic ground motion in complex media: the case of a sedimentary basin in the Friuli (Italy) area, *J. Appl. Geophys.*, **30**, 131-148.

Fäh, D., C. Iodice, P. Suhadolc and G.F. Panza (1993b): A new method for the realistic estimation of seismic ground motion in megacities: the case of Rome, *Earthquake Spectra*, **9**, 643-668.

Fäh, D., P. Suhadolc, P. St. Mueller and G.F. Panza (1994): A hybrid method for the estimation of ground motion in sedimentary basins: quantitative modelling for Mexico City, *Bull. Seismol. Soc. Am.*, **84**, 383-399.

Fäh, D. and P. Suhadolc (1994): Application of numerical wave-propagation techniques to study local soil effects: the case of Benevento (Italy), *PAGEOPH*, **143**, 513-536.

Feroci, M., R. Funiciello, F. Marra and S. Salvi (1990): Evoluzione tettonica e paleogeografica plio-pleistocenica dell'area di Roma, *Il Quaternario*, **3**, 141-158.

Florsch, N., D. Fäh, P. Suhadolc and G.F. Panza (1991): Complete synthetic seismograms for high-frequency multimode *SH*-waves, *PAGEOPH*, **136**, 529-560.

Funiciello, R., G. Loria and S. Salvi (1987): Ricostruzione delle superfici strutturali del sottosuolo della città di Roma, *Atti del 6° Convegno Gruppo Nazionale Geofisica della Terra Solida*, CNR, Roma, 395-415.

Giorgetti, F. and S. Stefanini (1989): Vulnerabilità degli acquiferi del campo di Osoppo-Gemona all'inquinamento (Provincia di Udine), Istituto di Geologia e Paleontologia, Università degli Studi di Trieste, Pubblicazione n. 125.

Haskell, N.A. (1960): Crustal reflection of plane *SH* waves, *J. Geophys. Res.*, **65**, 4147-4150.

Haskell, N.A. (1962): Crustal reflection of plane *P* and *SV* waves, *J. Geophys. Res.*, **67**, 4751-4767.

Houston, H. and H. Kanamori (1986): Source characteristics of the 1985 Michoacan, Mexico earthquake at periods of 1 to 30 seconds, *Geophys. Res. Lett.*, **13**, 597-600.

Jackson, P.S. (1971): The focusing of earthquakes, *Bull. Seismol. Soc. Am.*, **61**, 685-695.

Kanamori, H., P.C. Jennings, S.K. Singh and L. Astiz (1993): Estimation of strong ground motions in Mexico City expected for large earthquakes in the Guerrero seismic gap, *Bull. Seismol. Soc. Am.*, **83**, 811-829.

Korn, M. and H. Stöckl (1982): Reflection and transmission of Love channel waves at coal seam discontinuities computed with a finite difference method, *J. Geophys.*, **50**, 171-176.

Mena, E., C. Carmona, R. Delgado, L. Alcantara and O. Dominguez (1986): Catálogo de acelerogramas procesados del sismo del 19 de septiembre de 1985, parte I: Ciudad de México, *Series del Instituto de Ingeniería No. 497, UNAM, México, D. F. México.*

Ordaz, M. and E. Faccioli (1994): Site response analysis in the valley of Mexico: Selection of input motion and extent of nonlinear soil behaviour, *Earthq. Eng. Structural Dynamics*, **23**, 895-908.

Panza, G.F. (1985): Synthetic seismograms: the Rayleigh waves modal summation, *J. Geophysics*, **58**, 125-145.

Reidesel, M.A., T.H. Jordan, A.F. Sheehan and P.G. Silver (1986): Moment-tensor spectra of the 19 September 85 and 21 September 85 Michaocan, Mexico, earthquakes, *Geophys. Res. Lett.*, **13**, 609-612.

Sánchez Sesma, F.J., S. Chávez-Pérez, M. Suárez, M.A. Bravo and L.E. Pérez Rocha (1988): The Mexico earthquake of September 19, 1985 - On the seismic response of the Valley of Mexico, *Earthquake Spectra*, **4**, 569-589.

Singh, S.K., E. Mena, J.G. Anderson, R. Quaas and J. Lermo (1990): Source spectra and RMS acceleration of Mexican subduction zone earthquakes, *PAGEOPH*, **133**, 447-474.

Suárez, M., F.J. Sánchez-Sesma, M.A. Bravo and J. Lermo (1987): Caracteristicas de los depósitos superficiales del Valle de México, *Memorias VII Congreso Nacional de Ingenieria Sismica, Querétaro, México, November 19-21*, A61-A74.

Suhadolc, P. and C. Chiarilesi (1985): A theoretical study of the dependence of the peak ground acceleration on source and structure parameters, in *Strong ground motion seismology*, edited by M.Ö. Erdik and M.N. Toksoz, *Proceedings of the NATO ASI on Strong Ground Motion Seismology, Ankara, Turkey, 1985*, 143-183.

Trifunac, M.D. (1971): Surface motion of a semi-cylindrical alluvial valley for incident plane *SH* waves, *Bull. Seismol. Soc. Am.*, **61**, 1755-1770.

Valdes, C. M., W. D. Mooney, S. K. Singh, R. P. Meyer, C. Lomnitz, J. H. Luetgert, C. E. Helsley, B. T. R. Lewis and M. Mena (1986): Crustal structure of Oaxaca, Mexico, from seismic refraction measurements, *Bull. Seismol. Soc. Am.*, **76**, 547-563.

Ventriglia, U. (1971): La geologia della città di Roma, *Amm. Prov. Roma*, Roma.

Virieux, J. (1986): *P-SV* wave propagation in heterogeneous media: velocity-stress finite-difference method, *Geophysics*, **51**, 889-901.

Table II. Structural bedrock models representative of the path from the epicenters to the city of Rome ($Q_\alpha = 2.2\ Q_\beta$). For the computations with source 3, located in the Alban Hills, the mechanical parameters of the first layer are given in parenthesis. The velocity gradients in the models are approximated by a series of thin layers.

Thickness (km)	Density (g/cm^3)	*P*-wave velocity (km/s)	*S*-wave velocity (km/s)	Q_β
0.09	2.24 (2.21)	2.40 (1.85)	1.29 (1.00)	30 (20)
0.10	2.25	2.50	1.30	30
0.10	2.25	2.80	1.50	30
0.10	2.30	4.00	2.31	100
0.10	2.40	4.10	2.37	100
0.10	2.40	4.20	2.43	100
0.10	2.50	4.30	2.48	100
0.10	2.50	4.40	2.54	100
0.10	2.50	4.50	2.60	100
0.10	2.50	4.60	2.65	100
0.10	2.60	4.70	2.70	100
0.10	2.60	4.80	2.77	100
0.10	2.60	4.90	2.83	100
0.10	2.60	5.00	2.88	100
0.10	2.60	5.20	3.00	100
0.10	2.60	5.40	3.10	100
0.10	2.60	5.60	3.20	100
1.70	2.80	5.70	3.30	100
6.10	2.85	6.00	3.46	100
0.10	2.85	5.89	3.40	100
0.10	2.85	5.80	3.35	100
0.10	2.85	5.71	3.30	100
0.10	2.85	5.54	3.20	100
8.60	2.85	5.40	3.12	100
0.10	2.85	5.49	3.17	100
0.10	2.85	5.63	3.25	100
0.10	2.85	5.71	3.30	100
0.10	2.85	5.89	3.40	100
0.10	2.85	6.06	3.50	100
2.70	2.85	6.20	3.58	300
1.70	2.88	6.50	3.75	300
1.70	2.90	6.70	3.87	300
2.40	2.95	7.00	4.04	300
4.75	3.35	7.90	4.56	300
4.75	3.35	7.92	4.57	300
4.75	3.35	7.94	4.58	300
4.75	3.35	7.96	4.59	300
4.75	3.35	7.98	4.60	300
4.75	3.35	8.00	4.62	300
4.75	3.36	8.02	4.63	300
4.75	3.37	8.04	4.64	300
4.75	3.38	8.06	4.65	300
∞	3.39	8.08	4.66	300

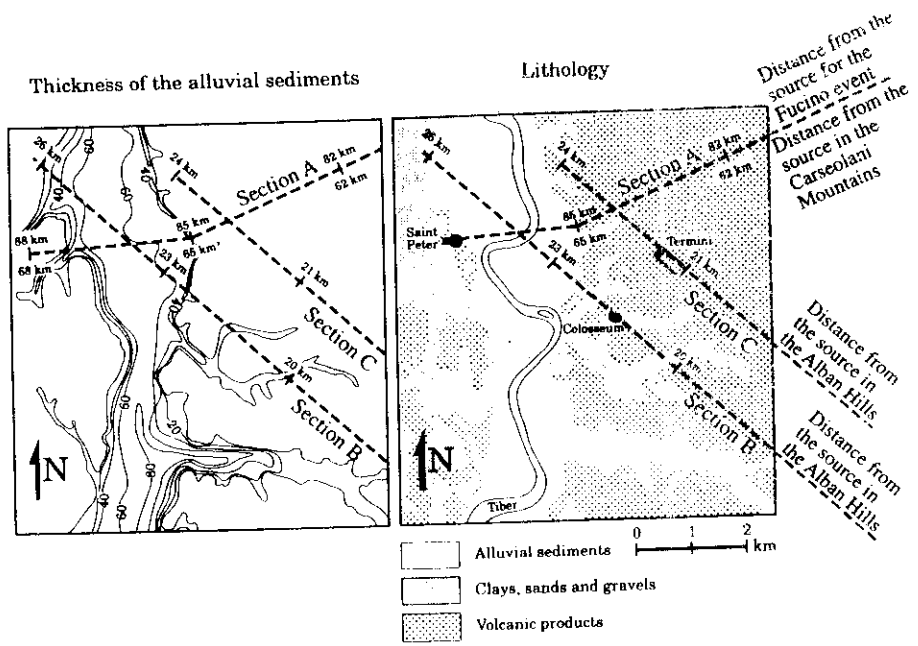

Fig. 2. Lithology and thickness of alluvial sediments in Rome (Ventriglia, 1971, Funiciello *et al.*, 1987 Feroci *et al.*, 1990). The dashed lines indicate the positions of the cross sections, for which numerical modelling is performed.

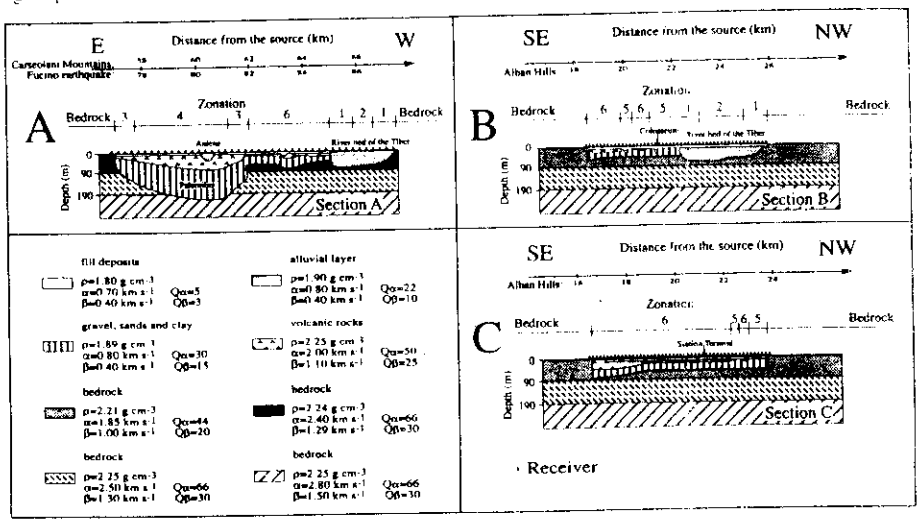

Fig. 3. Two-dimensional models corresponding to the dashed lines shown in fig. 2. Only the part near to the surface is shown, where the 2D model deviates from the horizontally-layered structural models shown in table II. The general microzonation is explained in the text.

35

1985; Florsch *et al.*, 1991). The mode-summation method allows the simulation of the complete incident wavefield in given phase-velocity and frequency bands. Explicit finite-difference schemes (Korn and Stöckl, 1982; Virieux, 1986) are then used to simulate the propagation of seismic waves in a two-dimensional model of the local structure. The hybrid method is particularly suitable to compute the ground motion in two-dimensional models of any complexity, and allows us to take into account the source and propagation effects, including local site conditions.

The area of Rome, considered here, is characterized by several sedimentary basins of considerable thickness, which in some parts are covered by volcanic rocks. The area is very vulnerable to earthquakes, as indicated, for example, by the well-documented damage distribution caused by the $M_L = 6.8$ January 13, 1915, Fucino (Italy) earthquake (Ambrosini *et al.*, 1986). In the absence of instrumental data in the city of Rome, a numerical simulation of the ground motion due to the January 13, 1915 Fucino earthquake was compared with the observed damage distribution (Fäh *et al.*, 1993). The macroseismic data in Rome shows essentially that the damage is concentrated at the edges of the alluvial basin of the Tiber River; the heavy and intermediate damage are located in that basin. The same distribution of damage can be expected on the basis of the numerical simulations of this event (Fäh *et al.*, 1993). The highest amplifications are observed at the edges of this alluvial basin, and large amplifications can be observed within the Tiber's River bed. The very good correlation between the damage statistics and the ground motion suggests using the hybrid technique for a microzonation of the entire town, which accounts also for events expected in other important seismogenetic areas. For this purpose, a series of different numerical simulations of the ground motion were performed, for different source positions and structural models of the Rome area. The results of such computations were then used for microzonation, based on the spectral amplifications expected in the different zones of the city.

2. Parametrization of the source and the propagation path

The most important seismogenetic zones (fig. 1) which can produce structural damage in Rome are the Central Apennines, whose earthquakes can cause, in the town, an observed maximum intensity VII-VIII on the Mercalli-Cancani-Sieberg intensity scale (MCS), and the Alban Hills, whose earthquakes are responsible for an observed maximum MCS intensity in Rome equal to VI-VII (Molin *et al.*, 1986). The source positions (fig. 1) used in this study include (1) the epicenter of the January 13, 1915 Fucino earthquake, (2) an epicenter close to the Carseolani Mountains where, from a study of pattern recognition (Caputo *et al.*, 1980), a strong earthquake is expected to occur, and (3) the Alban Hills. The source mechanisms assigned to these earthquakes are the mechanism of the Fucino earthquake (Gasparini *et al.*, 1985) for events 1 and 2, and the mechanism of a recent earthquake in the Alban Hills (Amato *et al.*, 1984) for event 3. The parameters of the focal mechanism of each event are given in table I.

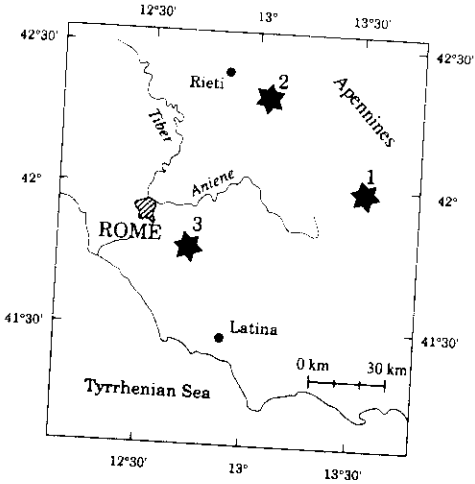

Fig. 1. Epicenter locations of the events used for the different numerical simulations. The source positions are (1) the epicenter of the January 13, 1915 Fucino earthquake, (2) an epicentre close to the Carseolani Mountains, and (3) the Alban Hills.

Table I. Source mechanisms of the events shown in fig. 1.

Event No.	Location	Source depth (km)	Dip	Rake	Strike-receiver angle
1	Fucino valley	8.00	39°	172°	38°
2	Carseolani Mountains	8.00	39°	172°	38°
3	Alban Hills	3.06	74°	266°	133°

The one-dimensional structural models for the region between the source positions and Rome are given in table II. The P-wave velocities in the crust are based on seismic refraction measurements made along the profile Latina-Pescara (Nicolich, 1981). The shear-wave velocities were chosen by assuming that $v_S^2 = v_P^2/3$. The Moho depth (28 km) is in good agreement with other published results (Nicolich, 1989; Suhadolc and Panza, 1989). These models were used as reference bedrock structures, and, for each seismic source, the ground motion computed with the hybrid method was always compared with that obtained for the related one-dimensional structure.

The position of the cross sections studied is shown in fig. 2, and the related two-dimensional structural models are shown in fig. 3. They are based on all the available geological and geotechnical information (Ventriglia, 1971; Serva *et al.*, 1986; Funiciello *et al.*, 1987; Boschi *et al.*, 1989; Feroci *et al.*, 1990). Alluvial sediments can be found in two major areas, the river beds of the Aniene and Tiber. The ancient river bed of the Tiber (referred as Paleotiber) is composed of Sicilian clays, sands and gravel. This sedimentary complex is covered by volcanic rocks which have their origin in the Pleistocene volcanic activity (Ventriglia, 1971). The volcanic rocks have greater wave velocities than the underlying sediments (Sicilian) which, therefore, define a buried low-velocity zone. The surficial layer consists of compacted fill, and of the foundations of man-made structures. The transition from the alluvial sediments in the Tiber River bed to the compacted clay is characterized by a very high impedance contrast. In fig. 3, the compacted clay is referred to as bedrock, and its material properties are related to the values given in table II. The velocity gradient in the uppermost part of the structure for the bedrock is approximated by a series of thin layers.

Since the mechanical properties and thickness of the different soils are not well known, we have used different material properties to test the stability of the microzonation and enhance its reliability. Our tests include: (1) two different models for which the seismic phase velocities given in fig. 3 are defined at 1 Hz and at 30 Hz, respectively, while the Q-values are not varied, and (2) two different models in which the surficial layer of man-made ground (fill deposits) has a thickness of 5 m and 10 m, respectively.

3. Properties of the ground motion caused by the Fucino event

Several ground motion related quantities can be extracted from the synthetic accelerograms obtained from our numerical modelling. The quantities that we consider here are: (1) the relative peak ground acceleration PGA(2D)/PGA(bedrock), (2) the so-called relative Arias intensity $W(2D)/W(\text{bedrock})$ (Arias, 1970), where W is defined as:

$$W = \frac{\pi}{2g} \lim_{t \to \infty} \int_0^t [\dot{x}(\tau)]^2 \, d\tau ,$$

where x is the ground displacement, and (3) the relative spectral accelerations or spectral amplification $Sa(2D)/Sa(\text{bedrock})$, where Sa is the spectral acceleration. PGA(2D), $W(2D)$,

amplification with respect to the bedrock model varies between 5 and 6, and it is due to the combination of resonance effects with the excitation of local surface waves (Fäh *et al.*, 1993). The general shape of the maximum and average spectral amplifications are similar for zones 1 and 2. In the frequency range from 1.0 Hz to 3.0 Hz, the maximum spectral amplification is of the order of 4 and the average spectral amplification is of the order of 2.

Similar observations can be made for the Paleotiber basin (zones 3 and 4), but in a different frequency band (0.4-1.0 Hz). The buried sedimentary complex (Sicilian) causes maximum spectral amplification between 3 and 4, due to resonance effects. These are most pronounced at frequencies around 0.6 Hz. Therefore, the presence of a near-surface layer of rigid material in the Paleotiber basin is not sufficient to classify that area as a «hard-rock site». A correct zonation requires the knowledge of both the thickness of the surficial layer and of the deeper parts of the structure, down to the real bedrock. This is especially important in volcanic areas, where pyroclastic material often covers alluvial basins. The maximum spectral amplification is larger at the edges of the Paleotiber basin (zone 3). For frequencies above 1.0 Hz, in the Paleotiber basin (zone 4), the volcanic layer acts as a shield reflecting part of the incoming energy, and the values of the average spectral amplification are smaller than 1.

For the sites in zones 5 and 6, the maximum and the average spectral amplifications are small for frequencies below 1 Hz. Since the sedimentary cover in these zones is thin, the amplification takes place at frequencies above 1.5 Hz, and changes rapidly from site to site. This rapid variation leads to average values of the order of 1.0-1.5.

5. Summary and conclusions

In the absence of instrumental data, realistic numerical simulations of the ground motion, successfully tested against macroseismic data, are used for the microzonation of Rome. The zonation is based on the numerical simulation of wave propagation along different profiles, by taking into account realistic seismic sources, the propagation paths of the seismic waves, and the uncertainty of material properties. The results of such computations are used to define the spectral amplifications expected in different zones of the city. Using as reference a bedrock model, six main zones can be distinguished, each one characterized by specific geological conditions. This characterization allows us to extend the results to sites in the Rome area which are not located on the cross-sections studied, but which have similar geological conditions as those defined in our modelling.

In general, for sites close to lateral heterogeneities, the amplification effects are maximum. The highest values of the spectral amplification (between 5 and 6), are observed at the edges of the sedimentary basin of the Tiber, and strong amplifications are observed in the Tiber's River bed. This is caused by the large amplitudes and long duration of the ground motion due to (1) the low impedance of the alluvial sediments, (2) resonance effects, and (3) the excitation of local surface waves. Similar observations can be made for the Paleotiber basin, where the buried sedimentary complex causes the maximum spectral amplification between 3 and 4, which can be explained by resonance effects.

Our technique can be applied routinely in microzonation studies, and it provides realistic estimates of amplification and attenuation effects for two-dimensional, anelastic models. Since geotechnical data are available for many areas, the proposed technique provides a scientifically and economically valid procedure for the immediate (no need to wait for a strong earthquake to occur) seismic microzonation of any urban area, and it can be very useful for the engineering design of earthquake-resistant structures and for the retrofitting of particularly important buildings.

Acknowledgements

We would like to thank ENEA for allowing us the use of the IBM3090E computer at the ENEA INFO BO Computer Center. D.F. has been supported by the Swiss National Science Foundation under Grant No. 8220-037189. This study has been made possible by the contracts CNR 91.02692.CT15, CNR 92.00068.CT12, CNR 92.02422.CT15, CNR 92.02867.PF54, and EEC EPOC-CT91-0042, and by MURST (40% and 60%) funds. This research has been carried out in the framework of the ILP Task Group II.4 contributions to the IDNDR project «Physical Instability of Megacities».

REFERENCES

AMATO, A., B. DI SIMONE and C. GASPARINI (1984): Considerazioni sulla sismicità dei Colli Albani, in *Atti del 3° Convegno del Gruppo Nazionale di Geofisica della Terra Solida*, CNR, Roma, vol. 2, 965-976.

AMBROSINI, S., S. CASTENETTO, F. CAVOLANI, E. DI LORETO, R. FUNICIELLO, L. LIPERI and D. MOLIN (1986): Risposta sismica dell'area urbana di Roma in occasione del terremoto del Fucino del 13 gennaio 1915. Risultati preliminari, *Mem. Soc. Geol. It.*, **35**, 445-452.

ARIAS, A. (1970): A measure of earthquake intensity, in *Seismic Design for Nuclear Power Plants*, edited by R. HANSEN (Cambridge, Mass.), 438-483.

BOSCHI, E., M. FEROCI, R. FUNICIELLO, L. MALAGNINI, A. ROVELLI and S. SALVI (1989): Valutazione della risposta sismica in ambiente urbano: risultati per la città di Roma, in *Atti dell'8° Convegno Gruppo Nazionale Geofisica della Terra Solida*, CNR, Roma, 317-326.

CAPUTO, M., V. KEILIS-BOROK, E. OBERTROVA, E. RANZMAN, I. ROTWAIN and A. SOLOVIEFF (1980): Pattern recognition of earthquake-prone areas in Italy, *Phys. Earth. Planet. Int.*, **21**, 305-320.

FÄH, D. (1992): A hybrid technique for the estimation of strong ground motion in sedimentary basins, *Ph. D Thesis No. 9767*, Swiss Federal Institute of Technology, Zurich.

FÄH, D., C. IODICE, P. SUHADOLC and G.F. PANZA (1993): A new method for the realistic estimation of seismic ground motion in megacities: the case of Rome, *Earthquake Spectra*, **9** (4), 643-668.

FÄH, D., P. SUHADOLC, ST. MUELLER and G.F. PANZA (1994): A hybrid method for the estimation of ground motion in sedimentary basins: quantitative modelling for Mexico City, *Bull. Seismol. Soc. Am.*, **84**, 383-399.

FEROCI, M., R. FUNICIELLO, F. MARRA and S. SALVI (1990): Evoluzione tettonica e paleogeografica pleistocenica dell'area di Roma, *Il Quaternario*, **3**, 141-158.

FLORSCH, N., D. FÄH, P. SUHADOLC and G.F. PANZA (1991): Complete synthetic seismograms for high-frequency multimode *SH*-waves, *PAGEOPH*, **136**, 529-560.

FUNICIELLO, R., G. LOMBA and S. SALVI (1987): Ricostruzione delle superfici strutturali del sottosuolo della città di Roma, in *Atti del 6° Convegno Gruppo Nazionale Geofisica della Terra Solida*, CNR, Roma, 395-415.

GASPARINI, C., G. IANNACCONE and R. SCARPA (1985): Fault-plane solutions and seismicity of the Italian peninsula, *Tectonophysics*, **117**, 59-78.

KORN, M. and H. STOCK (1982): Reflection and transmission of Love channel waves at coal seam discontinuities computed with a finite difference method, *J. Geophys.*, **50**, 171-176.

MOLIN, D., S. AMBROSINI, S. CASTENETTO, E. DI LORETO, L. LIPERI and A. PAGLIUCA (1986): Aspetti della sismicità storica di Roma, *Mem. Soc. Geol. It.*, **35**, 439-444.

NICOLICH, R. (1981): Il profilo Latina-Pescara e le registrazioni mediante OBS nel Mar Tirreno, in *Atti del Convegno Gruppo Nazionale Geofisica della Terra Solida*, CNR, Roma, 623-637.

NICOLICH, R. (1989): Crustal structures from seismic studies in the frame of the European Geotraverse (Southern Segment) and CROP projects, in *The Lithosphere in Italy: Advances in Earth Science Research, Atti dei Convegni Lincei*, **80**, 41-61.

PANZA, G.F. (1985): Synthetic seismograms: the Rayleigh waves modal summation, *J. Geophys.*, **58**, 125-145.

SERVA, L., A.M. BLUMETTI and A.M. MICHETTI (1986): Gli effetti sul terreno del terremoto del Fucino (13 gennaio 1915): tentativo di interpretazione della evoluzione tettonica recente di alcune strutture, *Mem. Soc. Geol. It.*, **35**, 893-907.

SUHADOLC, P. and G.F. PANZA (1989): Physical properties of the lithosphere-asthenosphere system in Europe from Geophysical Data, in *The Lithosphere in Italy: Advances in Earth Science Research, Atti dei Convegni Lincei*, **80**, 15-40.

VENTRIGLIA, U. (1971): La geologia della città di Roma, Amm. Prov. di Roma, Roma.

VIRIEUX, J. (1986): P-SV wave propagation in heterogeneous media: velocity-stress finite-difference method, *Geophysics*, **51**, 889-901.

36

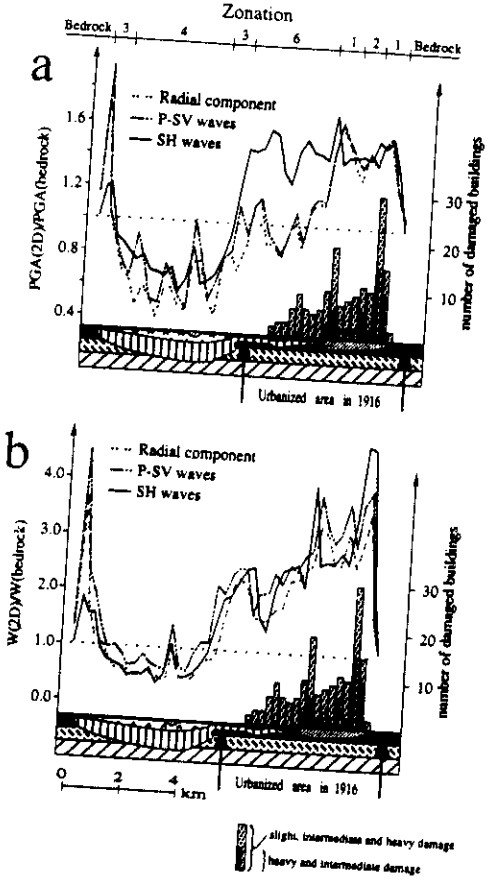

Fig. 4. Ratios of the peak ground acceleration, PGA(2D)/PGA(bedrock), and of the Arias Intensity, $W(2D)/W(bedrock)$, obtained for the numerical simulation of the Fucino earthquake (event 1 in fig. 1). They are compared with the damage distribution caused by the January 13, 1915 Fucino earthquake (Fäh *et al.*, 1993). The general microzonation is explained in the text.

$Sa(2D)$ indicate, respectively, PGA, W and Sa computed for the two-dimensional models shown in fig. 3. PGA(bedrock), W(bedrock), and Sa(bedrock) indicate, respectively, PGA, W and Sa obtained for the one-dimensional reference bedrock models given in table II. In order to remove the effects of the regional propagation, PGA(2D), $W(2D)$, and $Sa(2D)$ are always normalized with respect to the related quantities PGA(bedrock), W(bedrock), Sa(bedrock), computed in the reference bedrock model for the same seismic source and the same source-receiver distance.

For the Fucino event (event 1), relative PGA and relative Arias intensity, defined by the ratios PGA(2D)/PGA(bedrock) and $W(2D)/W$(bedrock), computed for the transverse component of motion (SH-waves), the radial component of motion, and the total P-SV wavefield (radial and vertical component of motion), are shown in fig. 4. High relative PGA values are observed for locations sitting on unconsolidated sediments (fig. 4a), while relative PGA values are low where the volcanic layer is thick. Relative peaks can be seen at the beginning of the alluvial valley of the Tiber and within the alluvial valley of the Aniene. The peaks and troughs are more evident in the curve representing the relative W values (fig. 4b). There are five relative peaks: two at the edges of the Tiber basin, one within the alluvial valley of the Aniene, a broad peak where the Sicilian low-velocity zone is close to the surface, and one at the margin of the Paleotiber basin.

The macroseismic data show essentially that, in Rome, the damage is concentrated in the basin of the Tiber with clear peaks at the edges of the alluvial basin. To quantify this observation, the damage distribution has been projected on the cross section used in the numerical modelling (Fäh *et al.*, 1993). The resulting histogram is shown in fig. 4, which shows that a similar distribution of damage is predicted by our direct numerical simulation.

4. Seismic microzonation

The results obtained from the modelling of the Fucino event (fig. 4) can be used directly for general microzonation purposes. Using as reference the bedrock models given in table II, six zones can be distinguished (see figs. 3 and 4): (1) *zone 1* includes the edges of the Tiber River, (2) *zone 2* extends over the central part

of the alluvial basin of the Tiber, (3) *zone 3* includes the edges of the Paleotiber basin, and (4) *zone 4* extends over the central part of the Paleotiber basin. *Zones 5* and *6* include areas which are located outside the large basins of the Tiber and Paleotiber where we distinguish between areas (5) without and (6) with a layer of volcanic rocks close to the surface. Due to analogous geological conditions, these zones can be recognized in the sections considered in relation with the events located in the Carseolani Mountains and the Alban Hills, as is shown in fig. 3.

For all the receivers of all two-dimensional models and studied events, we have computed the spectral amplification $Sa(2D)/Sa$(bedrock) for one hundred frequencies of the oscillator, in the frequency range 0.2 to 4 Hz. For a certain zone, we have computed the average of all spectral amplification curves obtained for the receivers in this zone. Moreover, we have determined the maximum spectral amplification observed for all receivers in this zone. The results obtained for zero damping and 5% damping of the oscillator are shown in fig. 5. With respect to bedrock, the maximum spectral amplification defines the maximum amplification effects to be expected in a certain zone. The average spectral amplification defines amplification and attenuation effects which are similar for all receivers in a certain zone, and the difference between the maximum and average spectral amplification is a measure for the variability of the ground motion in a zone.

The greatest spectral amplification is observed at the edges of the sedimentary basin of the Tiber River (zone 1), for frequencies between 2.0 and 2.5 Hz. The maximum spectral

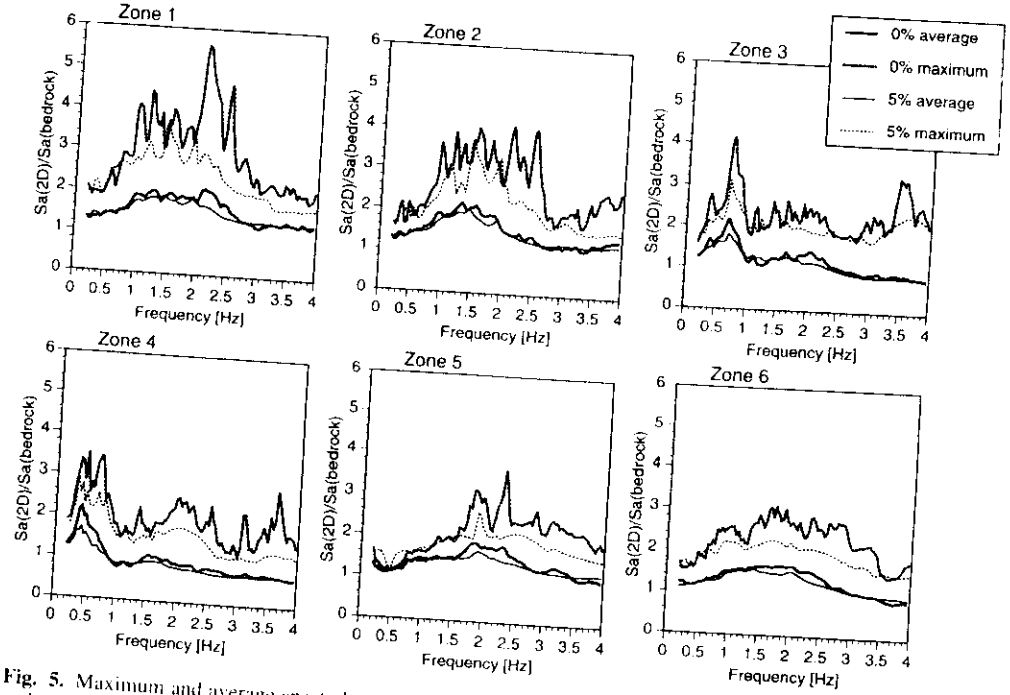

Fig. 5. Maximum and average spectral amplifications for the zones defined in figs. 3 and 4, for zero damping and 5% damping.

35

Mitigation of seismic hazard of a megacity: the case of Naples

CONCETTINA NUNZIATA, DONAT FÄH and GIULIANO F. PANZA

from

ANNALI DI GEOFISICA

Vol. XXXVIII, N. 5-6 Nov.-Dec. 1995, pp. 649-661

Editrice Compositori

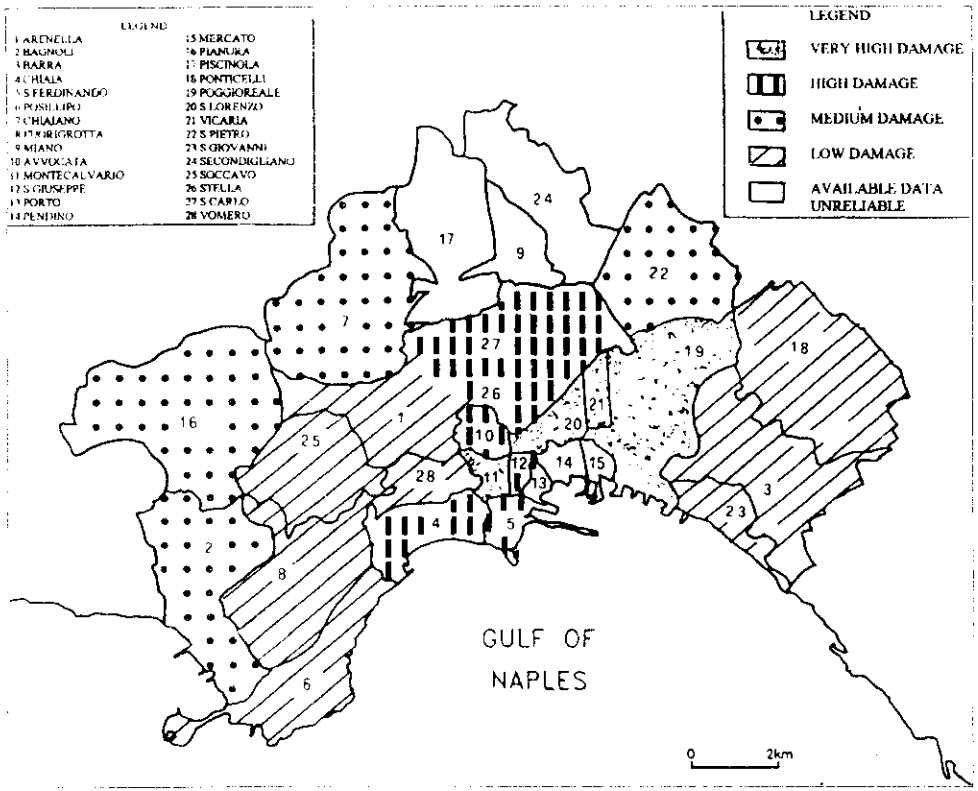

Fig. 1. Map showing the distribution of damage in Naples due to the 1980, Irpinia earthquake (modified from Esposito *et al.*, 1992).

Naples, lower peak ground accelerations might be expected on rock sites in the town. In addition, even if the epicentral distance is about 90 km, and therefore an increase in the peak ground acceleration with distance cannot be excluded (*e.g.* Suhadolc and Chiaruttini, 1985; Fäh *et al.*, 1993b), this increment should not exceed 30-40% of the maximum recorded at Torre del Greco. Hence, if for the historical buildings, the damage is easily explained by their degraded conditions, for the most damaged buildings in the eastern district, which are tall and made of reinforced concrete, it is necessary to consider the combined effects of the incident wavefield, the local soil conditions and the properties of the buildings.

The analysis of the strongest historical earthquakes, X and XI degrees on the Mercalli Cancani Sieberg (MCS) scale in the epicentral area, indicates that the maximum intensity observed in Naples is about VIII on the MCS scale for the most disastrous seismic event which occurred in Italian territory in December 1456. Intensity VII on the MCS scale was felt in Naples for the 1688, 1694 and 1805 historical earthquakes, as well as for the 1980 earthquake (Esposito *et al.*, 1992). The distribution of the damage caused by the historical earthquakes is obviously concentrated in the historical centre, but in 1805, the buildings present in the eastern part of Naples were completely destroyed.

Historical and archaeological data can be merged with geological information if synthetic isoseismals are computed considering the complete wavefield radiated from a point-source (Suhadolc *et al.*, 1988). This method, successfully applied to the modelling of the observed isoseismals of instrumentally recorded earthquakes (*e.g.* see Panza *et al.*, 1988; Panza, 1991), can easily be extended to historical earthquakes to infer their source mechanism (Panza *et al.*, 1991). For instance, it has been noted that, even if the observed isoseismals of the 1962 and the 1980 Irpinia earthquakes are differently elongated, the first being elongated perpendicularly to the axis of the Apennines and the second along the axis of the mountain chain, the source mechanism can be the same when the focal depths of the two events are assumed to be different. In accordance with the results of Panza *et al.* (1991), the focal depth of the 1962 event is greater than 12 km, *i.e.* the seismic source is close to the bottom of the thick, superficial sedimentary low velocity layers, while the focal depth of the 1980 earthquake is around 6 km. As a matter of fact, this is the method to assign a completely realistic seismogram to historical earthquakes, and hence to evaluate hazard in more rigorous terms.

The 1980 earthquake is the first strong event that occurred in the Southern Apennines, recorded by many instruments at different epicentral distances and in a wide range of frequencies. Several seismological studies considered the source geometry, the rupturing process, and the site effects (for a recent complete compilation of these studies see «Annali di Geofisica», 1993). The source process is complex, consisting of a main rupture episode (0 s subevent) followed by two smaller ones at about 18 s and 40 s from the origin time of the main episode. A general agreement exists about the geometry of the main rupture consisting of a fault dipping 60° toward NE and having a strike of about 315°. From levelling data (Pingue *et al.*, 1993), a fault dipping 20° toward NE is consistent with the second subevent (18 s), and another almost parallel to the main fault, but antithetic, dipping SW, is consistent with the third subevent (40 s). The largest moment release took place at a depth not exceeding 10 km, underneath the eastern flank of the Mt. Marzano ridge, near to the town of Laviano. This instrumental depth determination agrees quite well with the macroseismic depth estimate made by Panza *et al.* (1991).

The aim of this paper was (1) to perform the numerical modelling of the propagation of the wavefield, generated by the main rupture event of the 1980 earthquake, up to a profile trending N86°W, and located in a test area in the eastern district of Naples, and (2) to make an accurate and realistic evaluation of the seismic ground motion, taking into account the significant lateral variations which are present in the subsoil of this urban area.

For the computation of the local seismic response, we used (1) the standard one-dimensional method (computer program Shake), developed by Schnabel *et al.* (1972), that uses vertically incident *SH*-waves in a structure composed of plane parallel layers, here indicated as method 1, and (2) the hybrid method developed by Fäh (1992) and Fäh *et al.* (1993a,b), that accounts for the source and the propagation path, including anelasticity and local soil effects, here indicated as method 2. The results obtained with the two methods were compared in order to evaluate the possibilities of the commonly used 1-D computational techniques for reliable microzonation.

2. Numerical modelling of seismic ground motion for 2-D structures

Many computational techniques exist to estimate the ground motion at a site. The standard one-dimensional methods like Shake estimate the amplification of *SH* waves, vertically propagating through plane parallel layers of unconsolidated soils overlying the bedrock. Such techniques are very fast, but are uncertain for structures which are characterized by strong lateral heterogeneities or sloping layers.

ANNALI DI GEOFISICA, VOL. XXXVIII, N. 5-6, November-December 1995

Mitigation of seismic hazard of a megacity: the case of Naples

Concettina Nunziata([1]), **Donat Fäh**([2])(*) **and Giuliano F. Panza**([2])([3])
([1]) *Dipartimento di Geofisica e Vulcanologia, Università Federico II, Napoli, Italy*
([2]) *Istituto di Geodesia e Geofisica, Università degli Studi di Trieste, Italy*
([3]) *International Center for Theoretical Physics, Trieste, Italy*

Abstract
The seismic ground motion of a test area in the eastern district of Naples was computed with a hybrid technique based on the mode summation and the finite difference methods. This technique allowed the realistic modelling of source and propagation effects, including local soil conditions. In the modelling, as seismic source we considered the 1980 Irpinia earthquake, a good example of strong shaking for the area of Naples, located about 90 km from the source. Along a profile through Naples, trending N86°W, the subsoil is mainly formed by alluvial (ash, stratified sand and peat) and pyroclastic materials overlying a pyroclastic rock (yellow Neapolitan tuff) representing the Neapolitan bedrock. The detailed information available on the subsoil mechanical properties and its geometry warrants the application of the sophisticated hybrid technique. For *SH*-waves, a comparison was made between a realistic 2-D seismic response and a standard 1-D response, based on the vertical propagation of waves in a plane layered structure. As expected the sedimentary cover caused an increase in the signal's amplitudes and duration. If a thin uniform peat layer is present, the amplification effects are reduced, and the peak ground accelerations are similar to those observed for the bedrock model. This can be explained by the backscattering of wave energy at such a layer. The discrepancies evidenced between the 1-D and the 2-D seismic response suggest that serious caution must be taken in the formulation of seismic regulations. This is particularly true in the presence of the thin peat layer where the mismatch between the 1-D and the 2-D amplification functions is particularly evident in correspondence of the dominant peak and of the second significant peak.

Key words *seismic hazard – microzoning – numerical modelling – Naples*

1. Introduction

The main seismogenic areas of Southern Italy are located in the Southern Apennines. Naples is not within a seismogenic area, but it has often been severely damaged by Apennine earthquakes. The last strong event, the November 23, 1980 ($M_s = 6.9$, $M_L = 6.5$), Irpinia earthquake, produced serious damage in Naples (fig. 1), mostly in the historical centre and in the eastern area (Rippa and Vinale, 1983), despite the expected moderate ground shaking. In fact, peak ground accelerations of 0.06 g and 0.04 g, with dominant frequencies at 2.5 and 3 Hz, were recorded along the N-S and E-W directions at the seismic station Torre del Greco. This station is located on a lava deposit on the Vesuvius flanks, about 20 km from Naples, on a similar azimuth from the epicenter. Due to the larger epicentral distance of

(*) *Now at*: Institut für Geophysik, ETH-Hönggerberg, CH-8093 Zürich, Switzerland.

39

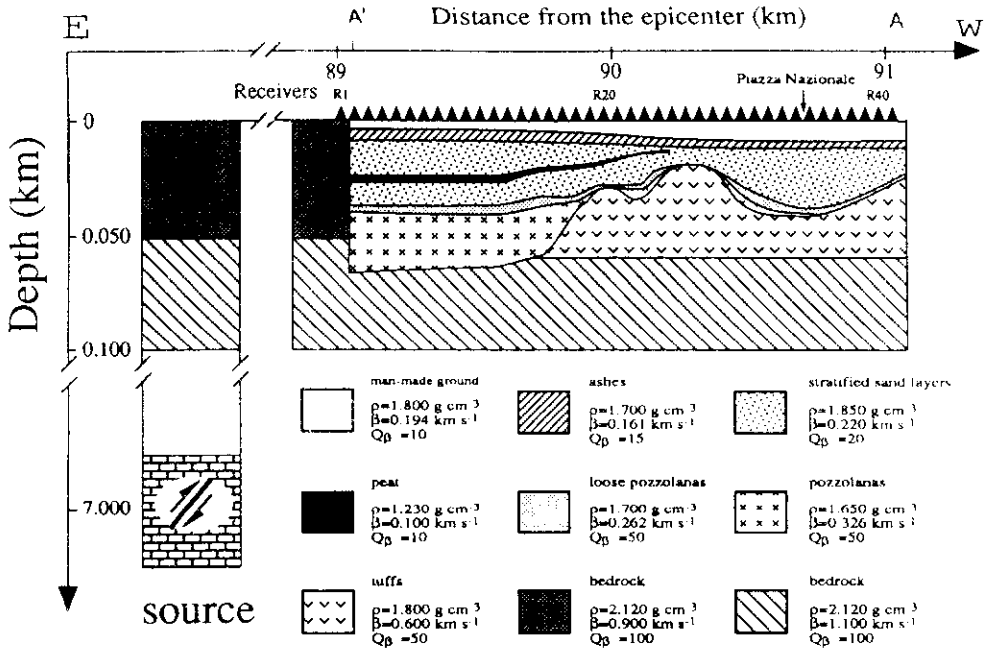

Fig. 3. Geological cross-section along the profile AA′ shown in fig. 2.

that we have taken as representative for the eastern part of Naples (fig. 3). The choice of the mechanism of the seismic source was made according to the mechanism of the main shock (0 s subevent) of the 1980 Irpinia earthquake: dip 65°, rake 270°, strike 315° and depth 7.0 km. The angle between the strike of the fault and the epicenter-cross section line is 36°.

The source is located in the laterally homogeneous part, and the propagation of the waves from the source up to the 2-D anelastic structure (fig. 3) was computed with the mode summation technique for the layered one-dimensional anelastic model representative of the path to the town of Naples (Vaccari *et al.*, 1990). Acceleration time series for *SH*-waves (fig. 4) were computed at an array of receivers over several different cross-sections: (1) the one-dimensional reference anelastic model for the bedrock, which represents the structural model for the region between the source position and Naples (table I), (2) the anelastic two-dimensional model with the peat layer, and (3) the same two-dimensional model without the peat layer. All scaling values were related to a source seismic moment of 10^{17} Nm, and all signals normalized to the same value. The time scale is shifted by 22 s with respect to the origin time, and the distance between two receivers is 100 m.

The presence of unconsolidated sediments increased the signal's amplitudes and duration, which is more pronounced for the model without the peat layer. For the model with the peat layer, between receivers 1 and 15, the maximum amplitudes are similar to the maximum amplitudes observed for the one-dimensional bedrock model. This can be explained by the backscattering of wave energy at such a layer. These effects could be different if the peat

layer is not laterally homogeneous, and the discussion of the effects of such fine details will be the subject of a future investigation.

The amplification and attenuation effects as a function of frequency can be identified through the analysis of the spectral ratios, that is the Fourier spectrum of the signals computed at the receivers in the 2-D structural model, normalized to the Fourier spectrum of the signals computed for the 1-D reference model (table I).

The maximum response spectrum of a simple oscillator is commonly used to quantify the ground motion for engineering purposes. We consider the spectral amplification for zero damping, which is defined as the response spectrum at a receiver in the 2-D structural model normalized to the response spectrum computed for the reference 1-D model. The spectral ratios and the spectral amplifications are computed in correspondence of the position of 5 receivers, representative of different stratigraphies in the 2-D section. Looking at the spectral ratios at the chosen receivers R7, R17, R23, R26, R33, the wide variability of ground motion is quite evident within a few hundred meters (fig. 5). The dominant peak moves from frequencies lower than 1 Hz (receiver R7), to

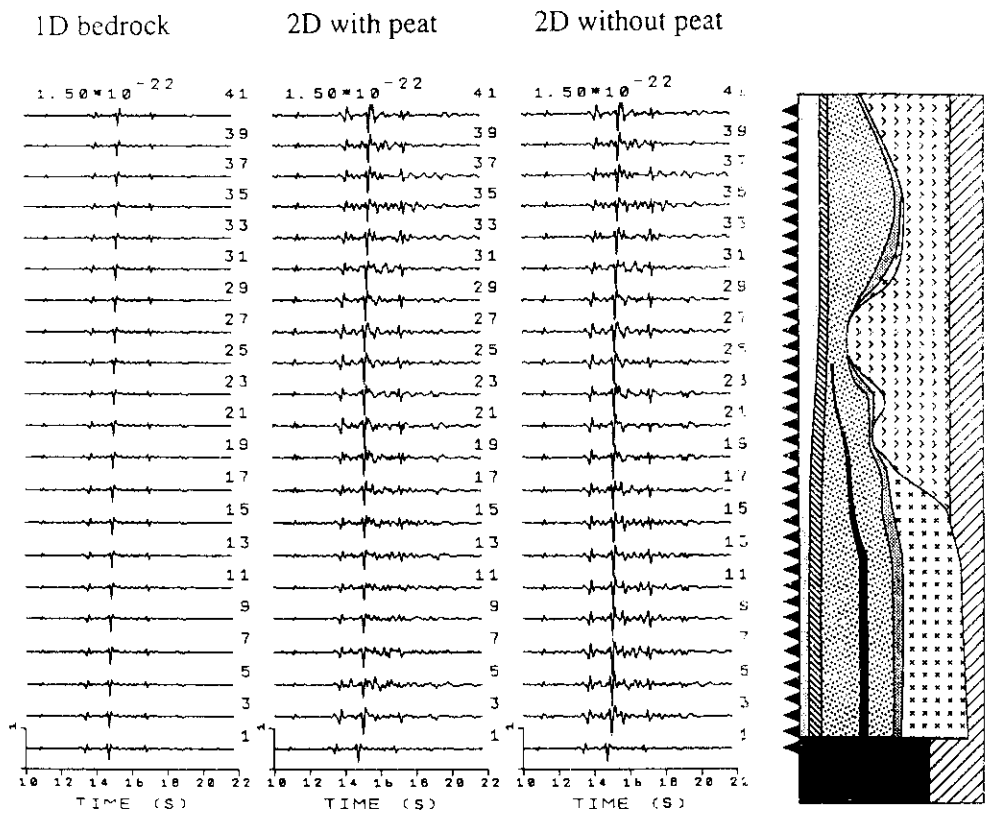

Fig. 4. Acceleration time series for *SH*-waves computed over the reference model (1D bedrock), the 2-D structural model with the peat layer, and the 2-D structural model without the peat layer.

In these cases, at least two-dimensional techniques may be necessary for a useful and realistic estimate of the ground motion.

The numerical hybrid approach recently proposed by Fäh (1992) and Fäh *et al.* (1993a,b) can account for the source and the propagation effects, including anelasticity and local soil effects. The propagation of the waves from the source up to the complex two-dimensional structure is computed with the mode summation technique (Panza, 1985; Florsch *et al.*, 1991), and in the complex, laterally heterogeneous structure it is computed with the finite difference method. This hybrid approach combines the advantages of both mode summation and finite difference technique. With the mode summation method it is possible to simulate a realistic rupture process on the extended fault, as a sum of point sources, properly distributed in space and time. The path from the source up to the region containing the 2-D heterogeneities is represented by a 1-D layered anelastic structure. The resulting wavefield is then used to define the boundary conditions to be applied to the 2-D anelastic region where the finite difference technique is used. The hybrid approach has been developed for both *SH*- and *P-SV*-waves (Fäh, 1992; Fäh *et al.*, 1993a,b). Here only *SH*-waves are considered since the program Shake handles only this kind of waves.

3. Geological setting of the studied area

Naples is located on volcaniclastic soils and rocks (various types of tuffs) erupted by the Campi Flegrei volcanoes (fig. 2). The original material that forms the tuffs and the volcanic soils is in general the same, with the volcaniclastic rocks being the result of the hardening of the volcaniclastic soils by post depositional hydrothermal alteration. The tuff formation is either outcropping or is located some tens of metres below the ground surface. Its thickness ranges from twenty metres in the eastern district to two hundred metres under the Posillipo hill.

The volcaniclastic soils derive from different types of explosive volcanic activity. When the magma was richer in gas, the products were magma fragments. As a consequence of a sudden cooling, the magma was solidified in a glassy state and with a spongy structure. These products are the pumiceous lapilli that have a coarse grain size. When the magma was poorer in gas, or the cooling rate was slower, scoriaceous lapilli were erupted, having a crystalline centre and a glassy outer part. Lava fragments were often thrown out and lithic lapilli were formed. Generally these three different types of volcanic activity occurred simultaneously, but with varying intensity. Therefore the different volcanic products were generally present in a variable composition, and led to the formation of four different volcaniclastic soils: pozzolana, pumice, lapillus and scoria. The pozzolana is the most widespread soil in the Campi Flegrei and surrounding areas and is mainly formed by ash with a minor percentage of pumiceous lapilli. Pumiceous lapilli prevail in the pumices, as do lithic lapilli in the lapilli and scoriaceous in the scoriae. The lapilli are mostly present along the coast of the gulf of Naples. The pozzolana has often undergone weathering and rill-wash processes, and has been carried away, far from the original deposition site. Depending upon the intensity of such a process, the grain size becomes finer with respect to that remaining in the original condition.

Croce and Pellegrino (1967) distinguished six homogeneous geotechnical zones in Naples (fig. 2), characterized by a tuff formation deepening or disappearing towards NE and SW. The pozzolana is almost everywhere, but soil covering can include sands along the coast (zone 5), and alternations of volcanic soils, alluvial soils and organic materials (zones 3, 6).

The test area, chosen to estimate the seismic ground response, is a flat area in the eastern district of Naples (zone 6), delimited to the South by the gulf of Naples, to the East by the flanks of Vesuvius and to the North by the hills of Capodimonte and Capodichino. The water table is at a depth of a few meters. Several laboratory and field measurements have been conducted on pyroclastic materials of the Campi Flegrei (Guadagno *et al.*, 1992), and in particular in our test area (Vinale, 1988), to define the geometry of the subsoil structures, and the physical (density, porosity, grain size, water content, etc.) and dynamic (*S*-wave velocities and damping ratios) properties of the materials.

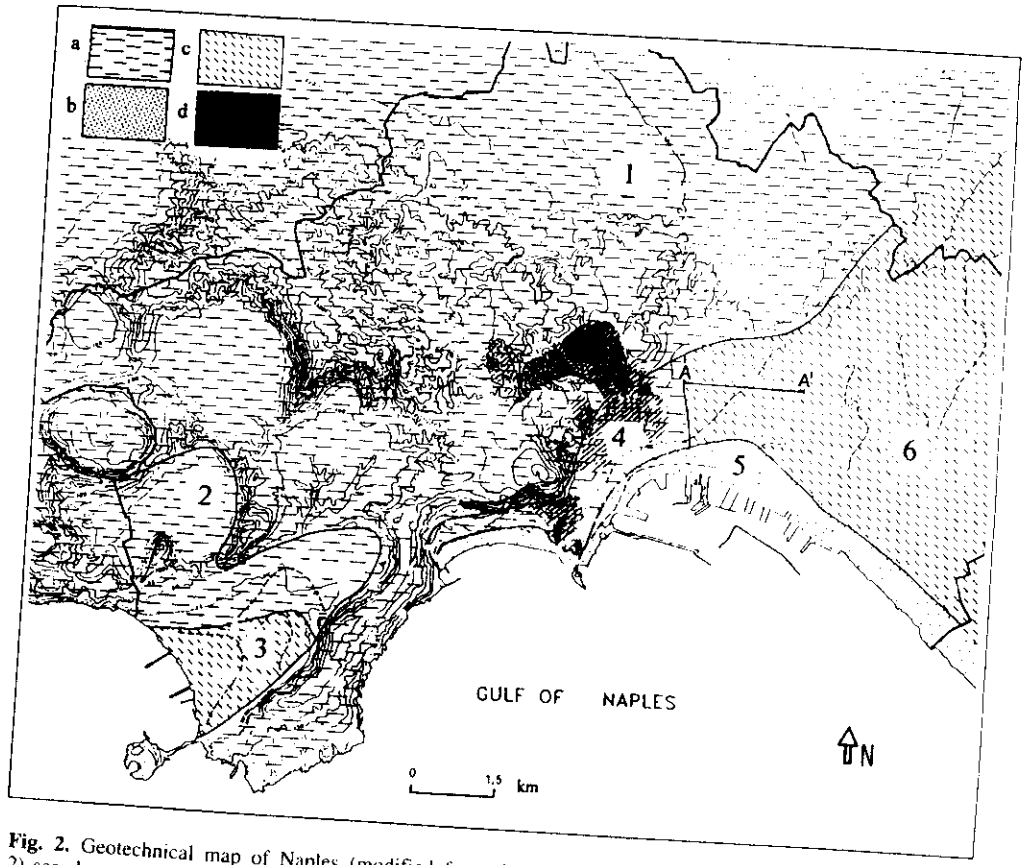

Fig. 2. Geotechnical map of Naples (modified from Croce and Pellegrino, 1967). Legend: 1) Pozzolana; 2) sea-shore sand; 3) alternations of volcanic soils, alluvial soils and organic materials; 4) cavities.

The reconstruction of the main geological pattern is shown along a N86°W profile (fig. 3). The subsoil is mainly formed by man-made ground, alluvial soils (ashes, stratified sands, peat), loose and slightly cemented pozzolanas, yellow tuff and marine sands. The eastern area of Naples was a marsh, supplied by the Sebeto river and small streams, recently drained both for urban development and for the reduction of water supply. Water channels were later filled with a variety of materials: bricks and waste materials. The alluvial cover is formed by volcanic soils, moved away by streams and redeposited with different texture.

4. Seismic response

The causative fault of the 1980 earthquake is located about 90 km from the cross-section,

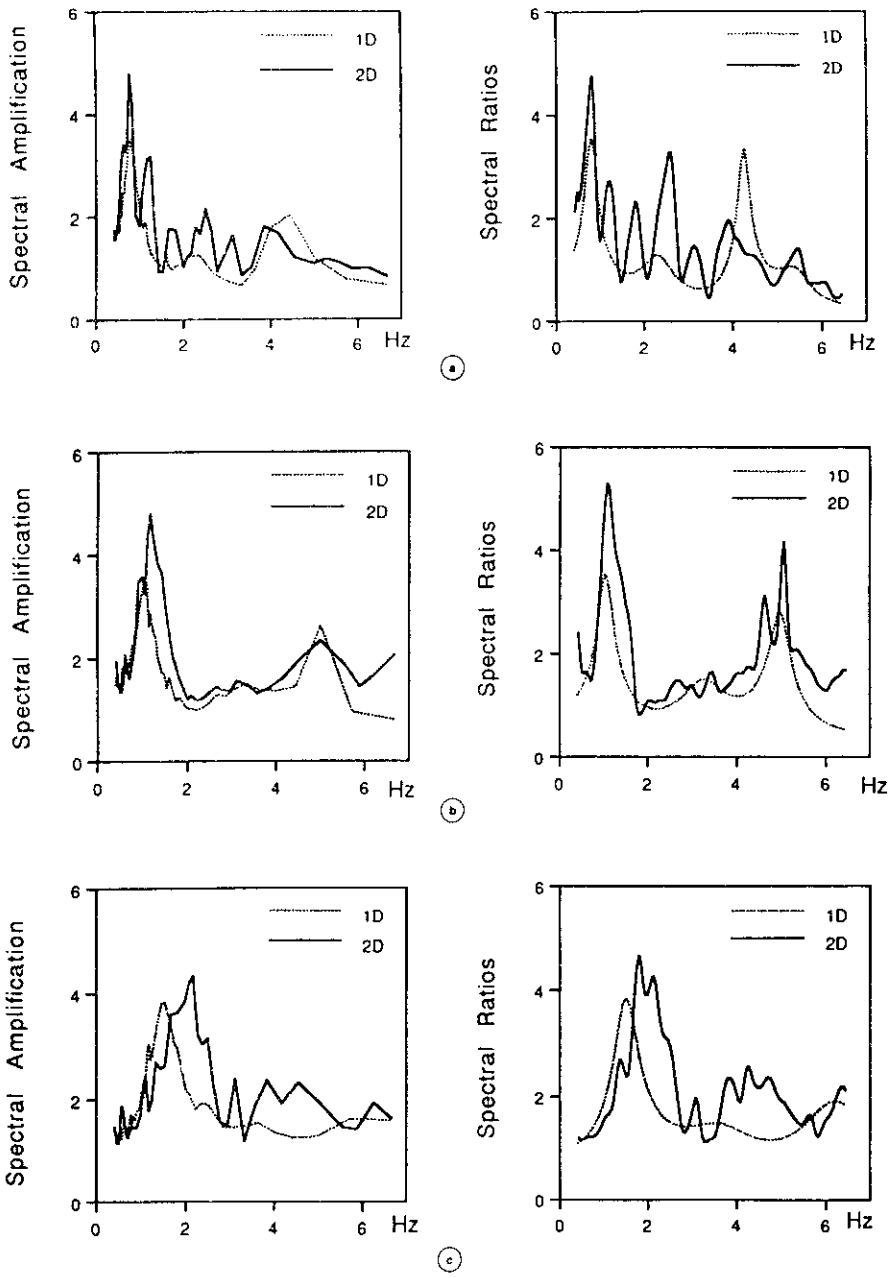

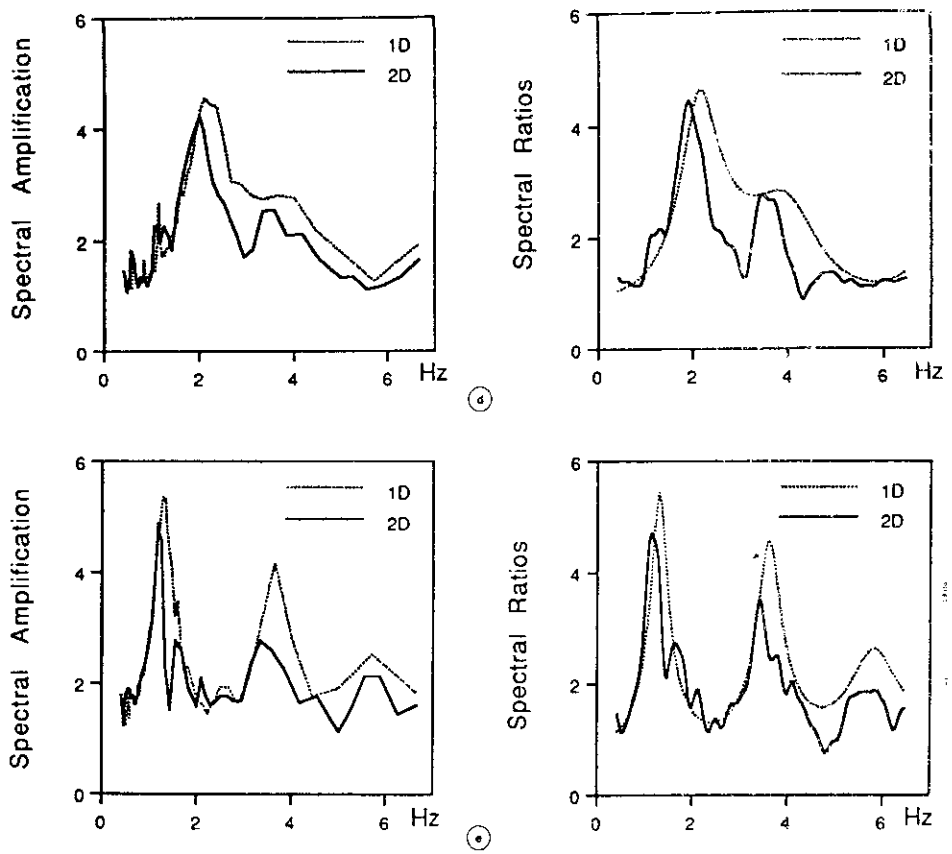

Fig. 7a-e. Spectral amplification for zero damping and spectral ratios computed with method 1 and method 2 at site R7 (a), at site R17 (b), at site R23 (c), at site R26 (d), at site R33 (e) (see fig. 3 for location). As in figs. 5 and 6, spectral ratios are smoothed; this is not the case for spectral amplifications, therefore spectral amplifications represent a quite reliable parameter, much more stable than spectral ratios.

seismogenic areas to suffer serious damage both because of the degraded conditions of the historical built-up environment and because severe local site amplification occurs. On the other hand, the high density of population and the kind of built-up environment to be protected increase the vulnerability of some areas of Naples, and consequently the seismic risk. Vulnerability may be reduced through the retrofitting of ancient buildings and monuments and through the design of reinforced concrete structures able to resist seismic shaking. Serious regulations are required since monuments must not be damaged by random injections of concrete. Sound anti-seismic criteria can be reliably based only on the knowledge of site seismic response, both in terms of peak ground acceleration and frequency content.

Ground motion modelling made with complete *SH*-wave seismograms shows that the superficial soil deposits composed of pyroclastic

Table 1. The 1-D model representative of the path from the source of Irpinia earthquake to the city of Naples (from Vaccari *et al.*, 1990).

Thickness (km)	Density (g/cm^3)	*P*-wave velocity (km/s)	*P*-wave attenuation	*S*-wave velocity (km/s)	*S*-wave attenuation
.50000E–01	.21200E+01	.15500E+01	.64516E–02	.90000E+00	.27778E–01
.20000E+00	.21200E+01	.19000E+01	.52632E–02	.11000E+01	.22727E–01
.25000E+00	.21400E+01	.22500E+01	.29630E–02	.13000E+01	.12821E–01
.25000E+00	.21600E+01	.26000E+01	.25641E–02	.15000E+01	.11111E–01
.25000E+00	.21800E+01	.27000E+01	.74074E–03	.17000E+01	.29412E–02
.25000E+00	.22000E+01	.28000E+01	.71429E–03	.17500E+01	.28571E–02
.25000E+00	.22200E+01	.29000E+01	.68966E–03	.18000E+01	.27778E–02
.25000E+00	.22400E+01	.30000E+01	.66667E–03	.18500E+01	.27027E–02
.25000E+00	.22600E+01	.31000E+01	.64516E–03	.19000E+01	.26316E–02
.25000E+00	.22800E+01	.32000E+01	.62500E–03	.19500E+01	.25641E–02
.25000E+00	.23000E+01	.33000E+01	.60606E–03	.20000E+01	.25000E–02
.25000E+00	.23200E+01	.34000E+01	.58824E–03	.20500E+01	.24390E–02
.25000E+00	.23400E+01	.35000E+01	.57143E–03	.21000E+01	.23810E–02
.25000E+00	.23600E+01	.36000E+01	.55556E–03	.21500E+01	.23256E–02
.25000E+00	.23800E+01	.37000E+01	.54054E–03	.22000E+01	.22727E–02
.25000E+00	.24000E+01	.38000E+01	.52632E–03	.22500E+01	.22222E–02
.25000E+00	.24200E+01	.39000E+01	.51282E–03	.23000E+01	.21739E–02
.25000E+00	.24400E+01	.40000E+01	.50000E–03	.23500E+01	.21277E–02
.25000E+00	.24600E+01	.41000E+01	.48780E–03	.24000E+01	.20833E–02
.25000E+00	.24800E+01	.42000E+01	.47619E–03	.24500E+01	.20408E–02
.25000E+00	.25000E+01	.43000E+01	.46512E–03	.25000E+01	.20000E–02
.25000E+00	.25200E+01	.44000E+01	.45455E–03	.25500E+01	.19608E–02
.25000E+00	.25400E+01	.45000E+01	.44444E–03	.26000E+01	.19231E–02
.25000E+00	.25600E+01	.46000E+01	.43478E–03	.26500E+01	.18868E–02
.25800E+00	.25800E+01	.47000E+01	.42553E–03	.27000E+01	.18519E–02
.25000E+00	.26000E+01	.48000E+01	.41667E–03	.27500E+01	.18182E–02
.25000E+00	.26200E+01	.49000E+01	.40816E–03	.28000E+01	.17857E–02
.25000E+00	.26400E+01	.50000E+01	.40000E–03	.28500E+01	.17544E–02
.25000E+00	.26600E+01	.51000E+01	.39216E–03	.29000E+01	.17241E–02

frequencies slightly higher than 1 Hz (receivers R17 and R33), and to frequencies around 2 Hz (receivers R23 and R26). The maximum amplification factor of the ground motion is in general around five, and this value is exceeded only at receiver R17. A secondary significant peak is present at higher frequencies, between 2 Hz and 3 Hz at receiver R7, between 3 Hz and 4 Hz at receivers R26 and R33, and around 5 Hz for receiver R17. The damping effect of the peat layer is clearly shown by the comparison of the spectral ratios computed at the same

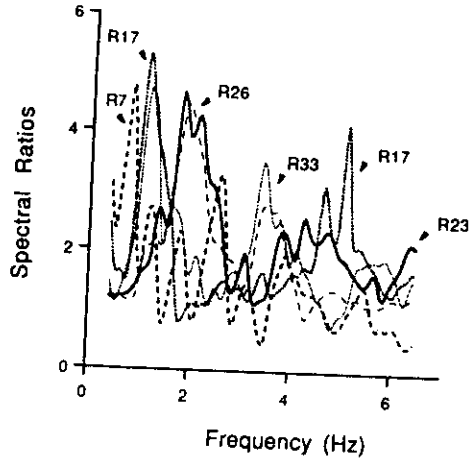

Fig. 5. Spectral ratios computed with the hybrid method at sites R7, R17, R23, R26, R33.

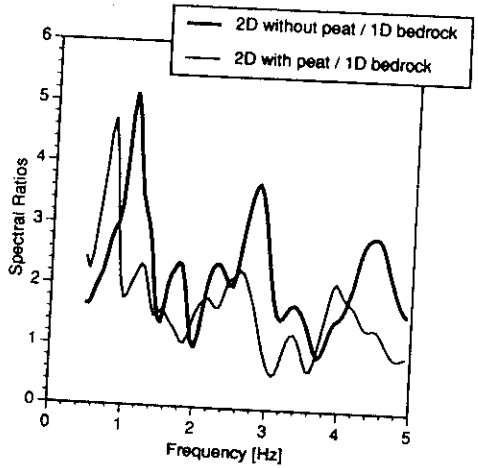

Fig. 6. Example of the effect due to the presence of the peat layer at site R9.

receiver R9 when the peat layer is removed (fig. 6). The maximum peak increases in amplitude and is shifted towards higher frequencies, when the peat layer is removed. The peat layer, even though with a thickness of only 3 m, significantly reduces the amplification effects induced by the unconsolidated sediments.

The discrepancies between the amplifications computed with method 1 and method 2 are illustrated in fig. 7a-e. At receiver R7, the dominant peak is estimated at the same frequency by both methods, but the amplitude obtained with method 1 is 30% smaller than that obtained with method 2. Moreover, other peaks, at frequencies which are very important for engineering purposes, and clearly visible in the results obtained with the hybrid method, are absent in the modelling made with method 1. The spectral ratios and the spectral amplifications for zero damping, obtained with method 1 and method 2, have similar peaks at receiver R17, but the amplification computed with the 1-D method is underestimated with respect to that determined with the 2-D method. At receiver R23 a frequency shift of the main peak is observed. The picture changes for receivers R26 and R33, as the spectral amplifications computed with method 1 overestimate those obtained with method 2, even if they have a similar shape.

5. Discussion

The main effort that is necessary to mitigate the seismic hazard is the definition of a correct seismic response, both in terms of peak ground acceleration and spectral amplifications. It is well known that these factors depend upon the mechanical characteristics of the local soil conditions, and the characteristics of the expected earthquake, like focal mechanism, hypocentral depth, epicentral distance, and magnitude or scalar seismic moment. The formulation of good building codes for engineers, should rely on the information which is supplied by many different disciplines, such as seismology, history, archeology, geology and geophysics. If properly used, synthetic seismograms may represent a fundamental tool to take into consideration most of this information simultaneously, with the important practical result of effectively reducing seismic vulnerability.

Naples represents a typical example of a non-seismogenic area, but close enough to

PROCEEDINGS OF
THE FIFTH INTERNATIONAL
CONFERENCE
ON

SEISMIC ZONATION

October 17-18-19, 1995
Nice, France

II

OUEST ÉDITIONS
Presses Académiques

PROCEEDINGS OF
THE FIFTH INTERNATIONAL
CONFERENCE ON
SEISMIC ZONATION

ISBN
2-908261-74-X

900 FF (160 USD
pour trois vol. / for three vc

OUEST ÉDITIONS
Presses Académiques

46

and alluvial materials, with lateral discontinuities, are responsible for an increase in amplitude and duration of the signal relative to the bedrock. Such an effect is reduced when a thin, laterally heterogeneous peat layer is present. Peak ground accelerations on rock sites and on surficial soil deposits with peat are similar, and they are about half of those observed on soil deposits without peat. Relevant differences are observed in the time series computed along the 2-D structure and they are even more clear when the seismic ground motion is considered in the frequency domain (fig. 5). It is evident that the unconsolidated sediments amplify particular frequencies contained in the seismogram computed for the 1-D reference model. Hence the built-up environment along the profile has to resist shear stresses up to five times larger than that on the rock site.

6. Conclusions

As a first step for the mitigation of seismic risk, the seismic ground motion of a flat test area in the eastern sector of Naples was modeled along a profile trending N86°W, considering as source the main shock of the 1980 Irpinia earthquake. Discrepancies are found between the amplifications computed with the 1-D standard method (method 1) and the more realistic 2-D hybrid method (method 2). These differences cannot be ignored when formulating building codes and retrofitting the old built-up environment. In the presence of a peat layer, for the dominant peak, the amplifications computed with method 1 are smaller than the ones computed with the more realistic method 2, while for the second significant peak random mismatches are observed. This is a clear evidence of the danger intrinsic in the application of method 1 for vulnerability assessment, even in a flat area. When the peat layer is absent, a similarity exists in the shape of the spectral amplification functions computed with the two methods, but method 1 overestimates the effects with respect to the more realistic method 2. Thus the use of the guidelines based on method 1, may imply unnecessary, higher costs for the reduction of vulnerability.

Acknowledgements

We would like to thank Dr. Claudio Iodice for his contribution to this research, and Dr. J. Vidale for his useful suggestions. We are grateful to ENEA for allowing us the use of the IBM3090E computer at the ENEA INFO BO Computer Center. D.F. has been supported by the Swiss National Science Foundation under Grant No. 8220-037189. This study has been made possible by CNR contracts 91.02692.CT15, 91.02550.PF54, 92.02867.PF54, 92.02876.54, and EEC-EPOCH contract EPOC-CT91-0042. This research has been carried out in the framework of the ILP Task Group II.4 contributions to the IDNDR project «Physical Instability of Megacities».

REFERENCES

Annali di Geofisica (1993): Special issue on the meeting «*Irpinia Dieci Anni Dopo*», Sorrento, November 19-24, 1990, **36** (1), 1-351.

CROCE, A. and A. PELLEGRINO (1967): Il sottosuolo della citta' di Napoli. Caratterizzazione geotecnica del territorio urbano, Ass. Geotecnica Italiana, in *Atti VIII Convegno di Geotecnica*, 233-253.

ESPOSITO, E., S. PORFIDO, G. LUONGO and S.M. PETRAZZUOLI (1992): Damage scenarios induced by the major seismic events from XV to XIX century in Naples city with particular reference to the seismic response, *Earthquake Engineering, Tenth World Conference*, 1075-1080.

FÄH, D. (1992): A hybrid technique for the estimation of strong ground motion in sedimentary basins, *Ph.D. Thesis* No. 9767, Swiss Federal Institute of Technology, Zurich.

FÄH, D., P. SUHADOLC and G.F. PANZA (1993a): Variability of seismic ground motion in complex media: the case of a sedimentary basin in the Friuli (Italy) area, *J. Appl. Geophys.*, **30**, 131-148.

FÄH, D., C. IODICE, P. SUHADOLC and G.F. PANZA (1993b): A new method for the realistic estimation of seismic ground motion in megacities: the case of Rome, *Earthquake Spectra*, **9** (4), 643-668.

FLORSCH, N., D. FÄH D., P. SUHADOLC and G.F. PANZA (1991): Complete synthetic seismograms for high-frequency multimode *SH*-waves, *PAGEOPH*, **136**, 529-560.

GUADAGNO, F.M., C. NUNZIATA and A. RAPOLLA (1992): Dynamic parameters of volcaniclastic soils and rocks of Campi Flegrei (Naples, Italy), Volcanic seismology, in *IAVCEI Proceedings in Volcanology* (Springer-Verlag), 533-546.

PANZA, G.F. (1985): Synthetic seismograms: The Rayleigh waves modal summation, *J. Geophys.*, **58**, 125-145.

PANZA, G.F. (1991): The theory and some appplications of synthetic seismograms to strong motion data and macroseismic informations, in *Earthquake Hazard Assessment, Proceedings European School, Athens, May 1988*, edited by R. FANTECHI and M.E. ALMEIDA-TEIXEIRA, Commission of the European Communities, 65-78.

PANZA, G.F. and P. SUHADOLC (1988): Prediction of strong ground motion and macroseismic intensity from assigned source and structural models, Senior Adv. ECE Governements on Science and Technology, Lisbon 1988, *Sc. Tech./Sem.* 16/R.21, 16.

PANZA, G.F., A. CRAGLIETTO and P. SUHADOLC (1991): Source geometry of historical events retrieved by synthetic isoseismals, *Tectonophysics*, **192**, 173-184.

PINGUE, F., G. DE NATALE and P. BRIOLE (1993): Modeling of the 1980 Irpinia earthquake source: constraints from geodetic data, *Annali di Geofisica*, **36** (1), 27-40.

RIPPA, F. and F. VINALE (1983): Effetti del terremoto del 23 Novembre 1980 sul patrimonio edilizio di Napoli, Ass. Geotecnica Italiana, in *Atti XV Convegno Nazionale di Geotecnica*, 193-206.

SCHNABEL, B., J. LYSMER and H. SEED (1972): Shake: a computer program for earthquake response analysis of horizontally layered sites, Rep. EERC 70-10, Earthquake Engineering Research Center, University of California, Berkeley.

SUHADOLC, P. and C. CHIARUTTINI (1985): A theoretical study of the dependence of the peak ground acceleration on source and structure parameters, in *Strong Ground Motion Seismology*, edited by M.O. ERDIK and M.N. TOKSOZ, 143-183, NATO ASI series C, 204.

SUHADOLC, P., L. CERNOBORI, G. PAZZI and G.F. PANZA (1988): Synthetic isoseismals: application to Italian earthquakes, in *Seismic Hazard in Mediterranean Regions*, edited by J. BONNIN, M. CARA, A. CISTERNAS and R. FANTECHI (Kluwer, Dordrecht), 205-228.

VACCARI, F., P. SUHADOLC and G.F. PANZA (1990): Irpinia, Italy, 1980 earthquake: waveform modelling of strong motion data, *Geophys. J. Int.*, **101**, 631-647.

VINALE, F. (1988): Caratterizzazione del sottosuolo di un'area campione di Napoli ai fini d'una microzonazione sismica, *Riv. Ital. Geotecnica*, **22**, 77-100.

over the central part of the Paleotiber basin. The *zones 5* and *6* include areas which are located outside the large basins of the Tiber and Paleotiber where we distinguish between areas (5) without and (6) with a layer of volcanic rocks close to the surface. These zones can be recognized also in the sections considered in relation with the events located in the Carseolani Mountains and the Alban Hills (Fig.1).

For all the receivers located in each of the six zones defined above, and for all the two-dimensional models, shown in Fig.1, and the studied events, the spectral amplification Sa(2D)/Sa(bedrock) has been computed. From these values the average and the maximum spectral amplification, which are shown in Fig.2, for zero and 5% damping of the oscillator, are determined for each given zone.

The greatest spectral amplification is observed at the edges of the sedimentary basin of the Tiber river (zone 1), for frequencies between 2.0 and 2.5 Hz. The maximum spectral amplification with respect to the bedrock model varies between 5 and 6, and it is due to the combination of resonance effects with the excitation of local surface waves. The general shape of the maximum and average spectral amplifications are similar for zone 1 and 2. In the frequency range from 1.0 Hz to 3.0 Hz, the maximum spectral amplification is of the order of 4 and the average spectral amplification is of the order of 2.

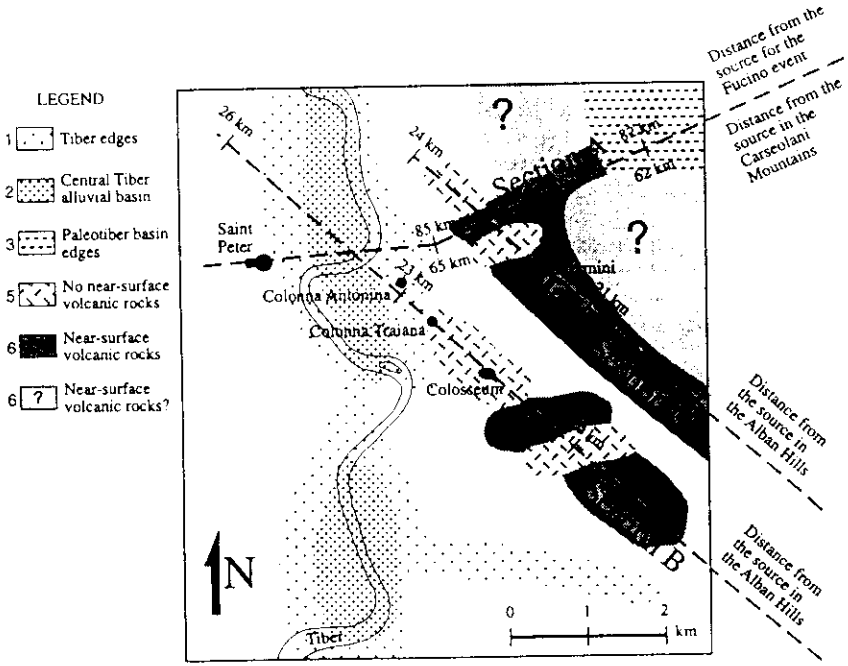

Fig.3: Microzoning for the city of Rome.

Similar observations can be done for the Paleotiber basin (zones 3 and 4), but in different frequency band (0.4-1.0 Hz). The buried sedimentary complex (Sicilian) cause maximum spectral amplification between 3 and 4, due to resonance effects. These are most pronounced at frequencies around 0.6 Hz. Therefore, the presence of a near-surface layer of rigid material in the Paleotiber basin is not sufficient to classify that area as "hard-rock site". A correct zonation requires the knowledge of both the thickness of the surficial layer and of the deeper parts of the structure, down to the real bedrock. This is especially important in volcanic areas, where pyroclastic material often covers alluvial basins. The maximum spectral amplification is larger at the edges of the Paleotiber basin (zone 3). For frequencies above 1.0 Hz, in the Paleotiber basin (zone 4), the volcanic layer acts as a shield reflecting part of the incoming energy, and the values of the average spectral amplification are smaller than 1.

For the sites in the zones 5 and 6, the maximum and the average spectral amplifications are small for frequencies below 1 Hz. Since the sedimentary cover in these zones is thin, the amplification takes place at frequencies above 1.5 Hz, and changes rapidly from site to site. This rapid variation leads to average values of the order of 1.0 - 1.5. The zoning performed along the three sections can be extrapolated, with cautions, to a larger area using the information available on geological and geotechnical conditions. The result of such tentative extrapolation is shown in Fig.3.

Thus, in absence of instrumental data, and without having to await for a strong earthquake to occur, a realistic numerical simulation of the ground motion, can be used for the first order microzonation of Rome. The highest values of the spectral amplification are observed at the edges of the sedimentary basin of the Tiber, strong amplification are observed in the Tiber's river bed. This is caused by the large amplitude and long duration of the ground motion due to (1) the low impedance of the alluvial sediments, (2) resonance effects, and (3) the excitation of local surface waves. The presence of a near-surface volcanic layer of rigid material is not sufficient to classify a location as a "hard-rock site", since the existence of an underlying sedimentary complex can cause amplifications due to resonance effects. A correct zonation requires the knowledge of both the thickness of the surficial layer and of the deeper parts of the structure, down to real bedrock. This is especially important in volcanic areas, where lava flows often cover alluvial basins.

Modelling of ground motion in Naples

Naples is not within a seismogenetic area of the Southern Apennines, but it has often been severely damaged by Apennines earthquakes. The last strong event, November 23, 1980 (M_S=6.9), produced serious damage in Naples, and mostly in the historical centre and in the eastern area (Rippa and Vinale, 1983), where a ten-storied building was completely destroyed causing tens of human deaths. For the historical buildings, the damage distribution is easily explained by their degraded conditions, but for the most damaged buildings of the eastern district, which are tall and made in reinforced concrete it is necessary to consider the combined effects of the incident wavefield, the local soil conditions and the properties of the buildings. The nearest available accelerogram was recorded at a seismic station set on a lava deposit at Torre del Greco, on the flanks of Vesuvius, about 20 km far from Naples and closer to the epicentral zone. Thus, at present, the only possibility for a detailed zoning for the town of Naples, that accordingly

REDUCTION OF SEISMIC VULNERABILITY OF MEGACITIES: THE CASES OF ROME AND NAPLES

Franco Vaccari[*,**,***], Concettina Nunziata[****], Donat Fäh[*****], Giuliano Francesco Panza[*,***]

Abstract: A hybrid technique, based on mode summation and finite differences, is used to simulate the ground motion induced in Rome and Naples by strong earthquakes (1915, Fucino and 1980, Irpinia) occurring in the Apennines. For the city of Rome we consider also earthquakes occurring in the Alban Hills.

Microzoning in Rome

In addition to the Central Apennines, whose earthquakes caused in the town maximum intensity VII-VIII (MCS) and may generate significant perturbations at long period, the most important seismogenetic zone which can cause structural damage in Rome are the Alban Hills (observed maximum MCS in Rome VI-VII) (Molin et al., 1986). Therefore, the source positions used in this study include (1) the epicenter of the January 13, 1915 Fucino earthquake, (2) the Carseolani Mountains where, from the study of pattern recognition (Caputo et al., 1980), a strong earthquake is expected to occur, and (3) the Alban Hills. The source mechanisms assigned to these earthquakes are the mechanism of the Fucino earthquake (Gasparini et al., 1985) for event 1 and 2, and the mechanism of a recent earthquake in the Alban Hills (Amato et al., 1984) for event 3. Synthetic seismograms have been computed along the three cross-sections shown in Fig.1 using the hybrid approach developed by Fäh (1992), which combines the advantages of mode summation and finite differences. The distances from the three seismogenetic zones are also given for each section.

For a first order microzoning of the town we consider the relative spectral accelerations or spectral amplification Sa(2D)/Sa(bedrock), computed along the profiles. Sa(2D) indicates the spectral acceleration computed for the two-dimensional models shown in Fig.1, while Sa(bedrock) indicates the spectral acceleration obtained for the one-dimensional reference bedrock models given by Fäh et al. (1993).

For each source, in order to remove the effects of the radiation pattern and of the regional propagation, Sa(2D) is always normalized with respect to the corresponding quantity, Sa(bedrock), computed in the reference bedrock model at the given source-receiver distance.

For general microzonation purposes, using the results obtained from the modelling of the Fucino event it is possible to define the six zones shown in Fig.1: (1) *zone 1* includes the edges of the Tiber river, (2) *zone 2* extends over the central part of the alluvial basin of the Tiber, (3) *zone 3* includes the edges of the Paleotiber basin, and (4) *zone 4* extends

* Ist. di Geodesia e Geofisica, Università degli Studi di Trieste, Trieste, Italia
** CNR-GNDT - Gruppo Nazionale per la Difesa dai Terremoti, Roma, Italia
*** ICTP - International Centre for Theoretical Physics, Trieste, Italia
**** Dip. di Geofisica e Vulcanologia, Università di Napoli "Federico II", Napoli, Italia
***** Institut für Geophysik, ETH-Hönggerberg, Zürich, Switzerland

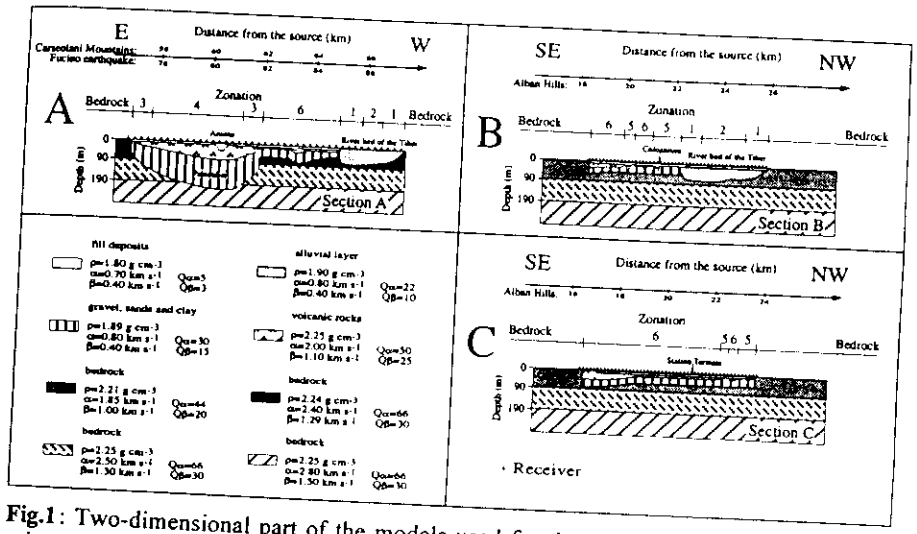

Fig.1: Two-dimensional part of the models used for the computation of the synthetic seismograms with the hybrid method. Only the part near to the surface is shown, where the 2D model deviates from the horizontally-layered reference models. The general microzonation is explained in the text.

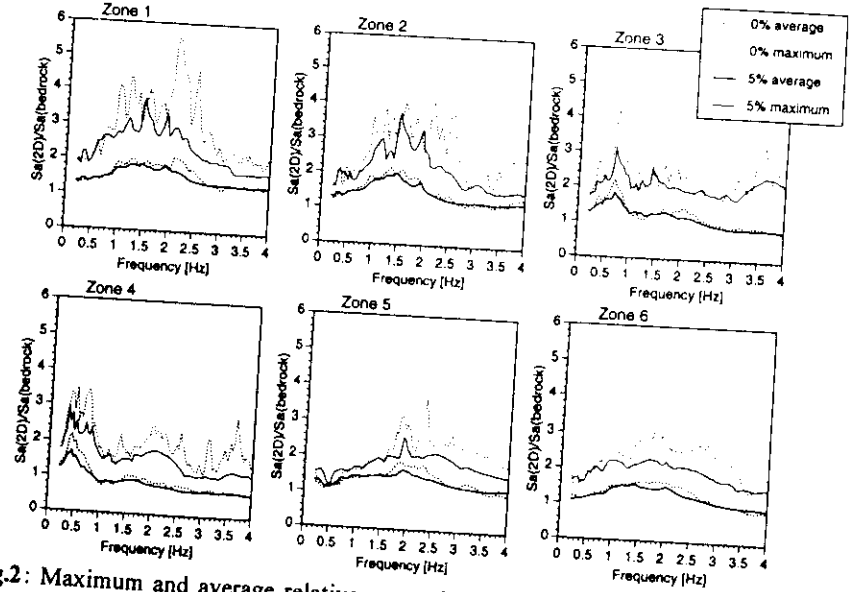

Fig.2: Maximum and average relative spectral accelerations for the zones defined in Fig.1, for zero damping and 5% damping.

The presence of unconsolidated sediments causes an increase of the signal's amplitudes and duration, more pronounced for the model without the peat layer. For the model with the peat layer, between receivers 1 and 15, the maximum amplitudes are similar to the maximum amplitudes observed for the one-dimensional bedrock model.

The amplification effects as function of frequency can be identified through the analysis of the spectral ratios and of the spectral amplification for zero damping, therefore these quantities have been computed in correspondence of the position of 5 receivers, representative of different stratigraphies in the 2-D section. Looking at the spectral ratios at the chosen receivers (R7, R17, R23, R26, R33) it is quite evident the large variability of ground motion within a few hundred meters (Fig.5). The main peak moves from frequencies less than 1 Hz, receiver R7, where the peat layer reaches the maximum thickness, to frequencies slightly higher than 1 Hz, receivers R17 and R33, and to frequencies around 2 Hz, receivers R23 and R26. The amplification factor of the ground motion is in general around five, and this value is exceeded only at receiver R17. A secondary significant peak is present at higher frequencies, between 2Hz and 3Hz at receiver R7, between 3Hz and 4Hz at receivers R26 and R33, and around 5Hz for receiver R17.

The damping effect of peat is clearly shown by the comparison of the spectral ratios computed at the same receiver R9 when the peat layer is removed (Fig.6). The maximum peak increases in amplitude and is shifted towards higher frequencies, when the peat layer is removed. The peat layer, even though with a thickness of only 3m, reduces significantly the amplification effects induced by the unconsolidated sediments.

Conclusions

The seismic vulnerability of a megacities like Rome and Naples, with a large cultural heritage and a very high number of people to safeguard, can be drastically reduced, without having to await for a strong earthquake to occur. The method used is, in fact, the only existing quantitative procedure that permits to compute reliable complete seismograms, that takes into account the propagation effects, including detailed local conditions and anelastic behaviour of soils, from which to obtain realistic seismic response, to be used for engineering purposes.

The results of the numerical simulations are used for a first order seismic microzonation in the city of Rome, which can be used for the retrofitting of buildings of special social and cultural value. Rome can be divided into six main zones: (1) the edges and (2) the central part of the alluvial basin of the river Tiber; (3) the edges and (4) the central part of the Paleotiber basin; the areas outside the large basins of the Tiber and Paleotiber, where we distinguish between (5) areas without, and (6) areas with a layer of volcanic rocks close to the surface. The strongest amplification effects have to be expected at the edges of the Tiber basin, with maximum spectral amplification of the order of 5 to 6, and strong amplifications occur inside the entire alluvial basin of the Tiber. The presence of a near-surface layer of rigid material is not sufficient to classify a location as a "hard-rock site", when the rigid material covers a sedimentary complex. The reason is that the underlying sedimentary complex causes amplifications at the surface due to resonance effects. This phenomenon can be observed in the Paleotiber basin, where spectral amplifications in the frequency range 0.3-1.0 Hz reach values of the order of 3 to 4.

50

In the eastern district of Naples, where the sub-soil is mainly formed by alluvial and pyroclastic materials overlying a pyroclastic rock representing the bedrock, the local seismic response is given in the form of spectral ratios and spectral amplifications for undamped oscillators. The comparison performed between the two-dimensional seismic response and a standard one-dimensional response, based on the vertical propagation of SH waves in a plane layered structure, suggests to take serious caution in the formulation of the appropriate seismic regulations to be adopted to reduce the seismic vulnerability of Naples, since commonly used methods, like for instance the vertical incidence of wavefield, can lead to very erroneous conclusions.

Acknowledgments

We acknowledge support by EU contracts EV5V-CT94-0491 and EV5V-0513, and CNR grants 92.02867.CT54 and 93.02492.CT54. Research carried out in the framework of ILP Task Group II.4 contribution to the IDNDR project "Physical Instability of Megacities".

Bibliography

Amato A., De Simoni B. and Gasparini C. (1984). *Considerazioni sulla sismicità dei Colli Albani*. Atti del 3° Convegno del Gruppo Nazionale di Geofisica della Terra Solida, CNR, Roma, 2, 965-976.

Bernard P. and Zollo A. (1989). *The Irpinia (Italy) 1980 earthquake: detailed analysis of a complex normal faulting*. J. Geophys. Res., 94, 1631-1647.

Caputo M. Keilis-Borok V., Oficerova E., Ranzman E., Rotwain I. and Solovjeff A. (1980). *Pattern recognition of earthquake-prone areas in Italy*. Phys. Earth. Planet. Int., 21, 305-320.

Fäh D. (1992). *A hybrid technique for the estimation of strong ground motion in sedimentary basins*. Ph.D. thesis Nr. 9767, Swiss Federal Institute of Technology, Zurich.

Fäh D., C. Iodice, P. Suhadolc and Panza G.F. (1993). *A new method for the realistic estimation of seismic ground motion in megacities: the case of Rome*. Earthquake Spectra, 9, 643-668.

Gasparini C., Iannaccone G. and Scarpa R. (1985). *Fault-plane solutions and seismicity of the Italian peninsula*. Tectonophysics, 117, 59-78.

Guadagno F. M., C. Nunziata and Rapolla A. (1992). *Dynamic parameters of volcaniclastic soils and rocks of Campi Flegrei (Naples, Italy)*. Volcanic seismology. IAVCEI Proceedings in volcanology. Springer-Verlag, 533-546.

Molin D., Ambrosini S., Castenetto S., Di Loreto E., Liperi L. and Paciello A. (1986) *Aspetti della sismicità storica di Roma*. Mem. Soc. Geol. It., 35, 439-444.

Nunziata C., Fäh D. and Panza G.F. (1994). *Reduction of seismic vulnerability of a megacity: the case of Naples*. In preparation.

Rippa F. and Vinale F. (1983). *Effetti del terremoto del 23 Novembre 1980 sul patrimonio edilizio di Napoli*. Ass. Geotecnica Italiana, Atti XV Convegno Nazionale di Geotecnica, 193-206.

Vaccari F., Suhadolc P. and Panza G.F. (1990). *Irpinia, Italy, 1980 earthquake. waveform modelling of strong motion data*. Geophys. J. Int., 101, 631-647.

Vinale F. (1988). *Caratterizzazione del sottosuolo di un'area campione di Napoli ai fini d'una microzonazione sismica*. Rivista Italiana di Geotecnica, 22, 77-100.

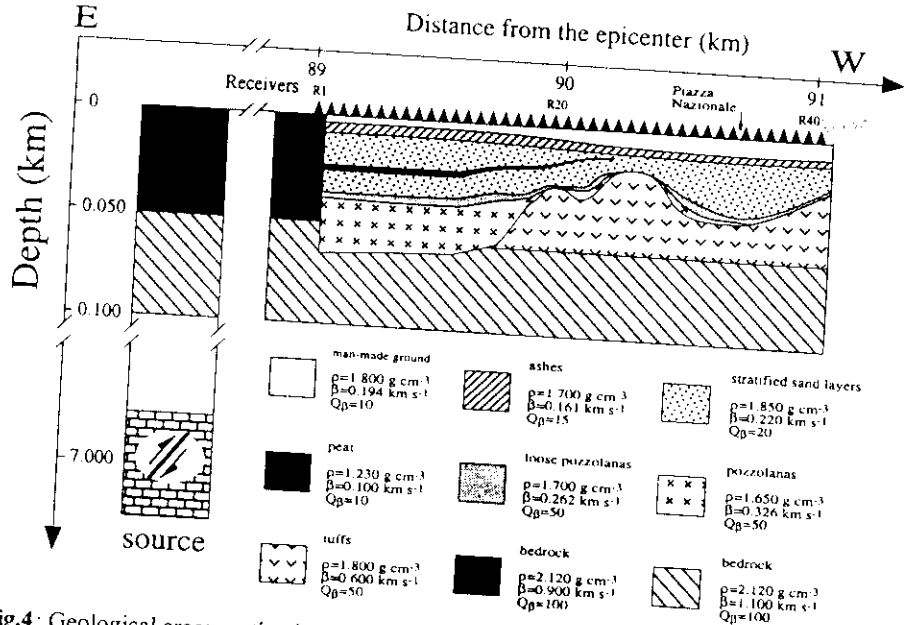

Fig.4: Geological cross-section in the eastern district of Naples, used in the computations.

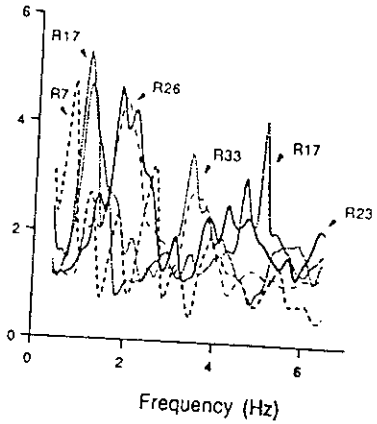

Fig.5: Smoothed spectral ratios computed with the hybrid method at the sites R7, R17, R23, R26, R33 (see Fig.4 for their location).

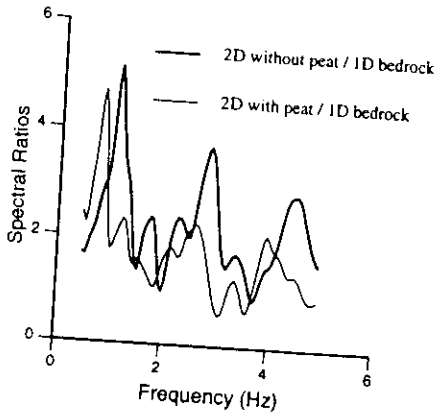

Fig.6: Example of the effect of the peat at site R9 (see Fig.4 for its location), with respect to its removal. Smoothing applied.

with historical records may experience a shaking of intensity VIII on the MCS scale, is given by the use of realistic synthetic seismograms.

Our aim here is (1) to perform the numerical modelling of the propagation of the wavefield, generated by the main rupture event of the 1980 earthquake, up to a profile trending N86°W, and located in a test area in the eastern district of Naples, and (2) to make an accurate and realistic evaluation of the seismic ground motion, taking into account the significant lateral variations, which are present in the subsoil of this urban area.

Naples is located on volcaniclastic soils and rocks (various types of tuffs) erupted by the Campi Flegrei volcano. The original material, forming the tuffs and the volcanic soils, is in general the same, with the volcaniclastic rocks being the result of the hardening of the volcaniclastic soils by hydrothermal post depositional phenomena. The tuff formation is often outcropping or is located some tens of metres deep from the ground surface. It has a thickness that ranges from twenty metres, in the eastern district, to two hundred metres under the Posillipo hill. The different volcanic products are always present in a variable composition, and led to the formation of four different volcaniclastic soils: pozzolana, pumice, lapillus and scoria (Nunziata et al., 1994).

The test area, in the eastern district of Naples, is a flat area delimited to the South by the gulf of Naples, to the East by the flanks of Vesuvius and to the North by the hills of Capodimonte and Capodichino. The water table is at a depth of a few meters. Several laboratory and field measurements have been conducted on pyroclastic materials of the Campi Flegrei (Guadagno et al., 1992) and, in particular in the test area (Vinale, 1988), to define the geometry of the sub-soil structures, the physical (density, porosity, grain size, water content, etc.) and dynamic (S-wave velocities and damping ratios) properties of the materials. The reconstruction of the main geological pattern is shown along a N86°W profile (Fig.4). The sub-soil is mainly formed by man-made ground, alluvial soils (ashes, stratified sands, peat), loose and slightly cemented pozzolanas, yellow tuff and marine sands.

The causative fault of the 1980 earthquake is located about 90 km from the cross-section, representative of the eastern part of Naples, shown in Fig.4. The choice of the mechanism of the seismic source is made accordingly with the mechanism of the main event: a normal fault with little transcurrent component. Since there is no agreement between authors about the amount of strike-slip component (e.g. Bernard and Zollo, 1989; Vaccari et al., 1990), we adopted a pure normal fault with dip 65°, rake 270°, strike 315° and depth 7.0 km. The angle between the strike of the fault and the epicenter-cross section line is 36°.

The source is located in the laterally homogeneous part, and the propagation of the waves from the source up to the 2-D structure (Fig.4) is computed with the modal summation technique for the layered one-dimensional model representative of the path to the city of Naples (Vaccari et al., 1990). Acceleration time series for SH-waves are computed at an array of receivers over different cross-sections: (1) a one-dimensional reference model for the bedrock, which corresponds to the structural model for the region between the source position and Naples, (2) a two-dimensional model with a peat layer, and (3) a two-dimensional model without the peat layer. All scaling values are related to a source seismic moment of 10^{-7} Nm, and in each column, the signals are normalized to the same value. The distance between two receivers is 100 m.

SEISMIC INPUT MODELLING FOR ZONING AND MICROZONING

Giuliano Francesco PANZA, Franco VACCARI, Giovanni COSTA,
Peter SUHADOLC and Donat FÄH

Earthquake Spectra - August 1996 issue
in press

ABSTRACT

The strong influence of lateral heterogeneities and of source properties on the spatial distribution of ground motion indicates that the traditional methods require an alternative when earthquake records are not available. The computation of broad-band synthetic seismograms makes it possible, as required by a realistic modelling, to take source and propagation effects into account, fully utilizing the large amount of geological, geophysical and geotechnical data, already available. For recent earthquakes, where strong motion observations are available, it is possible to validate the modelling by comparing the synthetic seismograms with the experimental records. The realistic modelling of the seismic input has been applied to a first-order seismic zoning of the whole territory of several countries. Even though it falls in the domain of the deterministic approaches, the method is suitable to be used in new integrated procedures which combine probabilistic and deterministic approaches and allow us to minimize the present drawbacks which characterise them when they are considered separately. Detailed modelling of the ground motion for realistic heterogeneous media (up to 10 Hz) can be immediately used in the design of new seismo-resistant constructions and in the reinforcement of existing buildings, without having to wait for a strong earthquake to occur. The discrepancies between the ground responses computed with standard methods and the results of our detailed modelling cannot be ignored when formulating building codes and retrofitting the built environment.

1. INTRODUCTION

The guidelines of the United Nations sponsored International Decade for Natural Disaster Reduction (IDNDR), for the drawing up of pre-catastrophe plans of action, have led to the consolidation of the idea that zoning can and must be used as a means of prevention in areas that have not yet been hit by disaster but are potentially prone to it. The optimisation of techniques

(GFP,FV,GC,PS) Univ. di Trieste - Dip. di Scienze della Terra, via Weiss 1, I-34127 Trieste, Italy
(GFP,FV,GC,PS) ICTP, SAND Group, P.O.Box 586, I-34100 Trieste, Italy
(FV) CNR - Gruppo Nazionale per la Difesa dai Terremoti, via Nizza 128, I-00198 Roma, Italy
(DF) Institut für Geophysik - ETH Hönggerberg Zürich - CH-8093 Switzerland

F-5

acceleration, velocity and displacement in a given frequency band (AMAX, VMAX and DMAX respectively) or any other parameter relevant to seismic engineering, which can be extracted from the computed theoretical signals. This procedure allows us to obtain a realistic estimate of the seismic hazard also in those areas for which scarce (or no) historical or instrumental information is available, and to perform the relevant parametric analyses.

To reduce the amount of computations the seismic sources can be grouped into homogeneous seismogenic areas, and for each group the representative focal mechanism can be kept constant. The scalar seismic moment associated with each source is determined from the analysis of the maximum magnitude observed in the epicentral area. The flow-chart of the procedure is shown in Figure 2.1.

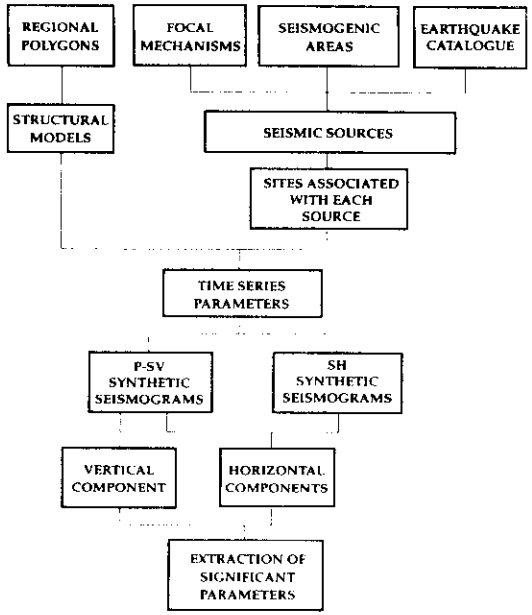

Figure 2.1 Flow chart describing the procedure for the first-order zoning of a territory (after Costa et al., 1993).

2.1.1. Synthetic models

The detailed description of the input data used in the procedure shown in Figure 2.1 is given by Costa et al. (1993) and Panza and Vaccari (1994). The NT file prepared by GNDT (Stucchi et al., 1993) and the ING (1980-1991) seismological reports are used for the definition of seismicity. The smoothed magnitude distribution for the cells belonging to the seismogenic zones defined by GNDT (1992) is given in Figure 2.2.

The synthetic signals are computed for an upper frequency limit of 1 Hz, and the point-source approximation is still acceptable. This is justified by practical considerations, since, for instance, several-story buildings might have a peak response in the frequency range around 1 Hz (e.g. Manos and Demosthenous, 1992) and by the fact that modern seismic design approaches and technologies, like seismic isolation, tend to lower the free oscillation frequencies of buildings.

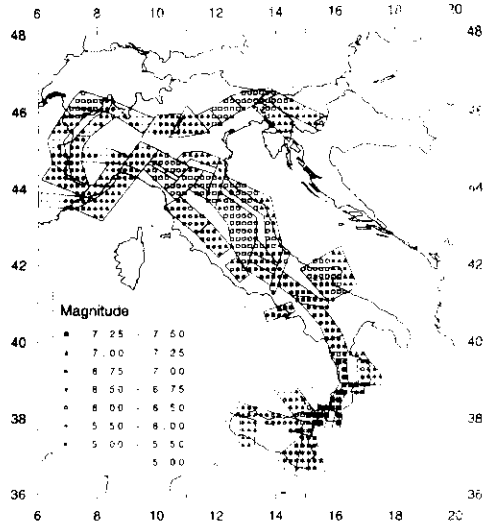

Figure 2.2 Smoothed magnitude distribution (Panza et al., 1990) for the cells belonging to the seismogenic zones defined by GNDT (1992).

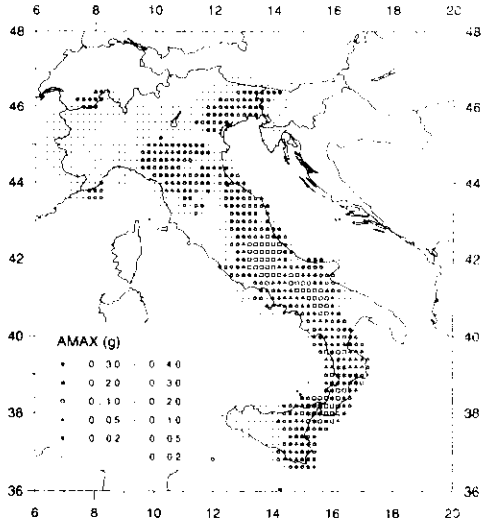

Figure 2.3a Horizontal AMAX (expressed in fractions of g, acceleration of gravity) distribution for Italy, obtained as a result of the application of the procedure described in Figure 2.1. Maximum frequency 1 Hz.

aimed at prevention will be one of the basic themes of the development of seismic zoning in the 21st century.

The first scientific and technical methods developed for zoning were deterministic and based on the observation that damage distribution is often correlated to the spatial distribution and the physical properties of the underlying terrain and rocks. The 1970s saw the beginning of the construction of probabilistic seismic zoning maps on a national, regional and urban (microzoning) scale. In the 1990s these instruments for the mitigation of seismic hazard are coming to prevail over deterministic cartography.

The most controversial question in the definition of standards to be used in the evaluation of seismic hazard may be formulated as follows: should probabilistic or deterministic criteria and methods be used? At the current level of development in the modelling of seismogenesis and of seismic wave propagation the best policy for the future is to combine the advantages offered by both methods, using integrated approaches (e.g. Reiter, 1990). In this way, among others, we have the main advantage of making possible the extension of seismic zoning to long periods, a period band up to now almost totally ignored by all methods, but that is acquiring a continuously increasing importance, due to the widespread existence in the built environment of special objects, with relatively long free periods.

Studies carried out following the most recent strong earthquakes (e.g. the 1985 Michoacan earthquake) have proved to be important sources of basic knowledge and have acted as catalysts for the use of zoning in seismic risk management. The impetus for this has come essentially from politicians and administrators particularly interested in rapid reconstruction according to criteria which reduce the probability of a repetition of disasters. These post-earthquake studies have led to the conclusion that the destruction caused by an earthquake is the result of the interaction of three complex systems: 1) the solid earth system, made up of a) the seismic source, b) the propagation of the seismic waves, c) the geometry and physical conditions of the local geology; 2) the anthropised system, whose most important feature in this context is the quality of constructions (buildings, bridges, dams, pipelines, etc.); 3) the social, economic and political system, which governs the use and development of a settlement before it is struck by an earthquake.

The most recent results have shown that in an anthropised area it is now technically possible to identify zones in which, by virtue of physical parameters of source, propagation and local conditions, the most serious damage can be predicted. Actual examples of this capability, closely linked to the ability to calculate realistic synthetic seismograms, are illustrated in Section 2.4.

With the knowledge acquired to date, a drastic change is required in the orientation of zoning, that must no longer be considered a post-disaster activity. It is necessary to proceed to pre-disaster surveys that can be usefully employed to mitigate the effects of the next earthquake, using all available technologies. As clearly indicated by the recent events in Los Angeles (1994) and Kobe (1995) we cannot confine ourselves to using what has been learned from a catastrophe in the area in which it took place, we must be able to take preventive steps, extending, in a scientifically-acceptable way, results obtained to areas in which no direct experience has yet been

gained. An opportunity is offered in this direction by the scientific community's ability to make realistic simulations of the behaviour of the solid earth system through the computation of increasingly realistic synthetic seismograms, with a broad frequency content. Thus seismic zoning can use scientific data banks, integrated in an expert system, by means of which it is possible not only to identify the safest and most suitable areas for urban development, taking into account the complex interaction between the solid earth system, the environmental system and the social, economic and political system, but also to define the seismic input that is going to affect a given building. The construction of an integrated expert system will make it possible to tackle the problem at its widest level of generality and to maintain the dynamic updating of zoning models, made necessary by the acquisition of new data and the development of new model-building methods.

2. DETERMINISTIC ZONING USING SYNTHETIC SEISMOGRAMS

The procedure for the deterministic seismic zoning developed by Costa et al. (1992, 1993) represents one of the new and most advanced approaches and can, at the same time, be used as a starting point for the development of an integrated approach that will combine the advantages of the probabilistic and of the deterministic methods, thus minimising their drawbacks.

Synthetic seismograms are constructed to model ground motion at the sites of interest, using the knowledge of the physical process of earthquake generation and wave propagation in realistic media. In first-order zoning a database of seismograms covering the area of interest (at a regional scale) is computed, taking into account the effects of lateral heterogeneities in a rough way. Synthetic seismograms are efficiently generated by the modal summation technique (Panza, 1985; Florsch et al., 1991), so it becomes possible to perform detailed parametric analyses at reasonable costs. For example, different source and structural models can be taken into account in order to create a wide range of possible scenarios from which to extract essential information for decision making. In this sense, an efficient technique, based on the analytical computation of partial derivatives, is currently under development.

Once the parametric analysis is performed and the gross features of the seismic hazard are defined, a more detailed modelling of ground motion, which can take into account the local geological and geotechnical conditions at a specific site of interest, is possible using the hybrid approach which combines, for the description of wave propagation in anelastic heterogeneous media, the modal summation with finite differences techniques (Fäh et al., 1990; Fäh, 1992). This deterministic modelling goes well beyond the conventional deterministic approach taken in hazard analyses - in which only a simple wave attenuation relation is invoked - in that it includes full waveform modelling.

2.1. FIRST-ORDER ZONING OF THE ITALIAN TERRITORY

Starting from the available information on the Earth's structure, seismic sources and the level of seismicity of the investigated area, it is possible to estimate the maximum ground

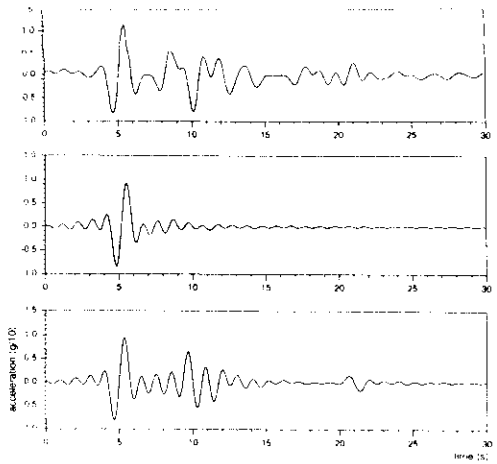

Figure 2.4a Irpinia (Southern Italy). Comparison between NS acceleration recorded at the Sturno station during the Irpinia earthquake of 23 November, 1980 (upper trace), one synthetic signal computed for that area (middle trace) in section 2.1.2 and the sum of four synthetic sub-events built using the middle trace (with proper weights and time shifts). Accelerations are low-pass filtered with a cut-off frequency of 1Hz.

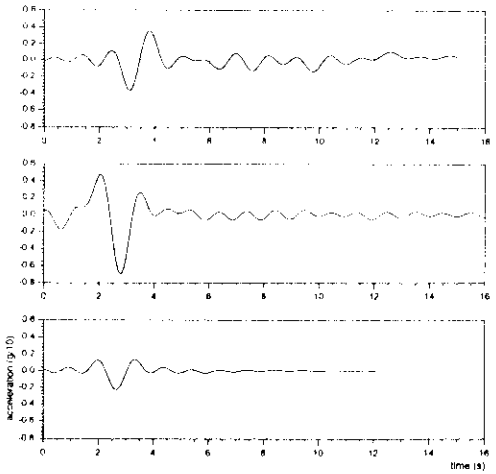

Figure 2.4b Friuli (Northern Italy). Comparison between NS acceleration recorded at the Tolmezzo station (upper trace) and two synthetic signals computed for that area (middle and lower traces).

source, which is deliberately neglected in the computation of the synthetic signal, to be used in the first-order zoning. The lower trace is shown as an example of modelling of the source complexity It is the result of a superposition of four sub-events, each one modelled with the middle trace properly weighted and shifted in time accordingly with the model by Vaccari et al (1990).

The same approach has been used in the comparison between the NS component recorded at Tolmezzo during the Friuli (1976) earthquake (Figure 2.4b, upper trace) and two synthetic signals obtained for that area (middle and lower traces). In the case of the Friuli event, the point-source approximation seems to be a sufficient approximation even for an event with M_S=6.1.

2.2. FIRST ORDER ZONING OF ETHIOPIA

Gouin (1976) produced the first seismic hazard map of Ethiopia using a probabilistic approach. Since the production of that map, quite a large number of destructive earthquakes have occurred in the country causing damages both to property and human life. Furthermore, destructive earthquakes that occurred in the neighbouring countries are not included in the production of the first map. Following the procedure described in section 2.1, Kebede and Vaccari (1996), produced a new seismic hazard map of Ethiopia and northern neighbouring countries.

The smoothed magnitude distribution for the seismogenic zones is given in Figure 2.5. The

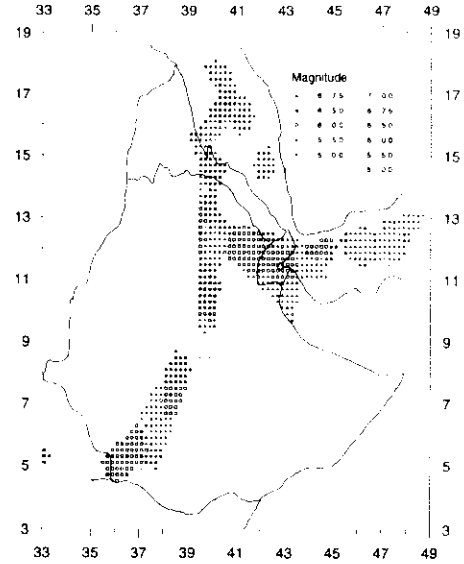

Figure 2.5 Smoothed magnitude (M_L) distribution for the cells belonging to the seven seismogenic zones, defined for Ethiopia after Kebede and Vaccari (1996).

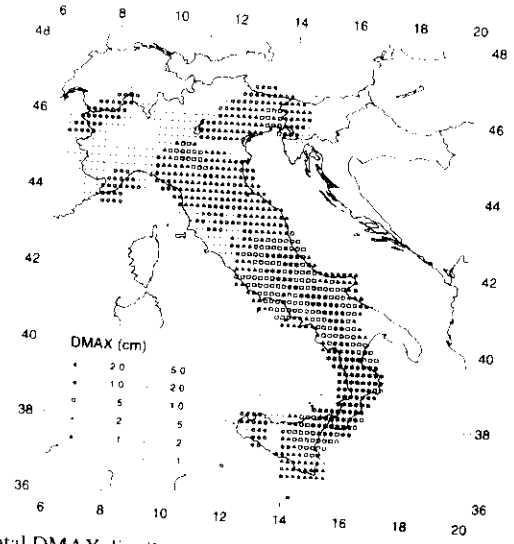

Figure 2.3b Horizontal DMAX distribution for Italy, obtained as a result of the application of the procedure described in Figure 2.1. Maximum frequency 1 Hz.

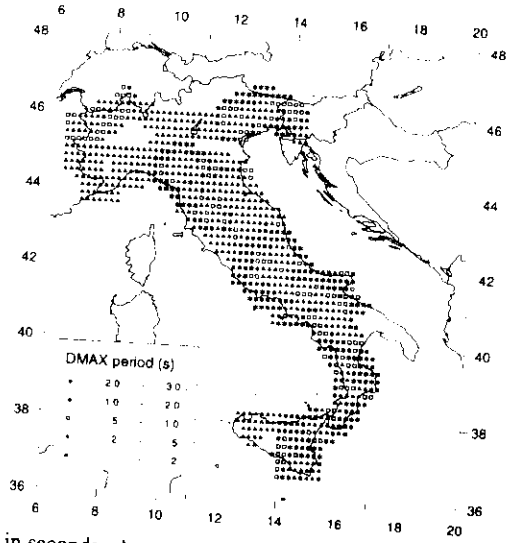

Figure 2.3c Periods, in seconds, characterised by the maximum amplitude, determined from the spectral analysis of the signals from which the DMAX values of Figure 2.3b have been derived.

P-SV (radial and vertical components) and SH (transverse component) synthetic seismograms are computed for a point-source with seismic moment of 10^{-7} Nm. The amplitudes are then properly scaled to a finite dimension source according to the (smoothed) magnitude (to be conservative we have assumed that all magnitude values given in the NT file are M_S) associated with the cell of the source, using the moment-magnitude relation given by Kanamori (1977) and the spectral scaling law proposed by Gusev (1983).

Among the parameters representative of the strong ground motion we have, for the moment, focused our attention on the maximum ground acceleration and displacement (AMAX and DMAX) in the considered range of frequencies (i.e. for frequencies up to 1 Hz). Since we compute the complete time series we are not limited to this choice, and it is also possible to consider other parameters, like Arias intensity (Arias, 1970) or other integral quantities that can be of interest in earthquake engineering or engineering seismology. Since recordings of many different sources are associated to each site, different maps can be produced. If one single value is to be plotted on a map (e.g. Figure 2.3), then only the maximum value of the analysed parameter is considered (e.g. maximum accelerations and displacements respectively in Figures 2.3a and b). In Figure 2.3c the periods associated with the displacements shown in Figure 2.3b are shown. It can be seen that in some regions, like for instance Central Italy around latitude 42°, long periods in the range between 20s and 30s are dominating. They are related with signals generated by strong earthquakes occuring at large distance from the site (about 90km), while the magnitude of the closer events, which are responsible for the higher frequencies (between 2s and 5s in our computations), is not big enough to let high frequencies dominate the scenario.

The results of the deterministic procedure are particularly suitable for civil engineers as seismic input for the design of special buildings. In fact, the relevance of the displacements at periods of the order of 10s or so is a particularly relevant issue for seismic isolation and in general for lifelines with large linear dimensions, like bridges and pipelines, where differential motion plays a relevant role on their stability.

2.1.2. Validation of the synthetic models against independent observations

A quantitative validation is made using the observed accelerograms recorded during the Irpinia earthquake on 23 November 1980 and the Friuli earthquake on 6 May 1976. The source rupturing process of the Irpinia event is very complex (e.g., Bernard and Zollo, 1989) and the dimension of the source has been estimated to be of the order of several tens of km. Nevertheless, it seems that the signal recorded at the station of Sturno is mostly due to a single sub-event that occurred rather close to the station itself, while the energy contributions coming from other parts of the source seem unimportant (Vaccari et al., 1990). With the cut-off frequency at 1 Hz, the horizontal components accelerograms recorded at Sturno have been low-pass filtered to be compared with the computed signals for the Irpinia region. The example shown in Figure 2.4a refers to the NS component but the same considerations can be applied to the EW component of motion. The early phases and the AMAX of the recorded signal (upper trace) and the synthetic one computed in the point-source approximation (middle trace), are in good agreement. The later part of the observed recording is more complicated and this is mostly related to the complexity of the

55

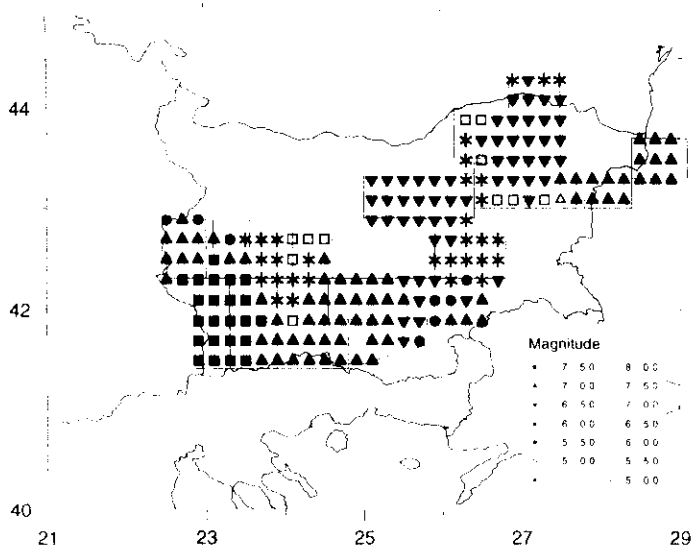

Figure 2.7 Smoothed M_S magnitude distribution for the cells belonging to the seismogenic zones, defined for Bulgaria after Orozova-Stanishkova et al. (1996).

2.4. DETAILED ZONING COMBINING OBSERVATION AND MODELLING OF GROUND MOTION

It is not possible to refine the results obtained with a first-order zoning by simply assuming a higher cut-off frequency (> 1 Hz) in the computation of the synthetic seismograms. A more detailed zoning requires a better knowledge of the seismogenic process in the region. Furthermore, to model wave propagation in greater detail the structural model used in the computation of synthetic seismograms must take into account lateral heterogeneities.

Detailed numerical simulations play an important role in the estimation of ground motion in regions of complex geology. They can provide synthetic signals for areas where recordings are absent. Numerical simulations are, therefore, useful for the design of earthquake-resistant structures, in particular when seismic isolation techniques are applied. In fact the number of available strong motion recordings containing reliable information at periods of a few seconds is very small, and will not increase very rapidly, since strong earthquakes in densely instrumented areas are rare events.

The computations that are at the base of the maps shown in Figures 2.3, 2.6 and 2.8 allow us to determine immediately the ground acceleration response spectra for periods, T, larger than 1 s, that are of special interest for seismically isolated buildings. For practical purposes, these

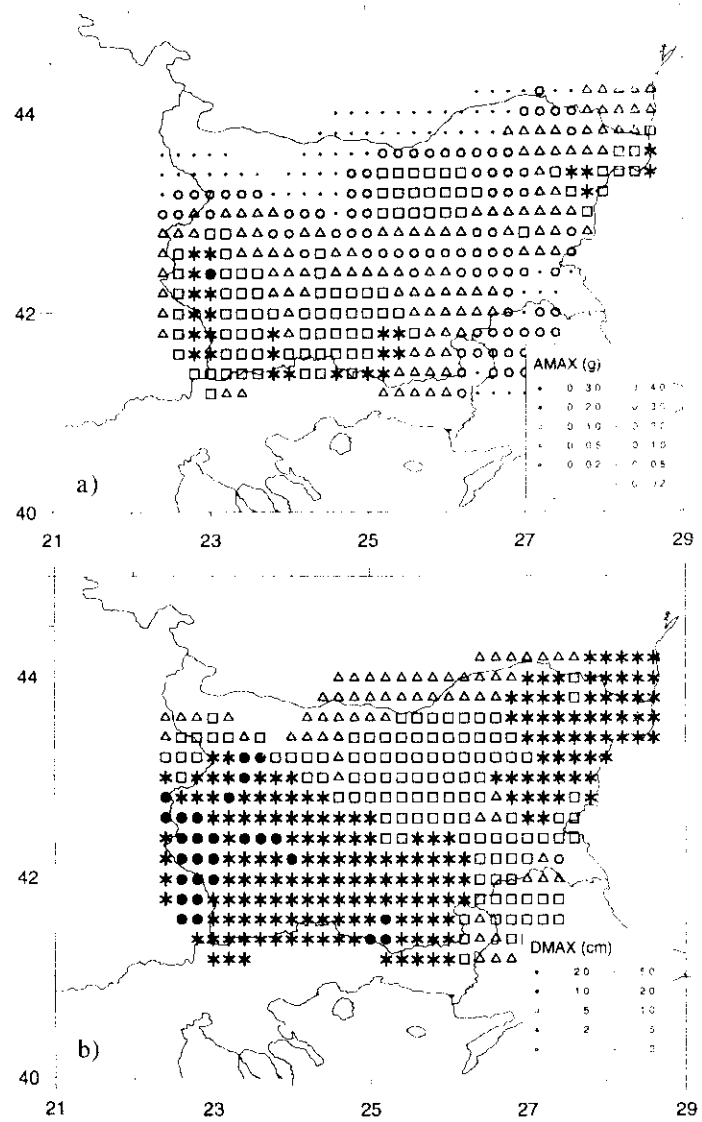

Figure 2.8 Horizontal AMAX (a) and DMAX (b) distribution for Bulgaria after Orozova-Stanishkova et al. (1996). Maximum frequency 1 Hz.

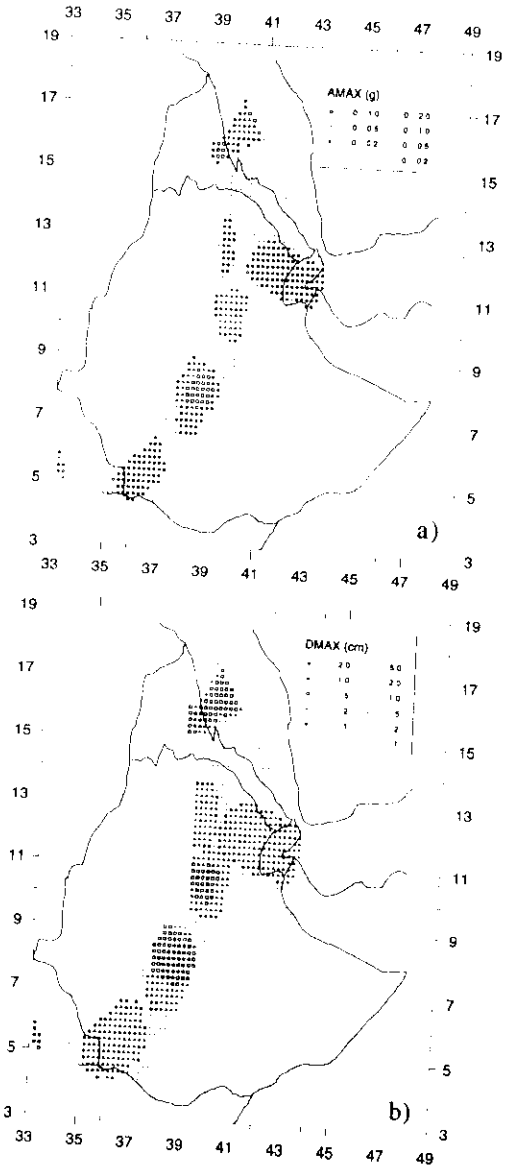

Figure 2.6 Horizontal AMAX (a) and DMAX (b) distribution for Ethiopia after Kebede and Vaccari (1996). Maximum frequency 1 Hz.

focal mechanisms and other related source parameters for the representative earthquakes that occurred in the seven seismogenic zones and the three main lithospheric structures (one for the rift and two for the eastern and western plateaux) used in this study, are based on the existing literature. The different magnitudes present in the earthquake catalogue have been converted to M_L, therefore, the magnitude-moment relation proposed by Boore (1987) has been used instead of the relation by Kanamori (1977).

Figure 2.6a shows the zoning map obtained for the region under study from the calculated AMAX, as a fraction of g (acceleration due to gravity). A glance at the figure shows that the higher values of AMAX (0.1 - 0.2g) are obtained for the main Ethiopian rift around latitude 8°N and in Eritrea around latitude 15°N, and are compatible with the values estimated by Gouin (1976) using a probabilistic approach. The corresponding displacements DMAX can be found in Figure 2.6b.

Given that the main Ethiopian rift is a region where various economic development activities are currently undertaken, and knowing that in this region the seismic hazard is high, necessary precautions should be taken both in the development of the new built environment and in the reinforcement of the existing one.

The seismic region of central and eastern Afar belongs to a different scenario. This area is characterised by the occurrence of intermediate-size earthquakes with M_L never exceeding 6.2. Even though the seismic activity rate is high (about 4 earthquakes per year with $m_b \geq 4.6$), a relatively low (as compared to that of the main Ethiopian rift) AMAX value is obtained for the region. The probabilistic approach used by Gouin (1976) leads to more conservative results than the deterministic one.

2.3. FIRST ORDER ZONING OF THE BULGARIAN TERRITORY

The same methodology (Section 2.1) has been applied to the Bulgarian territory by Orozova-Stanishkova et al. (1996), who discuss extensively the necessay input data. The map showing the smoothed distribution of seismicity within the seismogenic zones is given in Figure2.7.

As shown in Figure 2.8a, the highest values of AMAX are obtained in southwestern Bulgaria (0.3-0.4g), Struma zone, where the strongest earthquake in Bulgaria (M_S=7.8) occurred. Values between 0.2g and 0.3g have been estimated also in Southern Bulgaria and in the north-eastern part of the country. Near Trun, Sofia, and the western and central part of Maritza zone, as well as in Gorna Oryakhovitza zone AMAX varies in the range 0.1-0.2g. The northwestern and southeastern parts of Bulgaria are the less dangerous zones: AMAX is below 0.05g.

The largest Bulgarian cities, with relevant economical and cultural importance, such as Sofia, Plovdiv and Varna are situated in the zones with high seismic hazard. The values of AMAX calculated there are about 0.1-0.3 g. The corresponding displacements are shown in Figure 2.8b.

1985 (M_S=8.1), together with its aftershocks, produced the worst earthquake damage in the history of Mexico. More than 10,000 people died in Mexico City, 300,000 people were rendered homeless, and about 1,000 buildings were destroyed (Beck and Hall, 1986). Although the epicentre of the earthquake is close to the Pacific coastline, damage at coastal sites was relatively small. The reason for this is that most of the populated areas near the coast are sited on hard bedrock. In contrast, Mexico City, which is about 400 km from the epicentre, suffered extensive damage. This can be attributed to the geotechnical characteristics of the sediments in the valley of Mexico City. As the Michoacan earthquake was one of the most precisely-monitored events affecting a large metropolitan area, it is of particular interest to compare observed (Figure 2.10a) and computed (Figure 2.10b) strong ground motion, containing reliable information also at long periods.

The area of severe damage in Mexico City is characterized by the increasing thicknesses of the deep sediments and of the clay layer. The large impedance contrast between these two units causes strong resonance effects in the clay layer, as it is shown by the computed seismograms (Figure 2.10b) which are characterized by almost monochromatic wavetrains of long duration and large amplitude in the horizontal components, but absent in the vertical. The small influence of sedimentary basins on the vertical component of motion is frequently observed, and the computations (Fäh et al., 1994a) give a solid theoretical explanation of this fact.

The model used by Fäh et al. (1994a), directly obtained from the exisiting litterature, explains the observed difference in amplitudes for receivers located inside and outside the lake-bed zone in Mexico City, the ratio being in the range from 5 to 7 between the computed and the

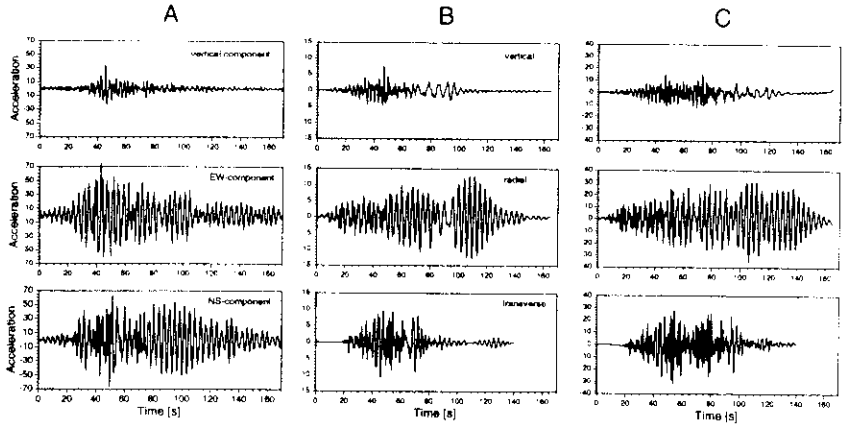

Figure 2.11 Michoacan earthquake (1985). Comparison between (A) the record at station CD and synthetic signals, computed at the eastern edge of the basin, 409.5 km from the source, corresponding to (B) one point source, (C), three point sources, with different strength and shifted in time (after Fäh and Panza, 1994).

observed time series. The use of an instantaneous source time-function gives rise to synthetic signals that contain too much energy at high frequency (above 0.6 Hz). This drawback can be removed by applying the ω^2 scaling law for the seismic moment rate spectrum, proposed by Kanamori et al. (1993) for the events occurring in the Mexican subduction zone:

$$\dot{M} = M_0 \omega_c^2 (\omega^2 + \omega_c^2)^{-1}$$

M_0 is the seismic moment and ω_c is the corner angular frequency. Following Kanamori et al. (1993), ω_c=0.196 s^{-1} and M_0=0.5·10^{21} Nm. These values permit to obtain a good reproduction of the shape of the observed signals over the entire frequency spectrum, but the absolute observed accelerations are underestimated by a factor ranging from 6 to 3. This last discrepancy can be reconciled considering the errors affecting the estimates of ω_c and M_0, and taking into account the subsequent rupture episodes of the Michoacan earthquake, mainly the one occurring about 26 s after the origin time, as shown in Figure 2.11 (Fäh and Panza, 1994). This data fitting is, however, unrelevant for the computation of spectral amplifications and for the more general purpose of defining the seismic input for engineering purposes.

At the site of interest, spectral amplification, computed with respect to a reference site, gives a good representation for micro-zoning purposes, especially from the engineering point of view. Fäh and Panza (1994) computed the spectral amplification, i.e. the relative spectral accelerations and velocities for one hundred frequencies of the oscillator in the frequency range 0.1-1.0 Hz. From these values the maximum spectral amplification (MSA) for the entire basin has been computed and is shown in Figure 2.12. The results for the relative spectral accelerations and velocities are similar, due to the approximate relation existing between them: $Sa(\omega) \approx \omega\, Sv(\omega)$, where ω is the angular frequency of the oscillator. In the following we will therefore limit ourselves to the relative spectral velocities, which we will call spectral amplification.

In two-dimensional modelling, the SH-waves (transverse component of motion) and the P-SV-waves (radial component of motion) are two independent wave fields. The direction of propagation of the local surface waves in the sedimentary basin is therefore well correlated with the source-receiver direction. In Mexico City, the local surface-waves are excited at different locations of the interface between the bedrock and the sediments, and the direction of propagation of the local surface-waves in the lake-bed zone may not correspond anymore to the source-receiver direction. Therefore, to justify the comparison between the observed ground motion and the synthetic signals, the spectral amplification for the complete horizontal ground motion must be computed. This has been done by Fäh and Panza (1994), who applied the horizontal ground motion to an oscillator with two degrees of freedom. The results for the synthetic signals are shown in Figure 2.12. Due to the large amplitudes of SH-waves, the MSA obtained for the horizontal ground motion are similar to the result obtained for the transverse component. The maximum peaks in the MSA in Figure 2.12 can be attributed to sites where a strong interaction between the deep sediments and the surficial clay layer occurs. At such sites, the resonance frequencies of the two layers are almost the same. The MSA obtained from the numerical simulation is rather independent from the shape of the seismic moment rate spectrum, as can be seen in Figure 2.13, where the results obtained with the seismic moment rate spectrum proposed by Kanamori et al. (1993) are compared with the results obtained for a frequency-independent spectrum.

results can be generalized to higher frequencies by the use of the existing standard codes. For instance, Eurocode 8 (1993) defines the normalized elastic acceleration response spectrum, β(T), of the ground motion, for 5% critical damping. Therefore, the matching of the long-period portion of the normalized spectra with the ones computed from synthetic accelerograms, allows us to obtain, for any portion of the considered territory, an absolute spectrum, provided a satisfactory classification of soils is available. An example is given in Figure 2.9. The preliminary soil classification of Eurocode 8 (1993) considers three classes, A, B, and C, ranging from hard rock to loose uncemented sands. Accordingly with Eurocode 8 (1993) for sites with soil conditions not matching the three classes A, B and C, special studies for the definition of the ground acceleration response spectrum are necessary (examples of such special studies are given in section 2.4.1).

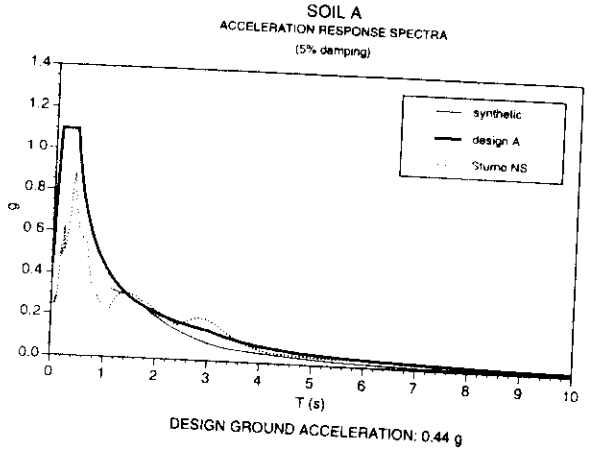

Figure 2.9 Elastic acceleration response spectra. Absolute values (thick line) have been obtained scaling the normalized Eurocode8 response spectrum for subsoil A with the long period response spectrum (thin line), determined from the synthetic signal obtained in section 2.1 for the Irpinia (Southern Italy) area. The spectrum of the NS component observed at Sturno during the 1980 Irpinia earthquake is shown by the dotted line.

When detailed special studies are required by Eurocode 8 or by the presence, in the built environment, of special objects, the standard seismic prospecting techniques, used for the detailed definition of the elastic properties of sub-surface geology, do not give satisfactory results since they treat wave propagation in laterally heterogeneous structures with asymptotic forms for high frequencies. These methods, called "ray methods", can only be applied to smoothly varying media, where the characteristic dimensions of the inhomogeneities are considerably larger than the prevailing wavelength. They fail to predict ground motion at sites close to lateral heterogeneities such as edges of sedimentary basins and at sites above irregular bedrock-sediment interfaces, where excitation of local surface waves and resonance effects can become important.

Far away from lateral heterogeneities, a local structure can sometimes be approximated by a horizontally-layered structural model, and the mode summation method is the most powerful tool for computing broadband synthetic seismograms. This method is still suitable when lateral variations can be schematized with vertical discontinuities (Vaccari et al., 1989), but it is presently not applicable to local irregular structures, which cannot be reduced to plane-layered models. When dealing with special detailed investigations the influence of these local and irregular heterogeneities must be included in the numerical modelling. This can be done combining the modal summation and the finite difference techniques (Fäh et al., 1990; Fäh, 1992).

2.4.1. Modelling strong ground motion observed in Mexico City

Mexico City has experienced extensive damage in the recent past from strong earthquakes with hypocentres in the Mexican subduction zone. The Michoacan earthquake of September 19,

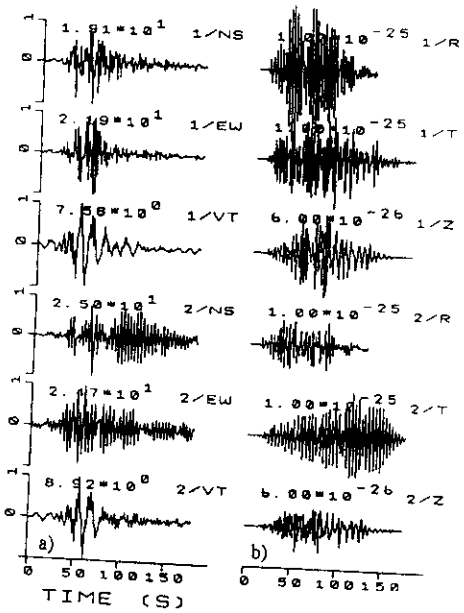

Figure 2.10 a) Observed horizontal and vertical components of displacements recorded at two stations (1 and 2) in the valley of Mexico City. N denotes the North-South, E the East-West and Z the vertical component. b) Synthetic displacements computed with the hybrid technique (Fäh et al., 1990; Fäh, 1992). R is the radial, T is the transverse and Z is the vertical component. The signals are normalised to a seismic moment of 10^{-7} Nm, and the peak displacement is indicated in units of cm (modified from Fäh et al., 1994a).

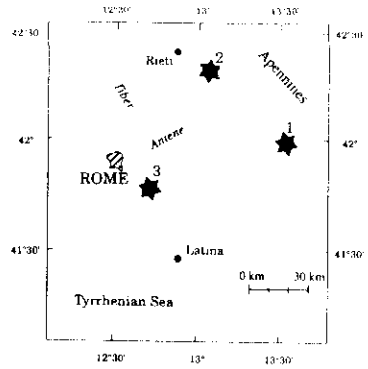

Figure 2.14 Epicenter locations of the events considered in the numerical simulations used for the microzoning. The source positions are (1) the epicenter of the January 13, 1915 Fucino earthquake, (2) the Carseolani Mountains, and (3) the Alban Hills.

spatial distribution of the spectral ratios can be due to the polarization of P-SV waves in the sediments, even when the geometry of the different sedimentary layers is relatively regular. This is a quite logical explanation of the often observed concentration of damage in very small, scattered zones, and is easier to accept than the often invoked presence of unlikely abrupt variations in the geotechnical properties of the subsoil.

Since the correlation is good between AMAX, W and the damage statistics, it is possible to extend the zoning to the entire city of Rome, thus providing a basis for the prediction of the expected damage from future strong events.

In addition to the Central Apennines, whose earthquakes caused in the town maximum intensity VII-VIII (MCS) and may generate significant perturbations at long period, the most important seismogenetic zone (Figure 2.14) which can cause structural damage in Rome are the Alban Hills (observed maximum MCS in Rome VI-VII) (Molin et al., 1986). Therefore, Fäh et al. (1993) used the sources shown in Figure 2.14: (1) the epicenter of the January 13, 1915 Fucino earthquake, (2) the Carseolani Mountains where, from the study of pattern recognition (Caputo et al., 1980), a strong earthquake is expected to occur, and (3) the Alban Hills. The source mechanisms assigned to these earthquakes are the mechanism of the Fucino earthquake (Gasparini et al., 1985) for event 1 and 2, and the mechanism of a recent earthquake in the Alban Hills (Amato et al., 1984) for event 3.

For a first order microzoning, in order to minimize the effects of the radiation pattern and of the regional propagation, Fäh et al. (1994b) consider the relative spectral accelerations or spectral amplification Sa(2D)/Sa(bedrock), computed along the profiles of Figure 2.15. Sa(2D) indicates Sa computed for the two-dimensional models of Figure 2.16, while Sa(bedrock) is the Sa obtained for the one-dimensional reference bedrock models given by Fäh et al. (1993).

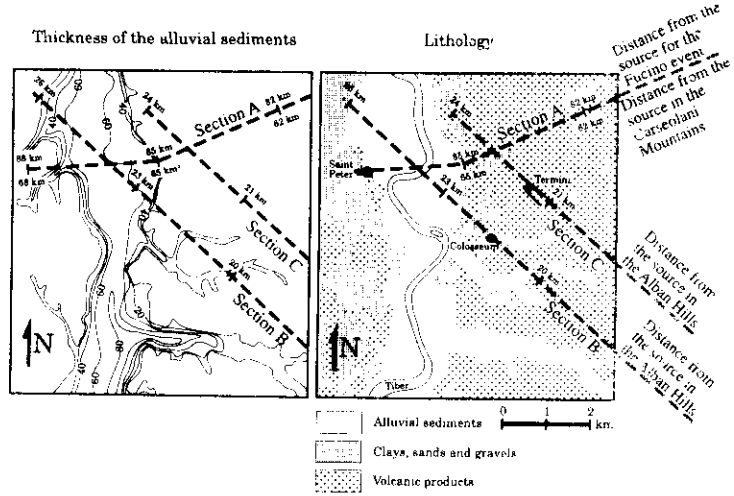

Figure 2.15 Lithology and thickness of alluvial sediments in Rome (Ventriglia, 1971; Funiciello et al., 1987; Feroci et al., 1990). The dashed lines indicate the positions of the cross sections, for which numerical modelling is performed.

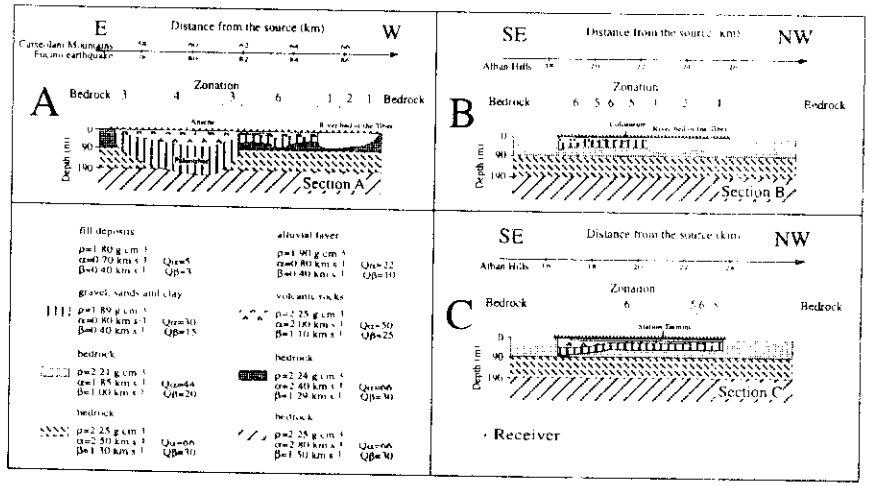

Figure 2.16 Two-dimensional models corresponding to the dashed lines shown in Figure 2.15. Only the part near to the surface is shown, where the 2D model deviates from the horizontally-layered reference models. The general microzonation is explained in the text (after Fäh et al., 1994b).

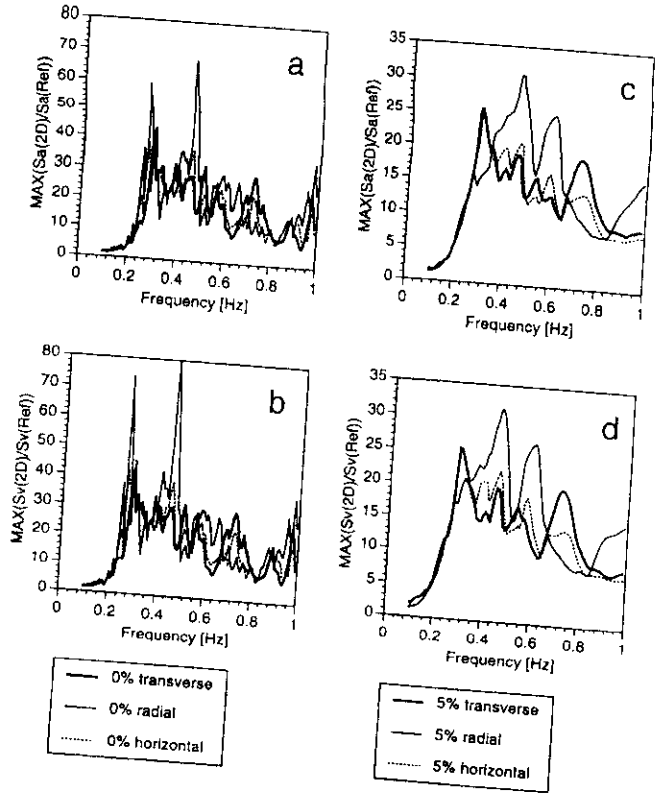

Figure 2.12 Maximum relative spectral accelerations Sa(2D)/Sa(Ref) and velocities Sv(2D)/Sv(Ref) for zero damping (a,b) and 5% damping (c,d) obtained with synthetic signals. The results are shown for a single-degree of freedom oscillator for the transverse and the radial component of motion, and for an oscillator with two degrees of freedom for the horizontal ground motion. The synthetic signals are scaled assuming the seismic moment rate spectrum proposed by Kanamori et al. (1993) (after Fäh and Panza, 1994).

The relation existing between the properties of strong motion records, the geological setting and the distribution of damage in Mexico City widens the spectrum of the possible applications of synthetic seismograms for seismic zoning purposes, allowing us the use of earthquakes for which instrumental data are not available (historical events). An example of such possibilities is given in Section 2.4.2.

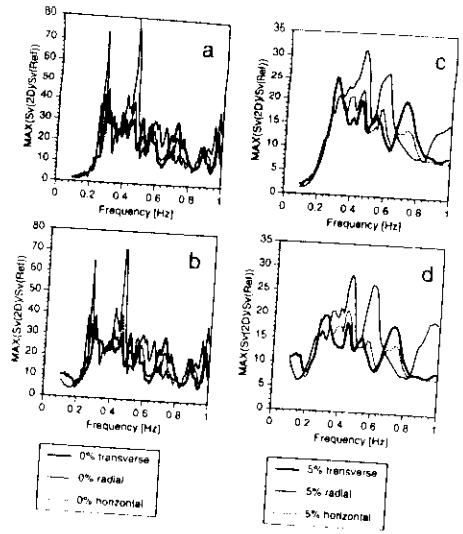

Figure 2.13 Maximum relative spectral velocities Sv(2D)/Sv(Ref) for zero damping (a,b) and 5% damping (c,d) obtained with the synthetic signals, which are scaled by assuming the seismic moment rate spectrum proposed by Kanamori et al. (1993) (a,c) and by assuming a constant, frequency independent, spectrum (b,d) (after Fäh and Panza, 1994).

2.4.2. Microzoning of Rome

A large quantity of descriptions of earthquakes that have been felt in Rome is available (Ambrosini et al., 1986; Molin et al., 1986; Basili et al., 1987). The use of the hybrid method (Fäh et al., 1993) allows us to give a simple and natural explanation of the damage disribution observed as a consequence of the the January 13, 1915 Fucino earthquake - one of the strongest events that have occurred in Italy during this century (Intensity XI on the Mercalli-Cancani-Sieberg, MCS, scale). The well-documented distribution of damage in Rome, caused by the Fucino earthquake, is successfully compared by Fäh et al. (1993) with the results of a series of different numerical simulations, using AMAX and the so called total energy of acceleration, W (Jennings, 1983), which is proportional to the Arias Intensity.

High relative AMAXs are obtained where the impedance of the surficial sediments is small, whereas relative AMAXs are low where the volcanic rocks are thick, and this is in good agreement with the observed damage distribution. An even better correlation with the observed damage is obtained considering the relative W. There are four peaks: at the edges of the Tiber basin, within the alluvial valley of the Aniene, and a broad peak at the end of the Siciliano low-velocity zone. An additional important result of Fäh et al. (1993) is the demonstration that sharp variations in the

sections we present examples of such predictions for areas where experimental data are not available or extremely scarce.

2.5. DETAILED ZONING FROM THE MODELLING OF GROUND MOTION, AND COMPARISON OF 1-D VERSUS 2-D METHODS.

The standard one-dimensional method, developed by Thomson (1950) and Haskell (1953), and by Schnabel et al. (1972) (computer program Shake), that uses incident SH-waves in a structure composed of plane parallel layers, when applied to laterally heterogeneous structures, is often not sufficient to account for effects such as the excitation of local surface waves, resonances, and different incidence angles relative to the geometry of the heterogeneities. This limitation produces significant discrepancies between the ground response predicted by one-dimensional modelling, and the response computed for realistic two-dimensional structural models and incident wavefields. Therefore, for the computation of the local seismic response, here we use (1) the standard one-dimensional method (Schnabel et al., 1972), from now on method 1, and (2) the hybrid method (Fäh et al., 1990; Fäh, 1992), from now on method 2. The results obtained with the two methods are compared in order to define the limits and possibilities of the generally used standard one-dimensional method for reliable microzoning actions.

2.5.1. Modelling of ground motion in Naples

Naples is not within a seismogenetic area, but it has often been severely damaged by earthquakes which occurred in the Southern Apennines. The last strong event, November 23, 1980 (M_s=6.9), produced serious damage in Naples, and mostly in the historical centre and in the eastern area (Rippa and Vinale, 1983), where a ten-storied building was completely destroyed causing tens of human deaths. For the historical buildings, the damage distribution is easily explained by their degraded conditions, but for the most damaged buildings of the eastern district, which are tall and made in reinforced concrete, it is necessary to consider the combined effects of the incident wavefield, the local soil conditions and the properties of the buildings. The nearest available accelerogram was recorded at a seismic station installed on a lava deposit at Torre del Greco, on the flanks of Vesuvius, about 20 km closer to the epicentral zone than Naples. Thus, at present, the only possibility for a detailed zoning for the town, that accordingly with historical records may experience a shaking of intensity VIII on the MCS scale, is given by the use of realistic synthetic seismograms.

Nunziata et al. (1995) performed the numerical modelling of the propagation of the wavefield, generated by the main rupture event of the 1980 earthquake, up to a profile trending N86°W, and located in a test area in the eastern district of Naples, and made an accurate and realistic evaluation of the seismic ground motion.

The causative fault of the 1980 earthquake is located about 90 km from the cross-section, representative of the eastern part of Naples, shown in Figure 2.19. The choice of the mechanism of the seismic source is made accordingly with the mechanism of the main event: a normal fault

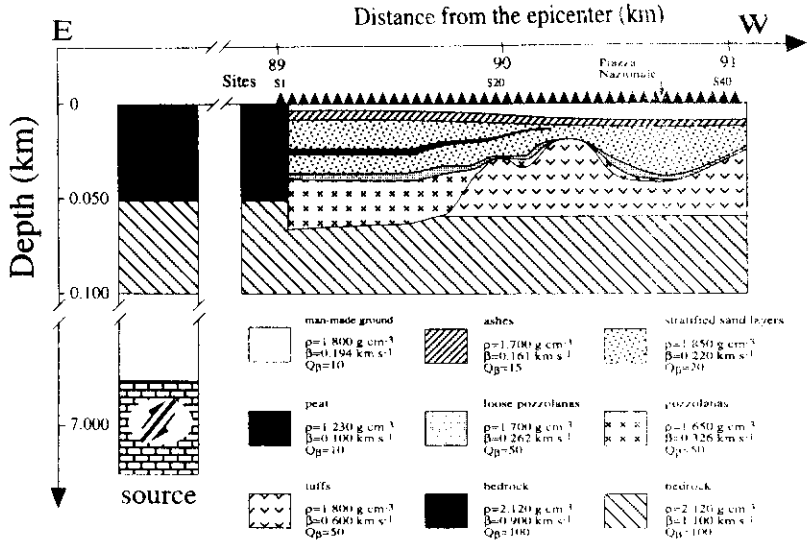

Figure 2.19 Geological cross-section in the eastern district of Naples, used in the computations (after Nunziata et al., 1995).

with little transcurrent component. Since there is no agreement between authors about the amount of the strike-slip component (e.g. Bernard and Zollo, 1989; Vaccari et al., 1990), Nunziata et al. (1995) adopt a pure normal fault with dip 65°, rake 270°, strike 315° and depth 7.0 km. The angle between the strike of the fault and the epicenter-cross section line is 36°.

The propagation of the waves from the source up to the two-dimensional structural model has been computed with method 2. The source is located in the laterally homogeneous part, and the propagation of the waves from the source up to the 2-D structure (Figure 2.19) is computed with the modal summation technique for the layered one-dimensional model representative of the path to Naples (Vaccari et al., 1990). Acceleration time series for SH-waves (Figure 2.20) are computed in several sites of different cross-sections: (1) a one-dimensional reference model for the bedrock, which corresponds to the structural model for the region between the source position and Naples, (2) a two-dimensional model with a peat layer, and (3) a two-dimensional model without the peat layer. All scaling values are related to a source seismic moment $M_0 = 10^{-7}$ Nm, and in each column, the signals are normalized to the same value. The time scale is shifted by 22 s with respect to the origin time, and the distance between two sites is 100 m. If we scale the signals of Figure 2.20 following Gusev (1983) relation using $M_0 = 2\ 10^{19}$ Nm, that is for M_s = 6.9 (Kanamori, 1977), we obtain acceleration values, associated with SH waves, in the range 45cm/s^2-60 cm/s^2, in good agreement with the regressions of Sabetta and Pugliese (1987).

For general microzonation purposes, using the results obtained from the modelling of the Fucino event, it is possible to define the six zones shown in Figure 2.16: (1) *zone 1* includes the edges of the Tiber river, (2) *zone 2* extends over the central part of the alluvial basin of the Tiber, (3) *zone 3* includes the edges of the Paleotiber basin, and (4) *zone 4* extends over the central part of the Paleotiber basin. The *zones 5* and *6* include areas which are located outside the large basins of the Tiber and Paleotiber where we distinguish between areas (5) without and (6) with a layer of volcanic rocks close to the surface. These zones can be recognized also in the sections considered in relation with the events located in the Carseolani Mountains and the Alban Hills (Figure 2.16).

For all the sites located in each of the six zones, and for all the two-dimensional models, shown in Figure 2.16, and the studied events, located in Figure 2.14, the spectral amplifications Sa(2D)/Sa(bedrock) have been computed. From these values the average and the maximum spectral amplification, which are shown in Figure 2.17, for zero and 5% damping of the oscillator, are determined for each given zone.

The zoning performed along the three sections can be extrapolated, with cautions, to a larger area using the information available on geological and geotechnical conditions. The result of such tentative extrapolation is shown in Figure 2.18.

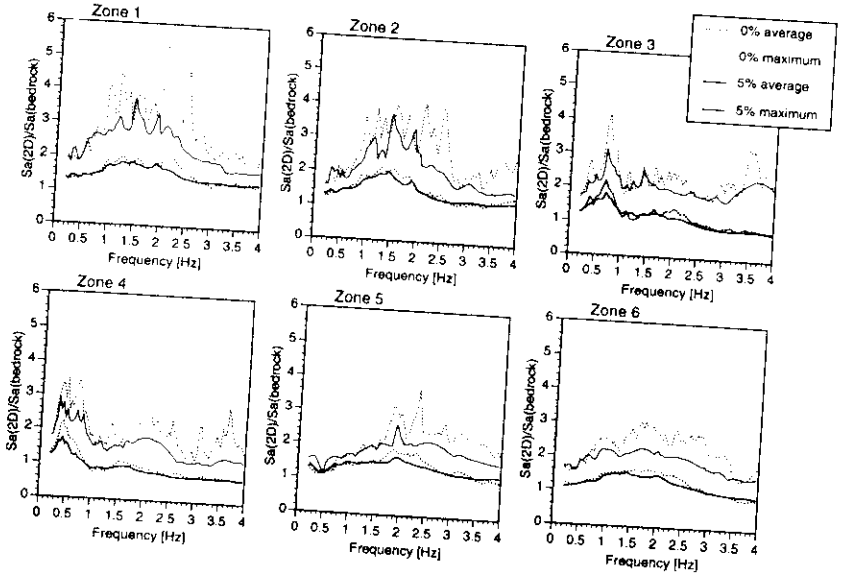

Figure 2.17 Maximum and average relative spectral accelerations for the zones defined in Figure 2.16, for zero damping and 5% damping (after Fäh et al., 1994b).

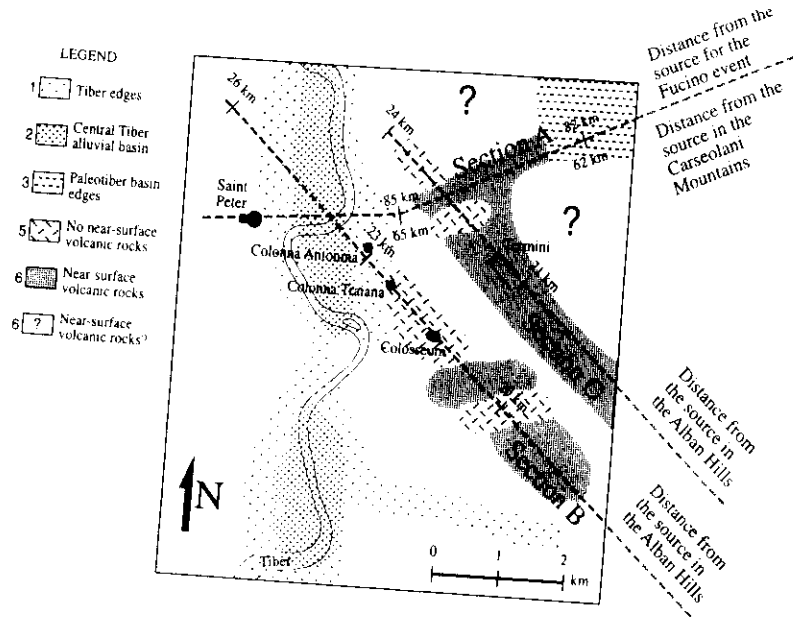

Figure 2.18 Microzoning for the city of Rome.

Thus, in absence of instrumental data, and without having to await for a strong earthquake to occur, a realistic numerical simulation of the ground motion, has been used for the first order microzonation of the city of Rome. The highest values of the spectral amplification are observed at the edges of the sedimentary basin of the Tiber, strong amplification are observed in the Tiber's river bed. This is caused by the large amplitudes and long duration of the ground motion due to (1) low impedance of the alluvial sediments, (2) resonance effects, and (3) excitation of local surface waves. The presence near to the surface of rigid volcanic rocks is not sufficient to classify a location as a "hard-rock site", since the existence of an underlying sedimentary complex can cause amplifications due to resonance effects. A correct zonation requires the knowledge of both the thickness of the surficial layer and of the deeper parts of the structure, down to the real bedrock. This is especially important in volcanic areas, where volcanic flows often cover alluvial basins.

Up to now we have seen examples of the possibility to reproduce most of the features of experimental records and to explain the damage distribution using as input data the information that can be retrieved in the literature. The agreement between observations and models is not obtained by an inversion procedure, that has not prognostic capabilities, but is the result of a direct computation. The ground motion is theoretically predicted on the base of the available knowledge about the seismic source and the medium through which waves propagate. In the following two

The peat layer, even though with a thickness of only 3 m, reduces significantly the amplification effects induced by the unconsolidated sediments.

The discrepancies between the amplifications computed with method 1 and method 2 are clearly illustrated in Figures 2.23, 2.24 and 2.25 for sites S7, S23 and S26. At site S7, the main peak is reached at the same frequency with both modellings, but the amplitude obtained with method 1 is 30% smaller than that obtained with method 2. Moreover, other peaks, at frequencies which are important for engineering purposes, and characterizing the results obtained with the finite differences method, are absent in the results obtained with method 1. At site S23 a frequency shift of the main peak is observed in addition to a disagreement for the other peaks. The picture changes for site S26, as the spectral amplifications, computed with method 1, overestimate those obtained with method 2, even if they have a similar shape.

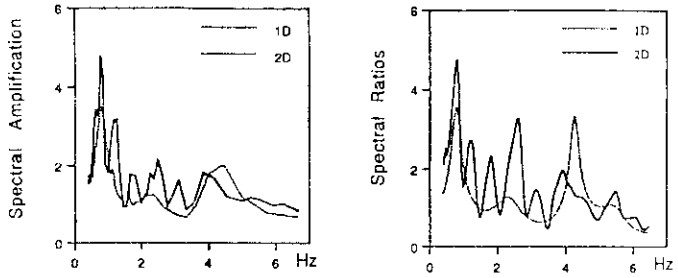

Figure 2.23 Spectral ratios (smoothed) and spectral amplification (not smoothed) for zero damping computed with 1-D and 2-D methods at site S7 - see Figure 2.19 for its location (after Nunziata et al., 1995).

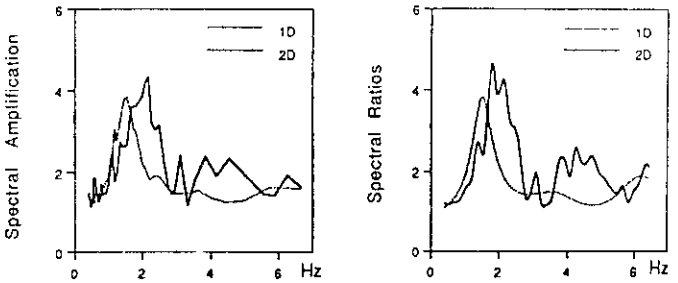

Figure 2.24 Spectral ratios (smoothed) and spectral amplification (not smoothed) for zero damping computed with 1-D and 2-D methods at site S23 - see Figure 2.19 for its location (after Nunziata et al., 1995).

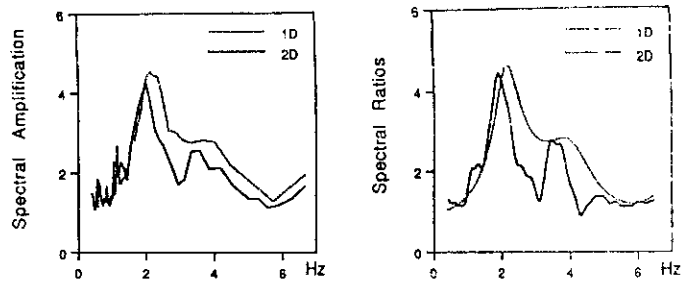

Figure 2.25 Spectral ratios (smoothed) and spectral amplification (not smoothed) for zero damping computed with 1-D and 2-D methods at site S26 - see Figure 2.19 for its location (after Nunziata et al., 1995)

Therefore, the seismic vulnerability of a megacity like Naples, with a large cultural heritage and a very high number of people to safeguard, can be drastically reduced, without having to await for another strong earthquake to occur.

2.6. THE SEISMIC MICROZONATION OF BENEVENTO: AN EXAMPLE OF PARAMETRIC STUDY

The average structural model for the region between the source position and the town of Benevento, used as the reference structure for the bedrock, is given by Vaccari et al. (1990). Following Fäh and Suhadolc (1994), the ground motion computed with the hybrid method for the different sites in the two-dimensional models is always discussed with respect to the results obtained for the same seismic source and this one-dimensional structure.

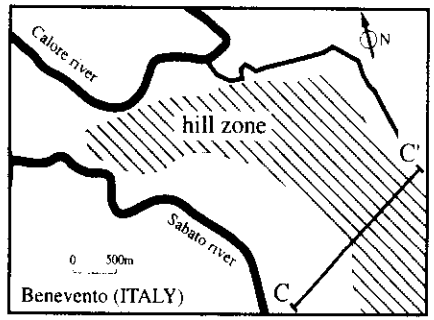

Figure 2.26 Area of the city of Benevento with the location of the profile C-C' used for the numerical modelling (after Fäh and Suhadolc, 1994).

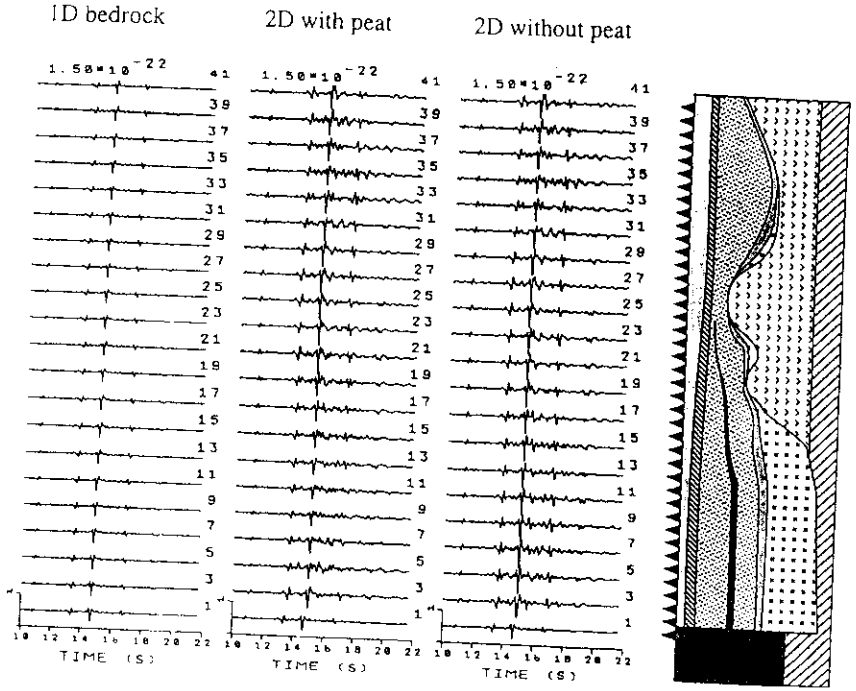

Figure 2.20 Acceleration time series for SH-waves computed for the reference model (1D bedrock), the 2-D structural model with the peat layer, and the 2-D structural model without the peat layer (after Nunziata et al., 1995).

The presence of unconsolidated sediments causes an increase of the signal's amplitudes and duration, more pronounced for the model without the peat layer. For the model with the peat layer, between sites 1 and 15, the maximum amplitudes are similar to the maximum amplitudes observed for the one-dimensional bedrock model.

Looking at the spectral ratios at the sites S7, S17, S23, S26, S33 it is quite evident the large variability of ground motion within a few hundred meters (Figure 2.21). The main peak moves from frequencies less than 1 Hz, site S7, where the peat layer reaches the maximum thickness, to frequencies slightly higher than 1 Hz, sites S17 and S33, and to frequencies around 2 Hz, sites S23 and S26. The amplification factor of the ground motion is in general around five, and this value is exceeded only at site S17. A secondary significant peak is present at higher frequencies, between 2Hz and 3Hz at site S7, between 3Hz and 4Hz at sites S26 and S33, and around 5Hz for site S17.

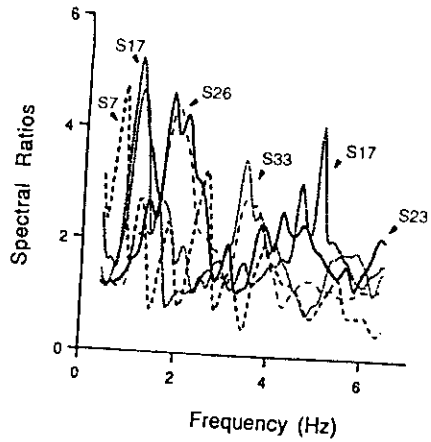

Figure 2.21 Smoothed spectral ratios computed with the hybrid method at the sites S7, S17, S23, S26, S33 - see Figure 2.19 for their location (after Nunziata et al., 1995).

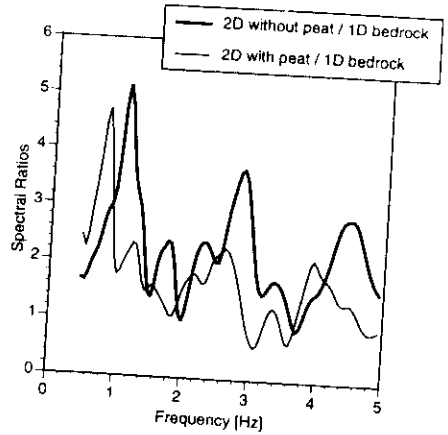

Figure 2.22 Example of the effect of the peat at site S9 (see Figure 2.19 for its location), with respect to its removal. Smoothing applied (after Nunziata et al., 1995).

The damping effect of the peat layer is clearly shown by the comparison of the spectral ratios computed at the same site (S9) when the peat layer is removed (Figure 2.22). The maximum peak increases in amplitude and is shifted towards higher frequencies, when the peat layer is removed.

The stability of the results obtained for the different models allows us to identify six zones, each characterized by a typical strong ground motion response, indicated in Figure 2.28. *Zone 1* extends over the lower valley of the Sabato river, where pliocenic clay is overlaid by a surficial layer of recent alluvium, including in some parts a thin buried layer of loose conglomerates. *Zone 2* represents the transition zone from the lower valley of the Sabato river to the hill zone of Benevento, where we have assumed a surface layer composed of loose conglomerate of variable thickness. Also present is a buried "silt lens". The hill zone of Benevento is divided into: *Zone 3* that includes the transition between pliocenic clay and cemented conglomerate, with a thick silt deposit, "made ground" within the surface layer, and in some parts a thin layer of loose conglomerate; *Zone 4* that extends over the areas of the hill where a thick layer of loose conglomerate is located close to the free surface; and *Zone 5* that spreads over the eastern part of the hill, where a silt layer is buried below the surface layer of "made ground". *Zone 6* is characterized by areas with only a thin sedimentary cover, located above the cemented conglomerate (bedrock).

In each of the six zones, for all sites and for all two-dimensional models, Fäh and Suhadolc (1994) have computed the relative spectral amplifications, Sa(2D)/Sa(bedrock), and the average and maximum spectral amplifications, that are shown, both for zero damping and 5% damping in Figure 2.29.

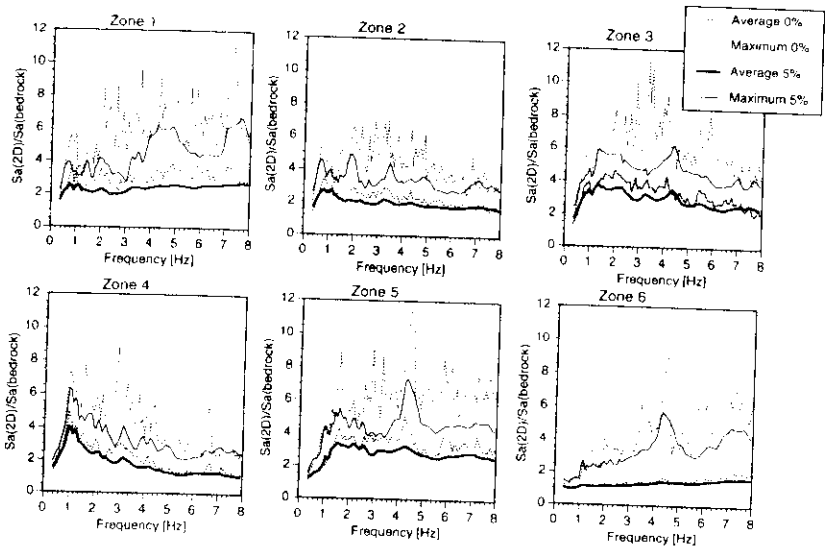

Figure 2.29 Maximum and average relative spectral amplifications, for the zones defined in Figure 2.28, for zero damping and 5% damping. The results include all computations made for the different two-dimensional structural models (after Fäh and Suhadolc, 1994).

3. CONCLUSIONS

Traditional deterministic methods for seismic zoning can only lead to a kind of "post-event" zoning whose validity cannot be easily extrapolated in time and to different regions and which, therefore, must be considered obsolete.

On the contrary the computation of realistic synthetic seismograms, using methods that make it possible to take source and propagation effects into account, utilizing the huge amount of geological, geophysical and geotechnical data, already available, goes well beyond the conventional deterministic approach and gives a powerful and economically valid scientific tool for seismic zonation and microzonation.

Because of its flexibility, the method is suitable for inclusion in new integrated procedures, a kind of compromise between probabilistic and deterministic approaches, that can be developed in order to minimize the drawbacks of each of the two procedures.

The ability to estimate accurately seismic hazard at very low probability of exceedance may be important in protecting, against rare earthquakes, the existence of special objects in the built environment. The deterministic approach, based upon the assumption that several earthquakes can occur within a predefined seismic zone, represents a conservative definition of seismic hazard for pre-event localized planning for disaster mitigation, over a quite broad-band of periods.

The results of tests made against instrumentally recorded accelerograms show that, even an approximate knowledge of the geometry and of the mechanical properties of the uppermost layers and the use of commonly available data on the seismic source geometry, is sufficient to make a realistic prediction of the ground motion.

Severe discrepancies are found between the amplifications computed with the 1-D standard method (method 1) and the 2-D hybrid method (method 2), and they cannot be ignored when formulating building codes and retrofitting the built environment. For example, in the area of Naples, in presence of a peat layer, the amplifications computed with method 1 are smaller then the "true" ones computed with method 2, and this is a clear evidence of the danger intrinsic in the application of method 1 for risk assessment. If the peat layer is absent, a similarity in shape exists between the amplifications computed with the two methods, but the amplification determined with method 1 overestimates the results obtained with method 2, with consequent implication of not necessary larger costs for the reduction of vulnerability.

Similar conclusion can be drawn from the computations made in Benevento. For an extended seismic source which is not located beneath the site of interest, in a laterally homogeneous structure, vertical incidence of waves (method 1) significantly overestimates the local hazard, with respect to the results obtained with the more realistic method 2. This is due to the different incidence angles related to different phase velocities of a realistic wavefield. The hybrid approach (method 2) allows us the simulation of the complete wavefield in given frequency and phase-velocity bands, and, in these bands, it accounts automatically for all surface waves and body waves, characterized by any incidence angle consistent with the bands considered. For a laterally

At the western border of the Benevento hill, a Pliocenic clay formation abruptly disappears, probably due to the presence of a fault. To study the influence of this abrupt transition, different geometries of the expected fault are considered, and since material properties of the different soils are not well known, a parametric study for the shear-wave velocities is performed (Fäh and Suhadolc, 1994).

The locations of the different layers and the values of the seismic velocities, shown in Figure 2.26, are based on the information given in Marcellini et al. (1991). The resulting cross-section and the examined different geometries of the transition between pliocenic clay and cemented conglomerate are shown in Figure 2.27. More details about the material properties which characterize the different layers and the type of extended seismic source considered are given by Fäh and Suhadolc (1994).

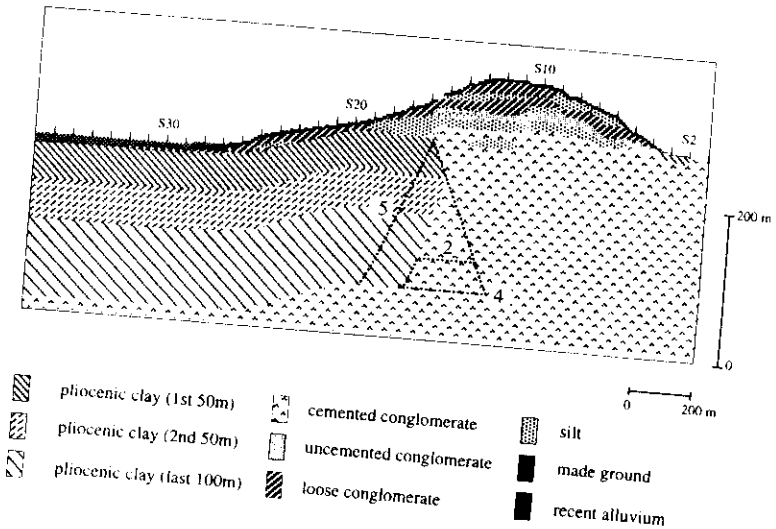

Figure 2.27 Two-dimensional model (1) of the studied Profile. Only the part of the structure near to the surface is shown, where the 2D model deviates from the 1D layered reference model. The assumed geometries of the transition between pliocenic clay and cemented conglomerate are indicated by numbers from 2 to 5, labeling the different thick dashed lines. The site positions are shown by small triangles - Site S1 at the right edge of the figure (after Fäh and Suhadolc, 1994).

The results of the study of the spatial variation of the site response, as determined by W, are shown in Figure 2.28a. The differences between the results obtained for the four geometries are smaller than the variations along the four single cross-sections. The biggest differences between

the four geometries are observed, as expected, just above the transition between pliocenic clay and cemented conglomerate. The peaks of relative W values, observed at distances between 13.7 and 13.9 km from the source, become slightly smaller for the two cases considered in Geometry 4 and Geometry 5. The result obtained for different shear-wave velocities are given in Figure 2.28b.

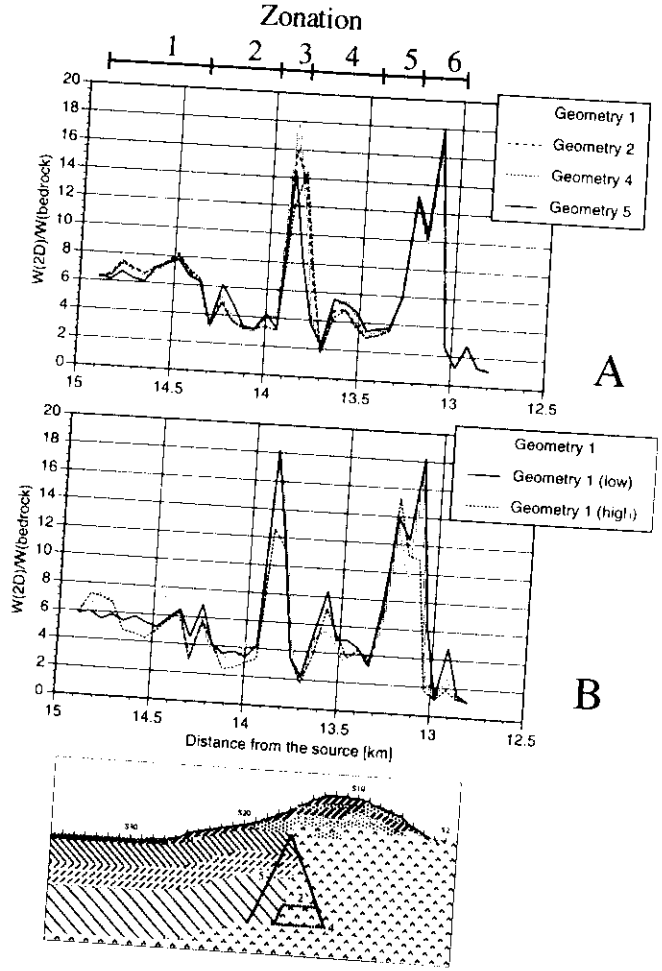

Figure 2.28 Relative energy of acceleration W: a) for different geometries, and b) by assuming low shear-wave velocities (low b), or high shear-wave velocities (high b) in the uppermost layer. The general zonation is explained in the text (after Fäh and Suhadolc, 1994).

Ph.D. thesis Nr. 9767, Swiss Federal Institute of Technology, Zürich.

Fäh D. and Panza G.F. 1994. Realistic modelling of observed seismic motion in complex sedimentary basins. *Ann. Geofis.* 37:1771-1797.

Fäh D. and Suhadolc P. 1994. Application of numerical wave-propagation techniques to study local soil effects: the case of Benevento (Italy). *Pure and Applied Geophys.* 143:513-536.

Fäh D., Suhadolc P. and Panza G.F. 1990. Estimation of strong ground motion in laterally heterogeneous media: modal summation - finite differences. Proc. 9-th European Conference of Earthquake Engineering, Sept. 11-16, 1990, Moscow, 4A, 100-109.

Fäh D., C. Iodice, P. Suhadolc and G.F. Panza 1993. A new method for the realistic estimation of seismic ground motion in megacities: the case of Rome. *Earthquake Spectra* 9: 643-668.

Fäh D., Suhadolc P., Mueller St. and Panza G.F. 1994a. A hybrid method for the estimation of ground motion in sedimentary basins: quantitative modeling for Mexico City. *Bull. Seism. Soc. Am.* 84: 383-399.

Fäh D., Iodice C., Suhadolc P. and Panza G.F. 1994b. Estimation of strong ground motion and micro-zonation for the city of Rome. Pre-print, IC/94/48, ICTP, Trieste, Italy.

Feroci M., Funiciello R., Marra F. and Salvi S. 1990. Evoluzione tettonica e paleogeografica plio-pleistocenica dell'area di Roma. *Il Quaternario* 3:141-158.

Florsch N., Fäh D., Suhadolc P. and Panza G.F. 1991. Complete synthetic seismograms for high-frequency multimode SH-waves. *Pure and Applied Geophys.* 136:529-560.

Funiciello R., Lori G. and Salvi S. 1987. Ricostruzione delle superfici strutturali del sottosuolo della città di Roma. Atti del 6° Convegno del Gruppo Nazionale Geofisica della Terra Solida, CNR, Roma, 395-415.

Gasparini C., Iannaccone G. and Scarpa R. 1985. Fault-plane solutions and seismicity of the Italian peninsula. *Tectonophysics* 117:59-78.

GNDT 1992. Convegno Nazionale sul Modello Sismotettonico d'Italia. Milano, 25-26 May 1992

Gouin P. 1976. Seismic zoning in Ethiopia, *Bull. Geophys. Obs.* (Ethiopia) 17:1-46.

Gusev, A.A. 1983. Descriptive statistical model of earthquake source radiation and its application to an estimation of short period strong motion. *Geophys. J.R. Astron. Soc.* 74:787-800.

Haskell N. A. 1953: The dispersion of surface waves in multilayered media. *Bull. Seism. Soc. Am.* 43:17-34.

ING 1980-1991. Istituto Nazionale di Geofisica, Seismological reports. ING, Roma

Jennings P.C. 1983. Engineering seismology. Terremoti: osservazione, teoria ed interpretazione. Rendiconti della Scuola Internazionale di Fisica 'Enrico Fermi', LXXXV Corso. Società Italiana di Fisica (ed.), 138-173.

Kanamori H. 1977. The energy release in great earthquakes. *J. Geophys. Res.* 82:2981-2987.

Kanamori H., Jennings P.C., Singh S.K. and Astiz L. 1993. Estimation of strong ground motions in Mexico City expected for large earthquakes in the Guerrero seismic gap. *Bull. Seism. Soc. Am.* 83:811-829.

Kebede F. and Vaccari F. 1996. Deterministic estimates of ground motion for Ethiopia, Djibouti and Eritrea. In preparation.

Manos G.C. and Demosthenous M. 1992. Design of R.C. structures according to the Greek Seismic Code Provisions. *Bull. of IISEE* 26:559-578.

Marcellini A., Bard P.-Y., Vinale F., Bousquet J.C., Chetrit D., Deschamps A., Franceschina L., Grellet B., Iannaccone G., Lentini E., Lopez Arroyo A., Meneroud J.P., Mouroux J.P., Pescatore T., Rippa F., Romeo R., Romito M., Sauret B., Scarpa R., Simoneili A., Tento A. and Vidal, S. 1991. Benevento Seismic Risk Project. Progress report (Report for the Commission of the European Communities, 1991).

Molin D., Ambrosini S., Castenetto S., Di Loreto E., Liperi L. and Paciello A. 1986. Aspetti della sismicità storica di Roma. *Mem. Soc. Geol. It.* 35:439-444.

Nunziata C., Fäh D. and Panza G.F. 1995. Mitigation of seismic hazard of a megacity: the case of Naples. *Annali di Geofisica* 38:649-661.

Orozova-Stanishkova I., Costa G., Vaccari F. and Suhadolc P. 1996. Estimates of 1Hz maximum acceleration in Bulgaria for seismic risk reduction purposes. *Tectonophysics* 258:263-274.

Panza G.F. 1985. Synthetic seismograms: The Rayleigh waves modal summation. *J. Geophysics* 58:125-145.

Panza, G. F., Prozorov, A. and Suhadolc, P. 1990. Is there a correlation between lithosphere structure and statistical properties of seismicity?, in: The structure of the Alpine - Mediterranean area: contribution of geophysical methods (Eds. R. Cassinis and G. F. Panza), *Terra nova* 2:585-595.

Panza, G. F. and Vaccari, F. 1994. Avanced criteria of seismic zoning and synthetic seismograms, Proc. Europrotech, Ed. G. Verri, CISM, Udine, 63-92.

Reiter L. 1990. Earthquake hazard analysis: issues and insights. Columbia University Press, New

40

heterogeneous area, one-dimensional modelling fails to correctly estimate the seismic hazard, whereas for a seismic source which is not located beneath the site of interest, two-dimensional modelling with vertical incidence of plane polarized body-waves does not allow us to correctly estimate the frequency bands at which amplifications occur.

These considerations point to the problem of the definition of the seismic source in time-domain compu ations, and to the differences that can be obtained when using an empirical definition of the incident wavefield or a numerical simulation of the seismic source. Numerical simulations of the seismic source are a more adequate technique than making estimates based on recorded accelerograms (empirical Green functions), since such records are always influenced by the local soil condition of the recording site. On the other hand, numerical simulations require the knowledge or the estimate of many parameters for the definition of the source-site path and of the source rupture process, which are often, but not always at hand. With method 2, it is possible to obtain, at low cost and exploiting large quantities of already available data - like geotechnical parameters, surface geology data, seismological and geophysical data - the definition of realistic seismic input for the existing or planned built environment, including special objects. The hybrid method is, at present, the only quantitative procedure that permits, for realistic seismic sources, to compute reliable complete seismograms that take into account the propagation effects, including detailed local conditions and the anelastic behaviour of soils.

The definition of realistic seismic input can be obtained from the computation of a wide set of time histories and spectral information, corresponding to possible seismotectonic scenarios for different source and structural models. Such a data set can be fruitfully used by civil engineers in the design of new seismo-resistant constructions and in the reinforcement of the existing built environment, and therefore supply a particularly powerful tool for the prevention aspects of Civil Defence.

The procedure is scientifically and economically valid for the immediate (no need to wait for a strong earthquake to occur), first order, seismic microzonation of any urban area, where the geotechnical data are available. The possibility to model broad-band seismic input is a useful tool for the engineering design and for the retrofitting of special objects, with relatively long free periods, that is acquiring a continuously increasing importance, due to the widespread existence, in the built environment, of special objects.

4. ACKNOWLEDGMENTS

We thank Dr. F. Kebede, Dr. C. Nunziata and Dr. I. Orozova-Stanishkova for their consent to use some results about the city of Naples (CN), the zoning of Bulgaria (IO-S) and Ethiopia (FK).

Most of the computations were performed on the IBM3090E computer at the ENEA INFO BOL Computer Center, to whom we would like to express our deep gratitude.

We acknowledge support by European Union contracts EPOC-CT91-0042, EV5V-CT94-0491 and EV5V-CT94-0513, Italian MURST 40% and 60% funds (1992-1994), and CNR grants 91.02550.PF54, 91.02539.PF54, 91.02692.CT15, 92.02867.CT54, 92.02876.CT54, 92.02422.CT15, 93.04179.CT15 and 94.00193.CT05, and Swiss National Science Foundation Grant Nr. 8220-037189. This research has been carried out in the framework of the ILP Task Group II.4 contribution to the IDNDR project "Physical Instability of Megacities".

65

5. REFERENCES

Amato A., De Simoni B. and Gasparini C. 1984. Considerazioni sulla sismicità dei Colli Albani. Atti del 3° Convegno del Gruppo Nazionale di Geofisica della Terra Solida, CNR, Roma, 2:965-976.

Ambrosini S., Castenetto S., Cevolani F., Di Loreto E., Funiciello R., Liperi L. and Molin D. 1986. Risposta sismica dell'area urbana di Roma in occasione del terremoto del Fucino del 13 gennaio 1915. Risultati preliminari. *Mem. Soc. Geol. It.*, 35:445-452.

Arias, A. 1970. A measure of earthquake intensity. In: Seismic design for nuclear power plants (Ed. R. Hansen), Cambridge, Massachussets.

Basili A., Favali P., Scalera G. and Smriglio G. 1987. Valutazione della pericolosità sismica in Italia centrale con particolare riguardo alla città di Roma. Atti del 6° Convegno del Gruppo Nazionale di Geofisica della Terra Solida, CNR, Roma, 379-393.

Beck J. L. and Hall J. F. 1986. Factors contributing to the catastrophe in Mexico City during the earthquake of September 19, 1985. *Geophys. Res. Lett.* 13:593-596.

Bernard P. and Zollo A. 1989. The Irpinia (Italy) 1980 earthquake: detailed analysis of a complex normal faulting. *J. Geophys. Res.*, 94:1631-1647.

Boore D.M. 1987. The prediction of strong ground motion. In: M.Ö. Erdik and M.N. Toksöz (Eds), Strong ground motion seismology. Reidel Publishing Company, Dordrecht, 109-141.

Costa, G., Panza, G.F., Suhadolc, P. and Vaccari, F. 1992. Zoning of the italian region with synthetic seismograms computed with known structural and source information. Proc. 10th WCEE, July 1992, Madrid, Balkema, 435-438.

Costa G., Panza G.F., Suhadolc P. and Vaccari F. 1993. Zoning of the Italian territory in terms of expected peak ground acceleration derived from complete synthetic seismograms. In: R. Cassinis, K. Helbig and G.F. Panza (Eds), Geophysical Exploration in Areas of Complex Geology, II. *J. Appl. Geophys.*, 30:149-160.

Eurocode 8 1993. Eurocode 8 structures in seismic regions - design - part 1 general and building, Doc TC250/SC8/N57A.

Fäh D. 1992. A hybrid technique for the estimation of strong ground motion in sedimentary basins.

York.

Rippa F. and Vinale F. 1983. Effetti del terremoto del 23 Novembre 1980 sul patrimonio edilizio di Napoli. Ass. Geotecnica Italiana, Atti XV Convegno Nazionale di Geotecnica, 193-206.

Sabetta F. and Pugliese A. 1987. Attenuation of peak horizontal acceleration and velocity from Italian strong-motion records. *Bull. Seism. Soc. Am.* 77:1491-1513.

Schnabel B., Lysmer J. and Seed H. 1972. Shake: a computer program for earthquake response analysis of horizontally layered sites. Rep. E.E.R.C. 70-10, Earthq. Eng. Research Center, Univ. California, Berkeley.

Stucchi M. et al., 1993. NT: il catalogo di lavoro del GNDT. GNDT internal report. Reserved.

Thomson W. T. 1950. Transmission of elastic waves through a stratified solid medium. *J. Appl. Phys.* 21:89-93.

Vaccari F., Gregersen S., Furlan M. and Panza G. F. 1989. Synthetic seismograms in laterally heterogeneous anelastic media by modal summation of P-SV-waves. *Geophys. J. Int.* 99:285-295.

Vaccari, F, Suhadolc, P. and Panza, G. F. 1990. Irpinia, Italy, 1980 earthquake: waveform modelling of strong motion data. *Geophys. J. Int.* 101:631-647.

Ventriglia U. 1971. La geologia della città di Roma. Amm. Prov. di Roma, Roma.

91